Thermal Stresses in End-Heated Layered Media

DISSERTATION
Jerry Rodney Couick
Major, USAF

AFIT/DS/ENY/95-6

DEPARTMENT OF THE AIR FORCE
AIR UNIVERSITY
AIR FORCE INSTITUTE OF TECHNOLOGY

Wright-Patterson Air Force Base, Ohio

DISCLAIMER NOTICE

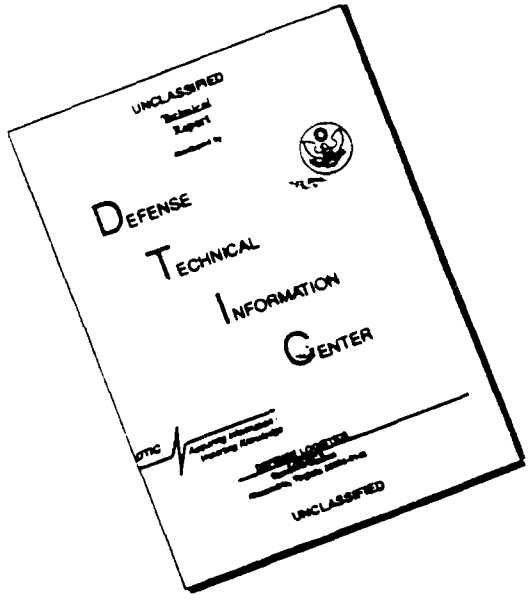

THIS DOCUMENT IS BEST QUALITY AVAILABLE. THE COPY FURNISHED TO DTIC CONTAINED A SIGNIFICANT NUMBER OF PAGES WHICH DO NOT REPRODUCE LEGIBLY.

AFIT/DS/ENY/95-6

Thermal Stresses in End-Heated Layered Media

DISSERTATION
Jerry Rodney Couick
Major, USAF

AFIT/DS/ENY/95-6

AFIT/DS/ENY/95-6

Thermal Stresses in End-Heated Layered Media

DISSERTATION

Presented to the Faculty of the School of Engineering

of the Air Force Institute of Technology

Air University

In Partial Fulfillment of the

Requirements for the Degree of

Doctor of Philosophy

Jerry Rodney Couick, B.S. Mathematics, B.S.A.E., M.S.A.E.

Major, USAF

December, 1995

AFIT/DS/ENY/95-6

Thermal Stresses in End-Heated
Layered Media

Jerry Rodney Couick, B.S. Mathematics, B.S.A.E., M.S.A.E.

Major, USAF

Approved:

Peter J. Torvik	1 Dec 1995
Wm. T. Bailey	1 Dec 95
Alan V. Pipes	1 Dec 95
Mark Hall	1 Dec 95
Anthony N. Palazotto	1 Dec 95

R. A. Calico

Dean

Acknowledgements

I am above all thankful to my Lord and Savior Jesus Christ for His favor and for the opportunity to have worked for the Doctor of Philosophy degree. Without Him I could not have succeeded. I am grateful to my loving and supportive wife, Janie, and my two dear children, Kristy and Roger, for all of their prayers, support and longsuffering endurance as I worked long hours to complete this dissertation. They were, for all practical purposes, without a husband and father for substantial periods during the performance and documentation of my research.

I am deeply indebted to my research advisor, Dr. Peter Torvik, for his guidance throughout my research activities and the preparation of this document. His patience, optimistic attitude, and expert advice gave me the encouragement I needed to press on when it wasn't clear how the research would turn out. I am especially grateful for his direction when my first solution attempt failed to address the problem of interest.

I wish to express my gratification to Mr. Christopher Clay of Wright Laboratory's Thermal Structures Section for his interest in this research and for his sponsorship. I also wish to thank Mr. Joseph Pokorski, my current supervisor, for his encouragement and for the countless times he helped me to rearrange my schedule in order that I might complete this research.

Jerry Rodney Couick

Table of Contents

List of Figures

List of Tables

Roman Symbols

Symbol	Units	Description
a_m, b_m, c_m		Constants in quadratic equation for characteristic roots in 2-D heat transfer model
A_i	MN/cm^3	Ratio of thermal strain to interfacial compliance coefficient, $\alpha_i T_{0i}/\kappa$
$\hat{A}$		Ratio of end thermal strains, A_2/A_1
b	cm	Thermal diffusion length, $2\sqrt{\kappa_{D1} t}$
$\hat{b}$		Square root of ratio of thermal diffusivities, $\sqrt{\kappa_{D2}/\kappa_{D1}}$
B		Ratio of stiffnesses, $\hat{E}\hat{h}$
C_i		Constant in solution to differential equation
E_i	MPa	Young's modulus of the ith layer
$\hat{E}$		Ratio of Young's moduli, E_2/E_1
h	cm	Total beam thickness, $h_1 + h_2$
h_i	cm	Thickness of the ith layer
$\hat{h}$		Ratio of layer thicknesses, h_2/h_1
h_f, h_m	cm	Fiber, matrix layer thicknesses in multi-layered model
H	W/cm^2°C	Effective convection heat transfer coefficient for the 2-D conduction model
i		Index denoting layer 1 or 2
I_i	cm^3	Rectangular beam moment of inertia
k^2	1/cm^2	Ratio of Λ to interfacial compliance coefficient, κ
k_{Ci}	W/cm°C	Thermal conductivity of the ith layer
$\hat{k}_C$		Ratio of thermal conductivities, k_{C2}/k_{C1}
$\bar{k}_C$	W/cm°C	Weighted average thermal conductivity
$\bar{k}$		Nondimensional form of k

Symbol	Units	Description
$\bar{k}$		Nondimensional form of k
k_N, p_N, q_N, Q_N		k, p, q, Q for N 3-layered repeating units in multi-layered model
L	cm	Length of finite-length beam or strip
m, n		Series summation indices
$\mathcal{M}_i$	MN	Internal bending moment of the ith layer, per unit width
N		Number of 3-layer repeating units in multi-layered model
q_f	MPa	Dimensional scale factor for $\hat{q}$
$\hat{q}$		Nondimensional interlaminar shearing stress
Q	MN/cm	Resultant interlaminar shearing force per unit width
p	MPa	Interlaminar normal (peeling) stress
p_f	MPa	Dimensional scale factor for $\hat{p}$
$\hat{p}$		Nondimensional interlaminar normal stress
P_0	MN/cm	Concentrated corner force per unit width at $(x, y) = (0, 0)$
$\hat{P}_0$		Nondimensional concentrated corner force
Q_f	MN/cm	Dimensional scale factor for $\hat{Q}$
$\hat{Q}$		Nondimensional resultant shearing force
$\hat{\mathcal{Q}}$		Ratio of end heat flux, $\mathcal{Q}_2/\mathcal{Q}_1$
$\bar{\mathcal{Q}}$	W/cm^2	Weighted average end heat flux
$\mathcal{Q}_i$	W/cm^2	Applied heat flux at end of the ith layer
t	sec	Time
$\hat{t}$		Nondimensional time, $4\kappa_{D1}t/L^2$
T_i	$^\circ C$	Temperature of the ith layer
T_{0i}	$^\circ C$	Temperature of the ith layer at $x = 0$
$\tilde{T}_i$		Nondimensional temperature in the ith layer in the 2-D heat transfer model
$\overline{T}_i$		Fourier cosine transform of $\tilde{T}_i$
u_0	cm	Displacement in x direction at $x = 0$
V	MN/cm	Vertical beam shearing force per unit width

Symbol	Units	Description
x	cm	Beam lengthwise (axial) distance coordinate
$\hat{x}$		Nondimensional axial coordinate, $x/b = x/2\sqrt{\kappa_{D1}t}$
$\tilde{x}$		Nondimensional axial coordinate, $\hat{x}/\hat{b} = x/2\sqrt{\kappa_{D2}t}$
y	cm	Beam thickness (transverse) coordinate

Greek Symbols

Symbol	Units	Description
α_i	cm/cm/°C	Coefficient of linear thermal expansion of the ith layer
δ_i		Nondimensional exponential temperature decay rate of the ith layer, η_i/k
ϵ_i	cm/cm	Total interface strain of the ith layer
$\epsilon_{iq}, \epsilon_{iQ}$	cm/cm	Interface strain of the ith layer due to $q(x), Q(x)$
$\epsilon_{iB}, \epsilon_{iT}$	cm/cm	Interface strain of the ith layer due to bending, thermal expansion
η_i	1/cm	Exponential temperature decay rate of the ith layer
κ	cm^3/MN	Total interfacial compliance coefficient
κ_i	cm^3/MN	Interfacial compliance coefficient of the ith layer
κ_{Di}	cm^2/sec	Thermal diffusivity of the ith layer
$\bar{\kappa}_D$	cm^2/sec	Weighted average thermal diffusivity
$\bar{\kappa}$		Nondimensional form of κ
Λ	cm/MN	Axial elongation per unit axial force
φ	cm	Equivalent moment arm for peeling stress
ν_i		Poisson's ratio of the ith layer
ξ	cm	Axial (lengthwise) coordinate
ρ	1/cm	Beam radius of curvature
σ_i	MPa	Normal (axial) stress in the ith layer
$\hat{\sigma}$		Nondimensional axial stress
ϕ		Nondimensional time, $k\sqrt{\kappa_{D1}t}$
ζ		Ratio of beam thickness to layer 1 thermal diffusion length, h/b
ω^2		Nondimensional effective convection heat transfer coefficient
γ_m		Length scale factor for Fourier series expansion
ψ_m		Temporal eigenvalues in 2-D heat transfer model
ϑ_m		Fourier sine series expansion coefficient
ϖ_m		Length scale factor for Fourier sine series expansion

Abstract

The role of thermal stresses in the failure of layered dissimilar materials is investigated using an extension to simple bimetallic thermostat theory. Of particular interest are the stresses generated in a freely supported semi-infinite layered beam with prescribed heat flux on the exposed end. The applicability of the solution to composite laminates is addressed.

Classical bimetallic thermostat solutions do not account for specified end tractions. For the freely supported thermostat, the classical solution yields self-equilibrating (but nonzero) axial stress distributions on the ends. Recently, other investigators have used the concept of interfacial compliance to formulate the bimetallic thermostat problem as a second-order boundary value problem, allowing for enforcement of the traction-free boundary conditions. This solution technique also provides for the calulation of interlaminar stresses, which cannot be obtained from the simple theory. The published work using the interfacial compliance concept was limited to beams of finite length subjected to a uniform temperature increase. In the present work, the bimetallic thermostat theory based on the interfacial compliance concept is extended to apply to semi-infinite layered beams subjected to end heating. A closed-form solution to the problem is then obtained.

The solution includes all the assumptions of Bernoulli-Euler beam theory and is not applicable within about one beam thickness (St Venant boundary region) of the end. Various classes of layered materials are analyzed to determine if significant stresses exist outside the boundary region. It is determined that thermal stresses of sufficient magnitude to cause failure are confined to the domain of nonapplicability (i. e. within the boundary region) if all the layers of a layered beam are poor thermal conductors. Significant axial and bending stresses are found to exist outside of the boundary region for layered beams in which one or more layers are relatively good thermal conductors. Very high stresses are found to exist in good conductors bonded to relatively poor conductors of similar stiffness. Significant interlaminar stresses are found to exist only in the boundary region, regardless of the magnitude of layer thermal conductivities.

Thermal Stresses in End-Heated

Layered Media

I. INTRODUCTION

1.1 Background

While working as a laser effects research engineer, the author was privileged to participate in experiments conducted to characterize the response of filament-wound composite pressure vessels (or *bottles*) to high energy laser radiation. The primary objective of the experiments was to define the laser beam parameters responsible for causing the bottle failure mode to transition from venting (i. e. depressurization over a relatively long time scale) to catastrophic bursting at a given value of the internal pressure.

Extensive modeling efforts were conducted in conjunction with the experiments in order to allow interpretation of the results and to facilitate a better understanding of the basic physics responsible for observed test results. The literature shows that six independent models evolved from the modeling activities. While all of them are not reported in the open literature, they are all documented in some form (1-6). All six models use finite elements to address fracture mechanics issues. Linear elastic fracture mechanics and free-edge delamination appear to be the phenomena of most interest to the researchers. While one of the models (2) accounts for through-the-thickness conduction, none of the existing models address the problem of thermal transport along the fiber direction and what role, if any, thermal stresses play in the failure of composite cylinders.

Interestingly, materials characterization tests on small test specimens indicated that heat loss via in plane conduction was significant. Also, postmortem analysis of numerous bottles revealed subsurface damage in the fiber direction at distances relatively far removed from the laser beam impingement area. As carbon and graphite fibers are known to be good conductors in the longitudinal direction, it is possible that conduction along the fibers away from the laser beam could cause thermal stresses to arise at some distance

removed from the immediate damage area. If thermal stresses of sufficient magnitude arise, the material will fail due to excessive stresses within one of the constituents or due to delamination along the interface. These failure possibilities, coupled with the absence of in-plane thermal transport consideration in the existing bottle failure models, strongly suggests the need for more research in this area.

1.2 The Overall Problem

The problem under consideration is quite complex and a comprehensive model should include a thorough treatment of the following issues:

- The physics of laser/target interaction, including;
  - Coupling of incident laser irradiation,
  - Ablation of target material.
- Heat transfer from the ablating region, including;
  - Lateral and transverse conduction,
  - Radiation to the environment,
  - Convection due to high velocity flow.
- The state of stress in the damaged cylinder, including;
  - Stress distribution around the impingement area,
  - Interlaminar stresses,
  - Thermal stresses,
  - Thermal degradation of mechanical properties.
- The target response, including;
  - Application of the most appropriate failure criteria,
  - Analysis of fracture following the onset of failure,
  - Determination of failure time and mode (i. e. vent or catastrophic burst).

The development of such a comprehensive model is dependent on the careful and thorough analyses of several simplified problems. The basic goal of the current research is to develop a simple thermoelastic solution which can be incorporated into a more sophisticated analytical model capable of predicting the failure mode and the time-to-failure for end-heated layered dissimilar media subjected to a wide variety of thermal boundary conditions. The specific problem to be studied in the current work is that of thermal transport in the lengthwise direction and the resulting thermal stresses. Valuable insight into this problem is obtained from a study of thermal stresses in layered beams with the appropriate temperature distribution. Therefore, an engineering solution to the problem of layered beams, with particular emphasis on lengthwise temperature variations and interlaminar stresses, is obtained and presented. Material failure predictions are then made based on the calculated values of interlaminar, extensional and bending stresses.

1.3 The Simplified Problem

When layered dissimilar media with different coefficients of thermal expansion are heated, thermal stresses are generated due to unequal thermal expansion in the layers. The stresses occur because free expansion of the layers is restricted by neighboring layers. Thermal stresses of significant magnitude are produced in layered dissimilar media subjected to even the simplest of temperature distributions, such as a uniform temperature increase or decrease. For example, two common engineering applications where thermal stresses due to uniform temperature distributions are of importance are; the deflection of a bimetallic thermostat, and the residual stresses present in laminated composite materials fabricated at one temperature but used in service at a significantly different temperature. If thermal stresses of sufficient magnitude arise in a layered medium, it will suffer damage due to failure of one or more of the individual layers or to delamination between layers.

As documented in Chapter II, most of the existing solutions to the problem of thermal stresses in layered dissimilar media are for temperature distributions that are either uniform or vary in the thickness direction. This is especially true concerning closed form engineering or strength of materials solutions. A fundamentally different problem results when a semi-infinite (or very long) layered dissimilar medium is heated on one end and maintained at

a constant temperature at infinity (or at the other end for very long finite media). The possibilities of failure are the same as for the uniform temperature problem. Stresses of sufficient magnitude will cause damage due to failure of individual layers or to delamination between layers. The temperature distribution is, however, quite nonuniform, decaying rapidly from its maximum value at the heated end to the prescribed temperature at infinity.

One expects, therefore, that the thermal stress distribution in end-heated, layered media will generally differ from the distribution in the same media subjected to uniform temperature variations. The objectives of the present work are to obtain a closed form engineering solution and to discuss its applicability to various types of layered dissimilar media.

The present study adds the capability to obtain closed form engineering calculations of the thermal stresses in layered dissimilar media subjected to known thermal boundary conditions resulting in nonuniform temperature distributions. This is an extension over the previous work, most of which has been restricted to layered media with uniform temperature distributions. Whereas a few of the previous studies address temperature variations in the thickness direction, the present study specifically addresses the problem of long, layered media with temperature variations in the lengthwise direction. The present study adds the capability to obtain closed form expressions for the thermal stresses in semi-infinite layered media. Most of the previous studies are for media of finite length and require that the temperature be symmetric about the middle (in the length direction) of the medium. The present study adds the capability to analyze many transient problems. Many of the previous studies were incapable of addressing transient problems because of the inherently nonuniform nature of transient temperature distributions. Finally, the present study adds the capability to analyze layered media of infinite length with a line heat source at the origin.

We now give a detailed description of the problem to be studied in the present work. The problem is to calculate the temperature and stresses in a layered Bernoulli-Euler beam consisting of two or more bonded dissimilar materials. Each individual layer is assumed to be isotropic, homogeneous and linearly elastic. The standard small displacement assumptions are invoked. The stress-strain relationship is assumed to be linear, thus restricting

the application to temperatures well below the melting or ablation temperature of the constituent materials. Each layer is assumed to be in perfect thermal and mechanical contact with neighboring layers. In general, each layer will have different thermal and mechanical material properites than adjacent layers. The beam is freely supported with no applied loads or tractions and with no residual stresses. The temperature is held constant at infinity, and the end is subjected to a known heat flux beginning at time zero. Initially, the beam is at a uniform temperature throughout. Convection and radiation heat transfer along the top and bottom surfaces of the beam is assumed to be negligible. The problem is assumed to be quasi-steady state, that is, while the temperature is a function of time, mechanical inertia terms in the equations of equilibrium are negligible. Therefore, time is merely a parameter in the equations for stress, strain and displacement. Finally, another key assumption is that the volumetric expansion occurs on a long enough time scale such that it does not cause the temperature to change. This final assumption allows the equilibrium and energy equations to be decoupled (7:Section 2.1). The temperature and stress distributions may then be calculated separately with temperature changes preceding stresses.

The temperature distribution in a two-dimensional bimaterial beam without convection and radiation transfer on its surfaces is governed by Fourier's law of heat conduction. In addition to satisfying the above initial and boundary conditions, the temperature and conduction in the thickness direction must also be continuous along the interface in order for the assumption of perfect thermal contact to be valid. If one of the constituents of the layered beam is a poor conductor while the other is a good conductor, the temperature distribution may be approximated as one-dimensional (i. e. the insulated rod solution).

The thermal stress distribution in a bimaterial Bernoulli-Euler beam is determined by forcing the curvature of the two layers to be identical and by enforcing strain continuity along the interface. The interface strain in a bimaterial beam with a nonuniform temperature distribution consists of an extensional term, a bending term, a term due to free thermal expansion, and a term due to the nonuniformity of the temperature. Note that for the mechanically free beam, the extensional and bending strains are entirely the result of material constraints against free thermal expansion.

1.4 Summary

The primary objectives of the present work are to obtain a simple analytical solution to the problem of thermal stresses in end-heated layered beams and use the resulting solution to make failure predictions. There appears to be very little literature addressing the problem as stated. However, there are numerous publications which address thermal stresses in layered beams and bimetallic strips subjected to less complicated temperature distributions. A review of the pertinent literature is now presented.

II. LITERATURE SURVEY

2.1 Elasticity Solutions

Elasticity solutions of the bonded strip problem are typically derived from Airy stress function solutions of the problem of bonded quarter-spaces. These solutions all indicate a singularity in the interlaminar stresses at the free-edge contact point. The free-edge contact point is the point of intersection between the interface of bonded dissimilar materials and the free edge. This point is also referred to as the corner point and is usually chosen for the origin of coordinates in Airy stress function analyses of bonded dissimilar materials. The two-dimensional solutions of bonded quarterplanes by Dundurs (9, 10) and Bogy (11, 12) are perhaps the classical solutions of this type. Raju et. al. (13) reported stress singularities for certain laminates but not for all laminates. Some other recent singularity solutions are those by Delale (14) and Blanchard and Ghoneim (15), in which a singular solution was developed using an eigenfunction expansion technique. There are many other singular solutions in the literature. (For example, see (16) and (17).) None of the singularity solutions considered appeared to be applicable to layered beams with nonuniform temperature distributions. Also, in an actual layered beam, there must be yielding or other forms of stress relaxation at the corner as predicted by the elasticity solutions. Therefore, some other solution must apply at this point and possibly in its neighborhood as well. For these reasons, an approximate nonsingular solution is sought for the problem at hand. It is anticipated that the approximate solution may not be accurate at and in the near vicinity of the corner.

2.2 Isothermal Solutions

There are no mechanical loads being applied to the bonded beams of interest in the current work. All stresses are brought about solely due to the nonuniform nature of the temperature distribution and the difference in material coefficients of thermal expansion. However, it is well-known that thermoelastic solutions can be found in theory from consideration of the appropriate isothermal problem (18). Only a few simple problems lend themselves to practical exact solutions using this approach. Nevertheless, since a theo-

retical solution exists, it is expected that phenomena observed in bonded materials under mechanical loads will be present in thermal problems as well. This should be especially true of the behavior of solutions near expected points of singularity. In other words, if mechanical solutions show a singularity to exist at the free-edge interface point, a singularity is also expected in thermal problems dealing with the same structure.

Pipes and Pagano (19) published what has become known as a classical solution dealing with free-edge interlaminar stresses. Classical elasticity theory was used to write the governing field equations. These were then solved using finite difference methods. The authors proclaim the solution to be an exact solution suitable for free-edge stress determination, subject to the generalized plane stress assumption. Interlaminar stresses were found to increase rapidly near the corner, indicating the possibility of a singularity there. Furthermore, the edge phenomena were observed to be applicable within only about one laminate thickness of the edge. Thus, edge effects are indeed confined to edges. The authors compared their results to those of Puppo and Evensen (20), who modelled a laminate as anisotropic layers joined with thin isotropic layers of adhesive. An eigenvalue problem was then formulated by assuming exponential forms of the displacements. Interlaminar normal stress was not addressed and the interlaminar shear stress was found to be zero in infinite laminates and maximum at the edge of finite laminates.

Goland and Reissner (21) appear to be the first to study *peeling* stresses, which they call tearing stresses. They did so in the course of analyzing stresses in the cement layer of cemented joints. They considered the beam to be a homogeneous beam with discontinuous thickness variation. The tearing stress was found to be high at the free edges, and was proposed as the primary failure mechanism in cemented joints.

While reviewing the literature on free-edge interlaminar stresses in bonded orthotropic laminae, Raju, Whitcomb and Goree (13) discovered an interesting discrepancy between published values of the interlaminar normal stress. Not only did the stresses for identical problems differ in magnitude near the free edge, but they also differed in sign. Due to the presence of a singularity at the corner, different solution techniques were expected to produce magnitude differences, but sign differences were unexpected. They analyzed the problem and suggested that the underlying cause of the sign discrepancy was the usual

assumption of symmetry in the stress tensor, which they showed to be invalid at singular points. They then performed careful finite element analyses of the problem with successively finer mesh sizes. This research showed the finite method to be accurate except for in the elements adjacent to the singular point. They showed their solutions to satisfy equilibrium considerations on a lamina, whereas the finite difference solution reviewed failed to satisty all the equilibrium equations. A very important conclusion was that the free-edge singularity effect is confined to a region very near the free edge. For the specific problem addressed they found no effects of the singularity to exist beyond a distance of about $.08h$ from the free edge, where h was the lamina thickness. The authors also commented that, while the shear stress should be zero at the corner because no shear load is applied on this face, all traditional solution techniques, both numerical and theoretical, predict a singularity at this point.

Ueng and Zhang (22) observed that, while many interlaminar stress solutions existed in the literature, they were cumbersome and impractical for thick laminates. They then developed an approximate solution by assuming the interlaminar stresses could be expressed as simple power series in the neighborhood of the free edge. In order to accomplish this, they divided the laminate into two regions; an end-effect region near the free edge, and a central region where classical laminated plate theory (CLPT) applies. They chose the effective edge width of the end-effect region to be either one or two laminate thicknesses, depending on which interlaminar stresses were being calculated. They noted that their solution required selection of the proper effective edge width in order for the results to be accurate, and that their particular selection seemed to explain some discrepancies discovered in the literature.

Lu and Liu (23) developed a theory for thick laminates which enforced interlaminar shear stress and displacement continuity for laminates with transverse shear deformation. Interlaminar normal stresses were not considered in their study. Their solution technique allows for determination of interlaminar shear stress directly from the constitutive relations, as opposed to the traditional method of using equilibrium considerations to recover shear stress after the fact. Their results were in excellent agreement with the benchmark results of Pipes and Pagano (19).

Kassapoglou and Lagace (24) used the Force Balance Method and the principle of minimum complementary energy to obtain closed-form expressions in angle-ply and cross-ply laminates due to mechanical loading.[1] An interesting feature of their solution was that the approximate solution developed satisfies the boundary conditions exactly. When comparing their solution to several others, they found all to match the Classical Laminated Plate Theory (CLPT) solution far from the free edge, but they found considerable differences in the published values of stress very near the edge. Some predicted nonzero values of the interlaminar shear stress at the free edge, which is somewhat consistent with the singularity solutions from elasticity theory, but seems to contradict the traction-free boundary conditions. The solution was obtained by requiring force and moment equilibrium to be satisfied in any section of the laminate. The stresses were then assumed to have a certain characteristic, exponential form. The unknown constants in these functions were then obtained by minimizing the complementary energy.

2.3 Solutions for Uniform Temperature Change

Very few solutions were uncovered addressing the problem of layered systems subjected to nonuniform temperature increases. With Goodier's method (18), one may determine the solution to a thermal problem from an equivalent isothermal problem where the effects of temperature are replaced by a body force distribution. The method is theoretically applicable for arbitrary temperature distributions, but in order to obtain solutions to physical problems, one must solve a problem in potential theory. The solution is tenable only for certain temperature distributions. An excellent example of applying Goodier's method to thermoelastic problems may be found in reference (25). A few solutions for specific types of nonuniform temperatures were found and are discussed later. No solutions were found for problems with temperatures similar to those in a long end-heated beam.

The classical engineering solution to the problem of thermal stresses in layered materials is the bi-metal thermostat solution due to Timoshenko (8). Timoshenko used standard Bernoulli-Euler beam theory to develop equations for the temperature of operation and

[1] The mechanical load consisted of normal traction in one direction only.

the total deflection during heating. He considered a layered strip of unit width with no applied forces or tractions. Bending due to thermal effects was simulated by applying fictitious concentrated forces and moments to the ends of the strip. The governing equations in Timoshenko's analysis were obtained from enforcing the curvature and interface strain of the two materials. The only stresses resulting from his theory are the axial and bending normal stresses. Interlaminar stresses cannot be calculated using his theory. He commented that there would be interlaminar normal and shear stresses for layers of different thickness or different moduli of elasticity, but only interlaminar shear stresses if both layers had the same thickness and modulus of elasticity. However, he described these stresses to be of *local* effect, confined very near the ends of the strip. He then showed that a fair amount of accuracy was possible when treating the layered strip as a homogeneous strip with material properties corresponding to the average of the constituent properties, for the case of equal layer thicknesses. Timoshenko applied his theory to several different beam configurations.

Pionke and Wempner (26) compared the stresses and deflections in bimetallic thermostats as calculated from elementary bonded beam theory, elementary bonded plate theory and finite element methods.[2] They found the closed form solutions to be adequate for calculating deflections and interior stresses, but inadequate for calculating interfacial stresses. Their criteria for an elementary solution to be called *adequate* seems to be how well it agrees with their finite element solutions. The bonded beam approximation was found to be adequate for calculating deflections while the the bonded plate approximation was found to be adequate for calculating both deflections and interior stresses. Note that interior stresses are bending stresses since interfacial stresses exist only near the free edges. The closed form solutions predicted finite values of the interfacial normal stress, whereas elasticity solutions insist on a singularity at the corner. Finally, the elementary closed form solutions failed to adequately predict interfacial stress magnitudes, gradients and signs very near the free edges.

[2]Note that the elementary plate solution can be obtained from the elementary beam solution by an appropriate change of Poisson's ratio.

Chen, Cheng and Gerhardt (27) considered the interface region of a bimaterial beam to be a third material with different material properties than either of the adjacent layers. Particular emphasis was placed on enforcing the traction-free boundary conditions on the ends of the beam. The problem was solved using a two-dimensional elasticity approach. The governing equations were solved using the principle of complementary energy. They found the peak interlaminar normal stress to be relatively independent of the thickness of the adhesive layer while the peak interlaminar shear stress was found to decrease as the thickness of the adhesive layer was increased. Also, they concluded that increasing the length of the beam had no effect on the interlaminar stresses. The only difference in this case was that the long mid-section of the beam, where interlaminar stresses are negligible, was longer.

Williams (28) considered the effects of the adhesive layer in a two-layered plate with particular emphasis on enforcing the traction-free boundary conditions on the ends of the plate. He solved the problem by developing an *inner* solution, valid only near the ends, and forcing it to match the classical Timoshenko (8) solution at the edge of the *inner* region. The method of matched asymptotic expansions was used in this process.

Seo et. al. (29) performed a systematic analysis to assess the role of various nondimensional parameters in the formation of thermal stresses in ceramic-metal plates. The parameters of interest were the ratio of Young's moduli, Poisson's ratios and the layer thickness-to-length ratios. Analyses were performed using both finite element methods and boundary element techniques, with the results from the two being indistinguishable. The variation of Poisson's ratios was shown to have practically no effect on thermal stresses. Variations of the ratio of Young's moduli and thickness-to-length ratios, on the other hand, produced significant differences in the thermal stresses. The most *damaging* stress, the interlaminar normal stress, was shown to achieve a maximum value at some ratio of Young's moduli. For small values of thickness-to-length ratios, which is the case for beams, the axial stresses were shown to be fairly constant over most of the length, except for near the ends, where they rapidly fell to zero. The interlaminar stresses (both shear and normal) remained constant (and approximately zero) over the same distance where axial stresses were nonzero, and then rapidly climbed to their peak values at the ends.

Chen and Nelson (30) considered the problem of bonded dissimilar materials where the interlaminar regions were considered to be a different material than either of the primary constituents. For example, their analysis would apply to structures such as a metal bonded to a different material with a nonmetallic adhesive. They considered three different materials with two different bond regions and two materials with a single bond region. In the three-material problem, bending was not allowed, whereas in the two-material problem, an analysis was conducted both with and without bending to assess the effects of bending on interlaminar shear stress. It is intuitively evident that unrestrained, bonded, dissimilar materials would bend when heated. Simple force and moment equilibrium considerations were used to derive the appropriate equations for stress and force. In all cases considered, shear stress was shown to be zero over most of the length, with rapid increase occurring near the free edge. Tensile stress, the authors' name for interlaminar normal stress, was found to behave in a similar manner for the problems with bending. There was no tensile stress when bending was disallowed. The tensile stress was shown to change sign near the edge, while shear stress maintained the same sign. According to the authors this is a common phenomenon in this type of problem. An additional conclusion was that bending serves to relax shear stress at the free edge.

Weitsman (31) studied the interlaminar stresses in a thin layer of adhesive situated between two rigid plates, when the edge of the layer was subjected to moisture or when the entire assembly was raised to an elevated temperature. An analysis based on variational principles showed the maximum interlaminar stresses to occur within one layer thickness of the free edge. This was reported to be consistent with unreferenced experimental results. This solution showed the interlaminar shear stress to be nonzero at the free edge. This result is qualitatively consistent with elasticity solutions which indicate a singularity at this point, but violates the traction-free boundary conditions. An important indication of the solution is that the interlaminar stresses depend very little on the Poisson's ratio of the adhesive layer. Finally, Weitsmann stated that his method was preferable to finite-element methods, especially for a single embedded layer of adhesive.

While Timoshenko was primarily interested in the operating temperature and deflection of bimetal thermostats, Suhir (32) was concerned about the possibility of thermostats

debonding due to the high interlaminar stresses near the free edges. He therefore sought to develop an engineering theory capable of predicting these stresses, while satisfying the necessary end boundary conditions. He observed that the reason Timoshenko's solution could not satisfy these conditions was that the stresses were not calculated from a differential equation, and end boundary conditions could not be used to affect the solution. Suhir reasoned that, if the shear stress must go from zero on the top (or bottom) of a bimetal thermostat to some value (the interlaminar value) at the interface, fibers of material near the interface must be strained more or less (depending on the sign of the shear stress) than they would be due to the resultant of the shear stress distribution applied at the midsection of the layer. Outer fibers of a layer should be strained less or more than they would be due to the average load. By studying the Ribière solution for a finite strip loaded with an antisymmetric shear load on one face such that the axial displacement is zero at the center of the strip, he was able to devise a *correction* term to Timoshenko's equation for interface strain compatibility. Since this term attempts to account for the variation of shear stress from zero to the interlaminar value, we see that it imparts a measure of two-dimensionality to Timoshenko's one-dimensional solution. The most significant effect of Suhir's extension is that it permits the curvature and strain matching conditions to produce a second order ordinary differential equation for the interlaminar shear force. The traction-free boundary conditions at the ends of the strip may then be enforced. The interlaminar shear stress is then found by differentiating the interlaminar shear force, and interlaminar normal (peeling) stress is related to shear stress via an equilibrium analysis. Suhir found that the maximum stresses were concentrated near the strip ends. Suhir's solution for uniform temperatures in each strip will be used as the basis for a solution for the problem of interest in the present work. The reader is referred to Chapter III for the mathematical details of this procedure.

Suhir (33) also developed a similar solution in which both the interlaminar shear force and the interlaminar shear stress are forced to approach zero at the ends of the strip. The key assumption in this solution is that the transverse normal stress can be written in terms of an effective through-the-thickness spring constant. This approach leads to coupled differential equations for the interlaminar normal and shear stresses. After some

interesting algebraic manipulation, Suhir reduces both equations to the same homogeneous sixth order ordinary differential equation. His equations are homogeneous because of the assumed uniform temperature distributions. The solutions for interlaminar normal and shear stress for the homogeneous problem differ solely due to different boundary conditions on the two stresses, since there are no particular solutions. For nonhomogeneous problems, solutions differ due to both different boundary conditions and different particular solutions.

Morton and Webber (34) used Kassapoglou and Lagace's method (24) to calculate free-edge stresses due to mechanical and thermal loads. They then used a quadratic interlaminar stress criterion to make failure predictions, which were found to agree reasonably well with experimental results. The authors did find that the stacking sequence of laminae was very influential in determining whether or not failure would occur.

Kuo (35) obtained a solution for a semi-infinite bimetallic thermostat with the free edge specified to be traction-free. He solved the problem by superposing the solutions to the following problems:

- The infinite bimetallic thermostat, solved using Timoshenko's theory;
- Bonded dissimilar quarter-spaces loaded on the free edge, solved using Bogy's elasticity solution (12);
- The infinite bimetallic strip loaded on the longitudinal surfaces, solved using Airy stress functions.

He also solved the problem using finite elements and found his analytical solution to be in close agreement with the finite element solution. At first glance, the problem Kuo solved appears to be very nearly the same problem for which a solution is sought in the current work. However, the particular solutions required by his technique (or any stress function technique) cannot be found in closed form except for certain temperature distributions. The most common restriction found in the literature is that the temperature be uniform. A few solutions have been found for harmonic temperature distributions. In spite of these limitations, Kuo's results suggest that the elementary beam theory solution due to Suhir (32) is accurate except in a boundary layer region near the free edge. Kuo's results indicate the boundary layer thickness to be less than or equal to three times the thickness

of the thinner strip, although he did not clearly state whether this suggested boundary layer thickness was applicable to all bimaterial beams, or only to the specific beam for which he obtained numerical results.

2.4 Solutions for Nonuniform Temperature Change

Ochoa and Marcano (36) extended elementary beam theory to include the effects of transverse normal strain and transverse shear strain. They used the resulting solutions to study the stresses in a layered beam subjected to various temperature distributions. The following forms of temperature distribution were considered:

- Uniform
- Linear in the longitudinal direction with no transverse variation
- Sinusoidal in the longitudinal direction with no transverse variation
- Simultaneously quadratic in both directions

The stresses calculated using classical beam theory agreed well with those predicted using the extended theory for the first two types of temperature distributions. However, significant differences were observed for the other two temperature distributions. No mention was specifically made of interlaminar stresses near the free edge of the beam. Also, none of the temperatures considered were of the type that decay along the length of the beam. In fact, they even increased or varied periodically with a constant peak amplitude.

Williams (37) analyzed the effects of the adhesive layer in solar cells by looking at a three-layer beam using a variational approach with displacement components that vary linearly through the thickness of the adhesive layer. This solution is limited to temperatures that vary in the thickness direction only. No variation in the longitudinal direction were allowed.

Tsai and Morton (38) employed finite element methods to show that the stress state near free edges is three-dimensional and they proposed that the only possibility of obtaining accurate free edge results was through the use of three-dimensional finite element analyses. None of the problems considered were of beam-type structures. That is, the ratio of

thickness to length was of order unity whereas this ratio is necessarily very small in the problems being addressed in the current research effort.

Yin (39) studied the effects of free-edge inclination in bimaterial beams, finding that tapering the free edge almost always led to lower interlaminar normal stresses and sometimes to lower interlaminar shear stresses as well. His variational method was developed assuming a through-the-thickness temperature distribution, but the specific example addressed was for a uniform temperature distribution. In any case, the temperature was assumed not to vary in the coordinate direction along the length of the beam. It is noted that through-the-thickness variations in temperature are simple to address using the extension of Suhir's method which will be presented in later chapters. This is because the governing differential equations do not include that coordinate direction. Therefore, particular solutions to inhomogeneous terms including only the thickness direction coordinate are simply those due to the appropriate constants.

More recently, Yang and Munz (40) used the Mellin transform in conjunction with stress functions to determine the regular (i. e. nonsingular) stress term in bonded dissimilar materials under thermal loading. The temperature distribution considered was that of a semicircle of constant temperature with the remainder of the materials at zero temperature. The technique requires existence and finiteness of the Mellin transform of the temperature distribution.

Kwon, Salinas and Neibert (41) used newly developed finite elements providing for both axial and lateral displacement continuity to analyze the stresses in trilayered systems subjected to various temperature distributions. Nonuniform distributions were considered, but while the temperature in the different layers was assumed to differ, the temperature within each individual layer was specified to remain constant.

2.5 Summary

An extensive review of the technical literature revealed that much work has been done to determine the state of stress in bonded dissimilar materials subjected to temperature changes. The majority of the work is restricted to uniform temperature changes. A few

solutions exist for through-the-thickness temperature variations. Very few solutions were found to exist for layered beams with temperature variations in the longitudinal direction. However, none of the solutions address the type of nonuniform temperature distribution in a layered beam heated on one end. It was shown in Chapter I that the thermoelastic response of a layered cylinder can sometimes be predicted by studying the simpler problem of a very long layered beam under the same thermal loads. One of the uniform temperature solutions (32) reviewed above can be extended to address this problem. We now present that solution and the necessary extensions in detail.

III. Thermal Stresses in a Bimaterial Beam with Nonuniform Temperature

3.1 Problem Description

Consider the semi-infinite bimaterial beam, illustrated in Figure 3.1, composed of two isotropic, homogeneous and linearly elastic materials. They are assumed to be perfectly bonded along the interface and the beam is assumed to behave according to standard Bernoulli-Euler beam theory. The ends of the beam are specified to be traction-free and its width is given to be unity.

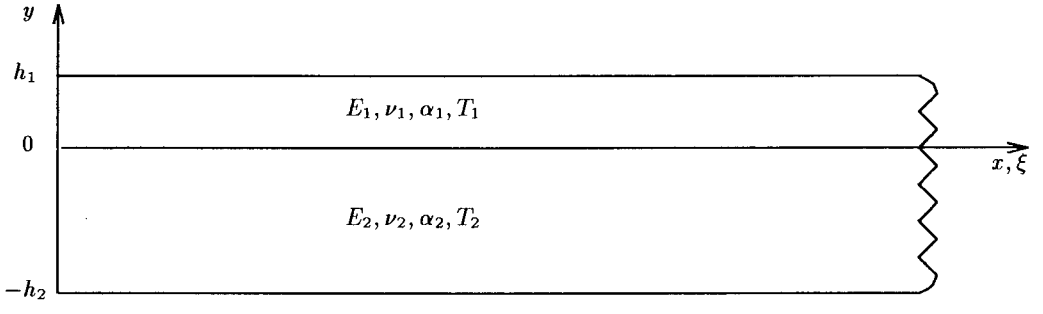

Figure 3.1 Illustration of the Bimaterial Semi-Infinite Beam

Due to the different temperature distributions and coefficients of thermal expansion in the two strips, interlaminar shear and normal stresses will occur along the interface of the two materials. Should these stresses exceed the strength of the interlaminar bond, failure will occur along the interface, initiating the process of delamination. Thermal expansion will also cause axial stresses, consisting of both extension and bending terms, to develop within the individual layers. If these stresses exceed the constituent material strengths, one or both of the layers will fail in either tension or compression. We desire a simple engineering solution to this problem for nonuniform temperature distributions. [1] Of particular interest are the stresses in the beam when either the temperature or the flux

[1] All temperatures are relative to the temperature at which the beam is stress-free, which is taken to be zero for convenience.

is specified at the exposed end ($x = 0$) of the beam. Note that, since the beam is of unit thickness, all forces and moments will be per unit thickness.

3.2 Suhir's Solution

Following the work by Suhir (32), we seek an elementary strength of materials type of solution as opposed to an exact elasticity solution. Suhir's solution is now presented in detail, with three exceptions. First, unless otherwise stated, the current analysis is for a beam of unit width, whereas Suhir's analysis is for a plate of unit width (i. e. a strip). The beam formulation of Suhir's strip solution is obtained by replacing the ratio, $E/(1-\nu^2)$, with E. Conversely, Suhir's strip formulation of the present beam solution is obtained by replacing the Young's modulus, E, with $E/(1-\nu^2)$. The second departure from Suhir's solution is that the current analysis is for a semi-infinite beam, whereas Suhir's analysis is for a strip of finite length. Finally, the current analysis is for an arbitrary temperature distribution, whereas Suhir's analysis is for a uniform temperature distribution.

Taking a section cut of the beam in Figure 3.1 at $\xi = x$ leads to the free body diagram shown in Figure 3.2.

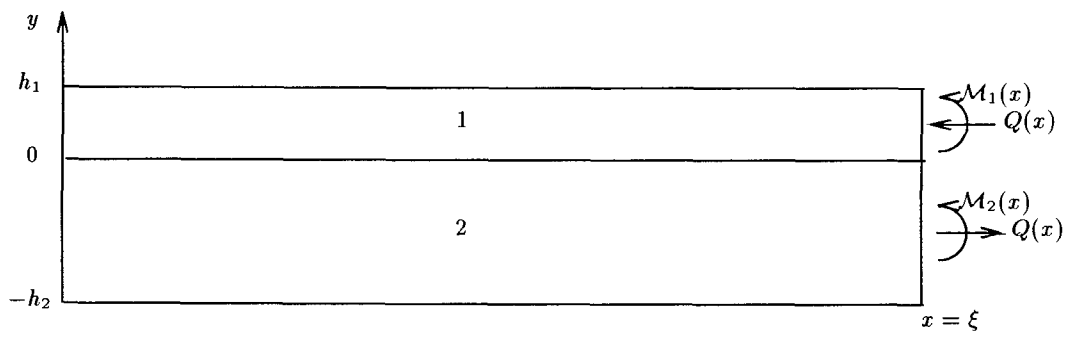

Figure 3.2 Section Cut of the Bimaterial Beam

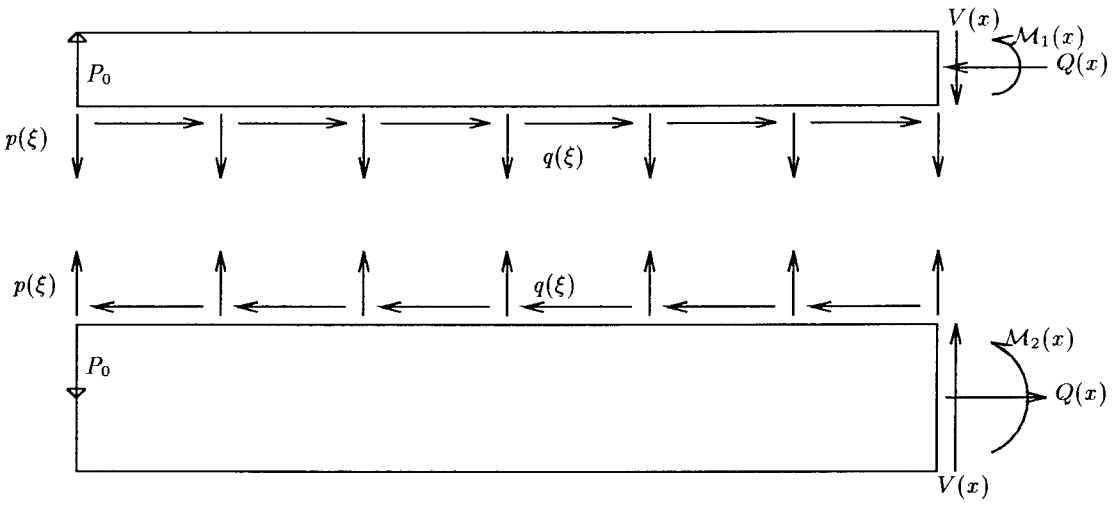

Figure 3.3 Interlaminar Forces in the Bimaterial Beam

Moment equilibrium of this section requires that

$$\mathcal{M}_1(x) + \mathcal{M}_2(x) = -\frac{h}{2}Q(x) \tag{3.1}$$

where $h = h_1 + h_2$. The radii of curvature of the two strips must be equal and are related to the bending moments by the standard formulae:

$$\mathcal{M}_1(x) = \frac{E_1 I_1}{\rho(x)} \tag{3.2}$$

$$\mathcal{M}_2(x) = \frac{E_2 I_2}{\rho(x)} \tag{3.3}$$

where E_i and I_i are the Young's modulus and moment of inertia, respectively, of the i^{th} layer. By substituting equations 3.2 and 3.3 into equation 3.1, the radius of curvature is found to be

$$\frac{1}{\rho(x)} = -\frac{h}{2}\left(\frac{1}{E_1 I_1 + E_2 I_2}\right) Q(x) \tag{3.4}$$

A system of interlaminar distributed forces must be present to hold the strips together, as shown in Figure 3.3. Note that, while the figure suggests these forces to be uniformly distributed, no assumption at all has been made regarding their distribution.

The section must be in force and moment equilibrium. Force equilibrium implies

$$Q(x) = \int_0^x q(\xi)\, d\xi \tag{3.5}$$

$$V(x) = P_0 - \int_0^x p(\xi)\, d\xi \tag{3.6}$$

The traction-free boundary condition at $x = \infty$ requires that the cross-sectional shear force, $V(x)$, be zero there. As research into the problem of thermal stresses in bonded dissimilar materials indicates a singularity in interlaminar normal stress at the corner, a pair of concentrated loads, P_0, acting at the origin of each strip, is assumed. Since $V(\infty) \to 0$,

$$P_0 = \int_0^\infty p(\xi)\, d\xi \tag{3.7}$$

In order to prevent dislocations from occuring along the interface, the strain must be compatible. The interface strains of the two beams are given as follows:

$$\epsilon_1 = \epsilon_{1Q} + \epsilon_{1q} + \epsilon_{1B} + \epsilon_{1T} \tag{3.8}$$

$$\epsilon_2 = \epsilon_{2Q} + \epsilon_{2q} + \epsilon_{2B} + \epsilon_{2T} \tag{3.9}$$

where ϵ_Q is the neutral axis strain due to the average force, $Q(x)$, ϵ_q is a correction term due to the nonuniformity in the x direction of the distributed lateral load, ϵ_B is the strain due to bending and ϵ_T is the neutral axis thermal strain. From simple beam theory we have

$$\begin{aligned} \epsilon_{1Q} = -Q(x)/(h_1 E_1) \quad &, \quad \epsilon_{2Q} = Q(x)/(h_2 E_2) \\ \epsilon_{1B} = h_1/(2\rho(x)) \quad &, \quad \epsilon_{2B} = -h_2/(2\rho(x)) \\ \epsilon_{1T} = \alpha_1 T_1(x) \quad &, \quad \epsilon_{2T} = \alpha_2 T_2(x) \end{aligned} \tag{3.10}$$

where α is the coefficient of linear thermal expansion and T_i represents the change in temperature of the i^{th} layer. The temperature change is measured with respect to an unstrained equilibrium temperature, which is taken to be zero for convenience.

The *correction term*, ϵ_q, requires a bit of clarification. Consider a strip of unit width with a self-equilibrating shear load applied along its bottom edge, as shown in Figure 3.4. The x direction displacement at $y = 0$ is given by the Ribière solution[2] for a long and

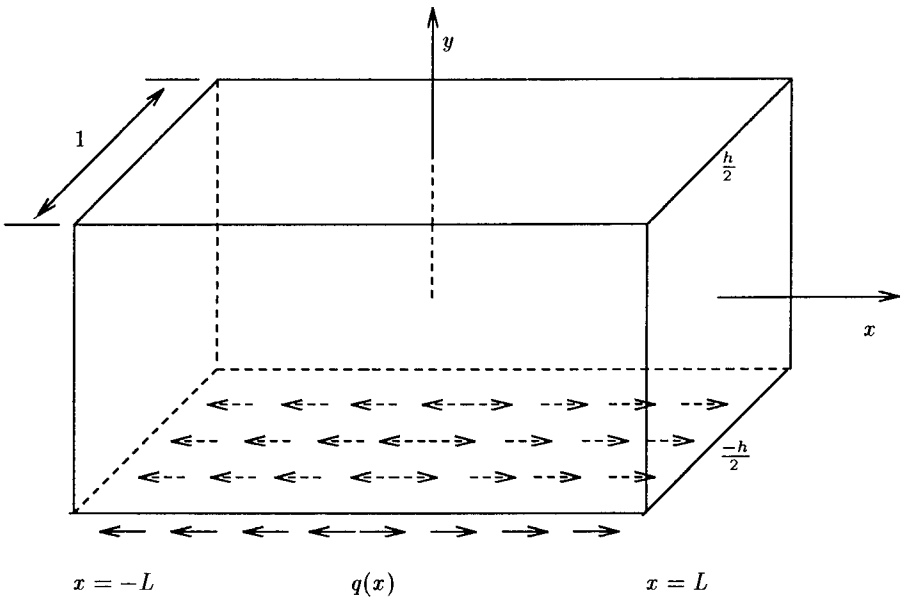

Figure 3.4 Strip Loaded in Shear Along One Face

narrow strip (32):

$$u_0 = \frac{1+\nu}{2E} \sum_{m=1,3,5,\ldots}^{\infty} \vartheta_m [\{3 - \nu - (1+\nu)\varpi_m h \coth \varpi_m h\} \coth \varpi_m h + (1+\nu)\varpi_m h] \sin \varpi_m x \tag{3.11}$$

where

$$\varpi_m = \frac{m\pi}{2L} \tag{3.12}$$

$$\vartheta_m = \frac{2}{\varpi_m h} \int_0^L q(x) \sin \varpi_m x \, dx \tag{3.13}$$

[2]The Ribière solution is an exact solution to the one-dimensional Navier equation obtained using a Fourier sine series expansion.

According to Gradshteyn and Ryzhik(42:page 23)

$$\coth \pi z = \frac{1}{\pi z} + \frac{2z}{\pi} \sum_{n=1}^{\infty} \frac{1}{z^2 + n^2} \tag{3.14}$$

For sufficiently small values of z this series reduces to

$$\coth \pi z = \frac{1}{\pi z} + \frac{\pi z}{3} \tag{3.15}$$

Therefore, if $h/L \ll 1$, the strain at $y = 0$ is given by

$$\epsilon_{0_R} = \frac{du_0}{dx} \approx \frac{1+\nu}{2E} \sum_{m=1,3,5,\ldots}^{\infty} \vartheta_m \varpi_m \left\{ \frac{4}{3} \varpi_m h + \frac{2(1-\nu)}{\varpi_m h} \right\} \cos \varpi_m x \tag{3.16}$$

where the R subscript denotes the Ribière solution. Consider now a section cut of the strip as shown in Figure 3.5. We seek a value of κ such that the strain at $y = 0$ due to the shear

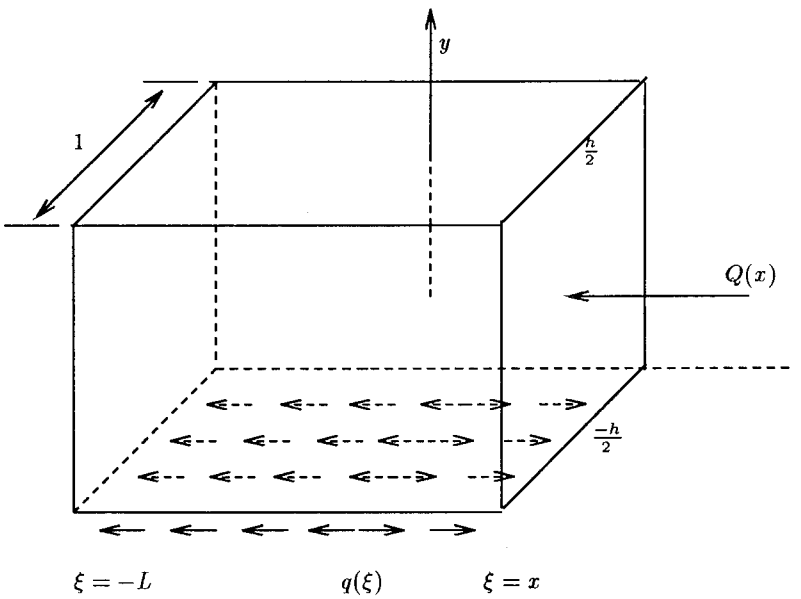

Figure 3.5 Section Cut of the Strip

load may be written in the form

$$\epsilon_{0_A} = -\frac{1-\nu^2}{hE} Q(x) + \kappa q'(x) \tag{3.17}$$

where the A subscript denotes an approximate solution and

$$\begin{aligned} Q(x) &= \int_{-L}^{x} q(\xi)\, d\xi \\ q'(x) &= \frac{dq(x)}{dx} \\ \kappa q'(x) &= \epsilon_q(x) \end{aligned} \tag{3.18}$$

From equation 3.13 we see that

$$q(x) = \sum_{m=1,3,5,\ldots}^{\infty} \varpi_m \vartheta_m \sin \varpi_m x \tag{3.19}$$

Substituting equations 3.19 and 3.18 into equation 3.17, we obtain

$$\epsilon_{0_A} = \sum_{m=1,3,5,\ldots}^{\infty} \left\{ \vartheta_m \frac{1-\nu^2}{hE} + \kappa \varpi_m^2 \vartheta_m \right\} \cos \varpi_m x \tag{3.20}$$

In order for equations 3.16 and 3.20 to be equal for all values of ϖ_m and ϑ_m, we must have

$$\kappa = \frac{2h(1+\nu)}{3E} \tag{3.21}$$

The analysis thus far follows that of Suhir (32). Equation 3.21 gives Suhir's interfacial shear compliance coefficient for bonded strips in plane stress, a configuration which more closely resembles plates than beams. Since the current analysis is for beams, κ must be adjusted by replacing E with $E(1-\nu^2)$. Performing the substitution results in

$$\kappa = \frac{2h}{3E(1-\nu)} \tag{3.22}$$

Substituting equations 3.10 into equations 3.8 and 3.9, we obtain

$$\epsilon_1 = -\frac{Q(x)}{h_1 E_1} + \kappa_1 q'(x) + \alpha_1 T_1(x) + \frac{h_1}{2\rho(x)} \tag{3.23}$$

$$\epsilon_2 = \frac{Q(x)}{h_2 E_2} - \kappa_2 q'(x) + \alpha_2 T_2(x) - \frac{h_2}{2\rho(x)} \tag{3.24}$$

where α_i is the coefficient of linear thermal expansion of the i^{th} layer and κ_1, κ_2 are shear compliance coefficients given by

$$\kappa_1 = \frac{2h_1}{3E_1(1-\nu_1)} \tag{3.25}$$

$$\kappa_2 = \frac{2h_2}{3E_2(1-\nu_2)} \tag{3.26}$$

with ν_i being Poisson's ratio. Equating equations 3.23 and 3.24, we obtain

$$-Q(x)\left(\frac{1}{h_1E_1}+\frac{1}{h_2E_2}\right)+\kappa q'(x)+\frac{h}{2}\frac{1}{\rho(x)}=\alpha_2T_2(x)-\alpha_1T_1(x) \tag{3.27}$$

where $\kappa = \kappa_1 + \kappa_2$. Substituting equation 3.4 into this equation, we obtain

$$-\Lambda Q(x)+\kappa q'(x)=\alpha_2T_2(x)-\alpha_1T_1(x) \tag{3.28}$$

where

$$\Lambda=\frac{1}{h_1E_1}+\frac{1}{h_2E_2}+\frac{h^2}{4}\left(\frac{1}{E_1I_1+E_2I_2}\right) \tag{3.29}$$

By differentiating equation 3.5 and substituting the result into equation 3.28, the following ordinary differential equation in $Q(x)$ results:

$$Q''(x)-k^2Q(x)=\frac{\alpha_2}{\kappa}T_2(x)-\frac{\alpha_1}{\kappa}T_1(x) \tag{3.30}$$

where

$$k^2=\frac{\Lambda}{\kappa}=\frac{3}{2h_1^2}\frac{(1-\nu_1)(1-\nu_2)}{(1+B\hat{h}^2)}\left[\frac{(B+1)(1+B\hat{h}^2)+3B(1+\hat{h})^2}{B(1-\nu_2)+\hat{h}^2(1-\nu_1)}\right] \tag{3.31}$$

with $B=\hat{E}\hat{h}=E_2h_2/(E_1h_1)$. Since the ends of the beam are specified to be traction-free, $Q(x)$ must be zero there.[3] The necessary boundary conditions are therefore

$$Q(0) = 0 \tag{3.32}$$

$$\lim_{x\to\infty} Q(x) = 0 \tag{3.33}$$

[3]Note that this condition will force only the axial stress, σ_{xx}, to be zero.

The solution to equation 3.30 is

$$Q(x) = C_1 e^{kx} + C_2 e^{-kx} + Q_p(x) \tag{3.34}$$

where C_1 and C_2 are constants to be determined by applying the boundary conditions, and $Q_p(x)$ is a particular solution to equation 3.30. Applying equations 3.32 and 3.33 to equation 3.34, we obtain

$$C_1 = -\lim_{x\to\infty}\left[Q_p(x)e^{-kx}\right] \tag{3.35}$$

$$C_2 = -Q_p(0) + \lim_{x\to\infty}\left[Q_p(x)e^{-kx}\right] \tag{3.36}$$

The interlaminar shear stress, $q(x)$, is obtained by differentiating Equation 3.5:

$$q(x) = Q'(x) = k\left(C_1 e^{kx} - C_2 e^{-kx}\right) + Q_p'(x) \tag{3.37}$$

The interlaminar normal stress, or *peeling* stress, may be obtained by considering the moment equilibrium of one of the beams shown in Figure 3.3. Moment equilibrium of strip 1 requires that

$$\mathcal{M}_1(x) + \mathcal{M}_p(x) + \frac{h_1}{2}Q(x) - P_0 x = 0 \tag{3.38}$$

where $\mathcal{M}_p(x)$ is the moment at x due solely to the distributed load, $p(\xi)$. In order to determine the relationship between the two, consider the free-body diagram of an incremental segment of the top strip as shown in Figure 3.6. Equilibrium of forces is guaranteed if equation 3.6 is satisfied. Equilibrium of moments about point O requires that

$$\Delta\mathcal{M}_p = V\Delta\xi - \bar{p}\frac{\Delta\xi^2}{2} \tag{3.39}$$

where $\bar{p}$ is the average value of p across the segment. Dividing by $\Delta\xi$ and taking the limit as $\Delta\xi \to 0$, we obtain

$$\frac{d\mathcal{M}_p}{d\xi} = V(\xi) \tag{3.40}$$

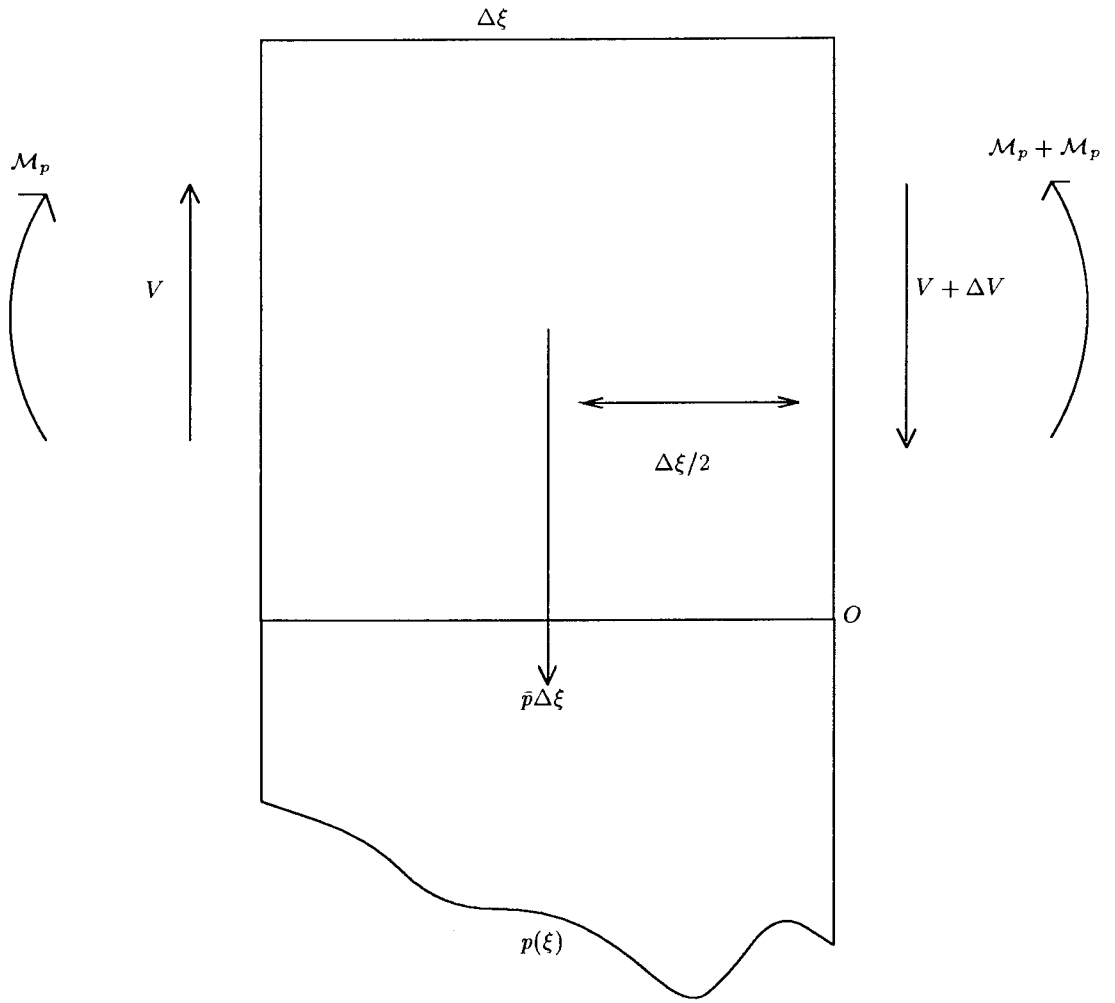

Figure 3.6 Free-Body Diagram of an Incremental Segment.

Substituting equation 3.6 into equation 3.40 and integrating, we obtain

$$\mathcal{M}_p(x) = -P_0 x + \int_0^x \left[\int_0^\xi p(\xi')\, d\xi' \right] d\xi \tag{3.41}$$

where the constant of integration is zero because there are no applied moments. Inserting this result into equation 3.38 produces the following equation:

$$\mathcal{M}_1(x) + \int_0^x \left[\int_0^\xi p(\xi')\, d\xi' \right] d\xi + \frac{h_1}{2} Q(x) - P_0 x = 0 \tag{3.42}$$

Substituting equations 3.2 and 3.4 into equation 3.42 yields

$$\int_0^x \left[\int_0^\xi p(\xi')\, d\xi' \right] d\xi = \varphi Q(x) + P_0 x \tag{3.43}$$

where

$$\varphi = \frac{h}{2} \frac{E_1 I_1}{E_1 I_1 + E_2 I_2} - \frac{h_1}{2} \tag{3.44}$$

Differentiating equation 3.43 twice, we obtain the normal stress:

$$p(x) = \varphi Q''(x) = \varphi \left[k^2 \left(C_1 e^{kx} + C_2 e^{-kx} \right) + Q_p''(x) \right] \tag{3.45}$$

The emphasis thus far has been on interlaminar stresses. Another important consideration is that of the axial stresses, which are given by

$$\sigma_x(x,y) = \begin{cases} -Q(x)/h_1 + \mathcal{M}_1(x) y_1 / I_1, & 0 < y \leq h_1 \\ Q(x)/h_2 + \mathcal{M}_2(x) y_2 / I_2, & 0 > y \geq -h_2 \end{cases} \tag{3.46}$$

where

$$y_1 = \frac{h_1}{2} - y \tag{3.47}$$

$$y_2 = -\left(\frac{h_2}{2} + y \right) \tag{3.48}$$

The axial stresses are found by substituting equations 3.2, 3.3, 3.47 and 3.48 into equation 3.46. All desired stresses have now been determined and the complete strength of materials solution to the problem is now given. The interface shearing force is given by

$$Q(x) = C_1 e^{kx} + C_2 e^{-kx} + Q_p(x) \tag{3.49}$$

the interface shearing stress is given by

$$q(x) = k \left(C_1 e^{kx} - C_2 e^{-kx} \right) + Q_p'(x) \tag{3.50}$$

the interface normal stress is given by

$$p(x) = \varphi \left[k^2 \left(C_1 e^{kx} + C_2 e^{-kx} \right) + Q_p''(x) \right] \tag{3.51}$$

and the axial stresses are given by

$$\sigma_{x_1} = -Q(x) \left\{ \frac{1}{h_1} + \frac{hE_1 (h_1/2 - y)}{2(E_1 I_1 + E_2 I_2)} \right\} \tag{3.52}$$

$$\sigma_{x_2} = Q(x) \left\{ \frac{1}{h_2} + \frac{hE_2 (h_2/2 + y)}{2(E_1 I_1 + E_2 I_2)} \right\} \tag{3.53}$$

The constants are given by

$$C_1 = -\lim_{x \to \infty} \left[Q_p(x) e^{-kx} \right] \tag{3.54}$$

$$C_2 = -Q_p(0) + \lim_{x \to \infty} \left[Q_p(x) e^{-kx} \right] \tag{3.55}$$

A concentrated force,

$$P_0 = \lim_{x \to \infty} \frac{C_1}{k} e^{kx} + \frac{1}{k}(C_2 - C_1) + \int_0^\infty Q_p(\xi)\, d\xi \tag{3.56}$$

is found to act at the corner on the heated end of the beam.

3.3 Extensions to Suhir's Solution

While the development given in the previous section is essentially due to Suhir, two modifications have been incorporated: all references to x becoming infinite, and the application to beams as opposed to strips. The key extension making it possible to use this technique for problems with nonuniform temperature distributions will now be presented.

Suhir's solution is for finite strips with a uniform temperature increase. The concept of an interfacial shear compliance coefficient is critical because it allows the shear force, $Q(x)$, to be defined by an ordinary differential equation, allowing the enforcement of zero normal stress (σ_{xx}) on the ends of the strip. While it does not appear necessary to modify Suhir's technique for the problem at hand, it is important to defend the use of the same

interfacial shear compliance coefficient. The interfacial shear compliance coefficient, κ, was shown above to apply to a finite bimaterial strip with a temperature distribution symmetric about the midlength of the strip. The problem of interest in the current study concerns a semi-infinite beam with a decaying temperature distribution. It is therefore appropriate to consider whether κ applies in this case. If both $T_1(x)$ and $T_2(x)$ decay to zero as $x \to \infty$, there is some value of x, say x_∞, for which all stresses are negligible for $x > x_\infty$. Consider now the beam of length $(2\ x_\infty)$ shown in Figure 3.7. Suhir's value of κ is applicable to this beam because it is of finite length and the temperature distribution is symmetric about $x = 0$. There exists a midsection of this beam, indicated by hash marks in the figure, where the temperature is very small and all stresses are negligible. The length of the relatively stress-free region may be made as long as desired by choosing x_∞ to be sufficiently large. Cutting the long, symmetrically heated beam at $x = 0$ results in two end-heated long beams. Consider now a semi-infinite beam with the same temperature distribution as one of the finite beams produced by taking the hypothetical cut we have just described. If the temperature in the semi-infinite beam decays to zero sufficiently before $x = x_\infty$, the stresses in this beam from $x = 0$ to $x = x_\infty$ should be indistiguishable from those in the finite beam, for which Suhir's value of κ is applicable. We conclude, therefore, that Suhir's value of κ is applicable to the semi-infinite layered beam with a decaying temperature distribution.

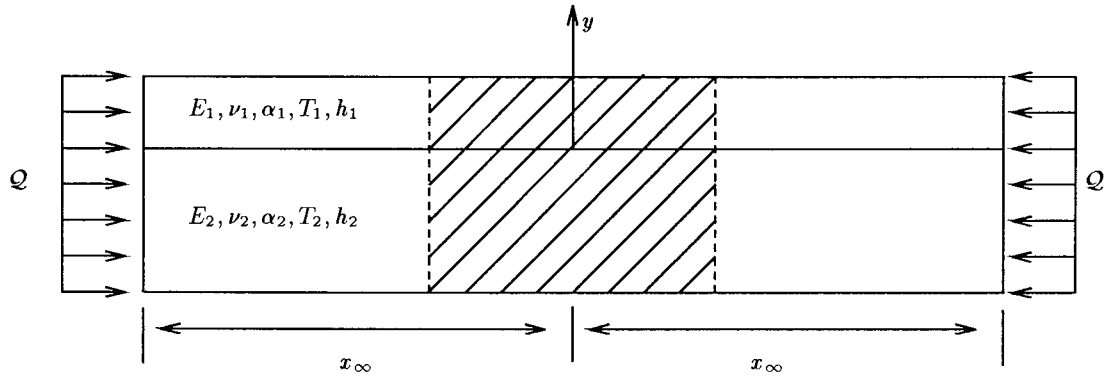

Figure 3.7 A Very Long Beam Heated Equally on Both Ends

3.4 Summary

An engineering solution to the problem of thermal stresses in semi-infinite (or very long) layered beams with nonuniform temperature distributions has been proposed. The solution is based on the technique developed by Suhir (32) for a finite bimetallic thermostat with a uniform temperature increase, but required extensions in order to address the problem of interest. It was shown that the concept of interfacial compliance proposed by Suhir for a bimaterial strip subjected to a uniform change in temperature could be applied to a semi-infinite layered beam subjected to an arbitrary change in temperature. The only restriction placed on the temperature distribution is that it must decay to zero at infinity. The expanded solution will now be used to determine the thermal stresses in a generic layered beam with various nonuniform temperature distributions.

IV. Thermal Stresses in End-Heated Bimaterial Beams

Without specifying a particular temperature distribution, an elementary bimetallic thermostat solution was extended in Chapter III to apply to problems in very long layered beams with arbitrary temperature distributions. The bimetallic thermostat solution was published for strips of finite length with a uniform temperature distribution. The interfacial compliance coefficient, κ, used in the baseline solution, was known to apply only to finite strips loaded symmetrically on one face (see Figure 3.4). The applicability of the same interfacial compliance coefficient was extended for semi-infinte layered strips and beams, provided the temperature decays to zero at infinity. The generic solution to the problem was found to be

$$Q(x) = C_1 e^{kx} + C_2 e^{-kx} + Q_p(x) \tag{4.1}$$

$$q(x) = Q'(x) \tag{4.2}$$

$$p(x) = \varphi Q''(x) \tag{4.3}$$

$$\sigma_{x1} = -Q(x)\left\{\frac{1}{h_1} + \frac{hE_1(h_1/2 - y)}{2(E_1I_1 + E_2I_2)}\right\} \tag{4.4}$$

$$\sigma_{x2} = Q(x)\left\{\frac{1}{h_2} + \frac{hE_2(h_2/2 + y)}{2(E_1I_1 + E_2I_2)}\right\} \tag{4.5}$$

$$P_0 = \lim_{x\to\infty} \frac{C_1}{k} e^{kx} + \frac{1}{k}(C_2 - C_1) + \int_0^\infty Q_p(\xi)\, d\xi \tag{4.6}$$

$$C_1 = -\lim_{x\to\infty} \left[Q_p(x)e^{-kx}\right] \tag{4.7}$$

$$C_2 = -Q_p(0) + \lim_{x\to\infty} \left[Q_p(x)e^{-kx}\right] \tag{4.8}$$

where k is given by equation 3.31 and $Q_p(x)$ is a particular solution to

$$Q_p''(x) - k^2 Q_p(x) = \frac{\alpha_2}{\kappa} T_2(x) - \frac{\alpha_1}{\kappa} T_1(x) \tag{4.9}$$

In order for this solution to be valid, the only restriction on $Q_p(x)$ is that

$$-\lim_{x\to\infty} [-Q_p(0)e^{-kx} + Q_p(x)e^{-2kx}] = 0 \tag{4.10}$$

Equation 4.10 shows that a closed form solution to the problem exists for any function $Q_p(x)$ that is bounded at $x = 0$ and grows exponentially at a rate less than e^{2kx}. This implies that the solution is applicable to a layered beam where the temperature increases with x (see the right hand side of equation 4.9). However, the constant, k^2, has in its denominator the interfacial compliance coefficient, κ, which was shown in Chapter III to be applicable to a semi-infinite beam with nonuniform temperature only when the temperature decays to zero at infinity. Also, equation 4.6 shows that the concentrated corner force, P_0, becomes infinite unless $Q_p(x)$ decays to zero at infinity. For these reasons the above solution is deemed to be suitable only for problems in which the temperature decays to zero at infinity.

Before turning to the problem of interest, i. e. stresses due do the temperature in an end-heated semi-infinite layered beam (the insulated rod solution), let us first consider a less complicated decaying temperature distribution. In order to assess the feasibility of our solution technique, it is not necessary for the temperature distribution to be the solution to any heat transfer problem. The only requirement levied on the temperature thus far is that it decays to zero at infinity. One of the simplest types of temperature distributions meeting this requirement is an exponentially decaying distribution. It offers the additional benefit that particular solutions to ordinary differential equations with exponential forcing functions are easily obtained. Therefore, let us first consider the problem where both layers of a bimaterial beam are subjected to exponentially decaying temperature distributions.

4.1 A Semi-Infinite Beam with Constant End Temperature

Let $T_1(x) = T_{01}e^{-\eta_1 x}$ and $T_2(x) = T_{02}e^{-\eta_2 x}$, where η_1 and η_2 are strictly positive and $\eta_1 \neq \eta_2$. The general solution for this problem is found to be

$$\hat{Q}(x) = -1/(1-\delta_1^2)\left[e^{-kx} - e^{-\delta_1 kx}\right] + \hat{A}/(1-\delta_2^2)\left[e^{-kx} - e^{-\delta_2 kx}\right] \quad (4.11)$$

$$\hat{q}(x) = -1/(1-\delta_1^2)\left[\delta_1 e^{-\delta_1 kx} - e^{-kx}\right] + \hat{A}/(1-\delta_2^2)\left[\delta_2 e^{-\delta_2 kx} - e^{-kx}\right] \quad (4.12)$$

$$\hat{p}(x) = -1/(1-\delta_1^2)\left[e^{-kx} - \delta_1^2 e^{-\delta_1 kx}\right] + \hat{A}/(1-\delta_2^2)\left[e^{-kx} - \delta_2^2 e^{-\delta_2 kx}\right] \quad (4.13)$$

$$\hat{\sigma}_{x1} = -\left\{\hat{h}(1+\hat{E}\hat{h}^3) + 3\hat{h}(1+\hat{h}) - 6\hat{h}(1+\hat{h})\frac{y}{h_1}\right\}\hat{Q}(x) \quad (4.14)$$

$$\hat{\sigma}_{x2} = \left\{1 + 3\hat{E}\hat{h}^2(1+\hat{h}) + 6\hat{E}\hat{h}^2(1+\hat{h})\frac{y}{h_2}\right\}\hat{Q}(x) \tag{4.15}$$

$$\hat{P}_0 = \frac{-(1+\delta_2) + \hat{A}(1+\delta_1)}{(1+\delta_1)(1+\delta_2)} \tag{4.16}$$

where

$$\hat{Q}(x) = k^2 Q(x)/A_1 \qquad \hat{q}(x) = kq(x)/A_1$$
$$\hat{p}(x) = p(x)/(\varphi A_1) \qquad \hat{\sigma}_{x1} = h_2 k^2(1 + \hat{E}\hat{h}^3)\sigma_{x1}/A_1$$
$$\hat{\sigma}_{x2} = h_2 k^2(1 + \hat{E}\hat{h}^3)\sigma_{x2}/A_1 \qquad \hat{P}_0 = k\int_0^\infty \hat{p}(\xi)\,d\xi$$

and

$$A_1 = \alpha_1 T_{01}/\kappa \qquad A_2 = \alpha_2 T_{02}/\kappa$$
$$\delta_1 = \eta_1/k \qquad \delta_2 = \eta_2/k$$
$$\hat{E} = E_2/E_1 \qquad \hat{h} = h_2/h_1$$
$$\hat{A} = A_2/A_1 \qquad \kappa = 2h_1/(3E_1(1-\nu_1)) + 2h_2/(3E_2(1-\nu_2))$$

In deriving equations 4.14 and 4.15, the moments of inertia were taken to be those of rectangular cross-sections of unit width. Note that $\hat{A} = 0$ corresponds to the case when strip 1 is heated while strip 2 remains at zero temperature. When this is the case, the maximum values of $\hat{Q}, \hat{q}$ and $\hat{p}$ are found in closed form to be

$$\hat{Q}_{\max} = \begin{cases} \delta_1^{\delta_1/(1-\delta_1)}/(1+\delta_1) \;@\; kx = \ln\delta_1/(\delta_1 - 1), & \text{if } \delta_1 \neq 1 \\ 1/(2e) \qquad\qquad @\; kx = 1, & \text{if } \delta_1 = 1 \end{cases} \tag{4.17}$$

$$\hat{q}_{\max} = \begin{cases} 1/(1+\delta_1) \qquad @\; x = 0, & \text{if } \delta_1 \neq 1 \\ 1/2 \qquad\qquad @\; x = 0, & \text{if } \delta_1 = 1 \end{cases} \tag{4.18}$$

$$\hat{p}_{\max} = -1, \qquad @\; x = 0 \tag{4.19}$$

Equations 4.11, 4.12 and 4.13 are plotted in Figures 4.1 through 4.3 for various values of the parameters, $\hat{A}, \delta_1$ and δ_2. Equations 4.14 and 4.15 are plotted in Figure 4.4 for various values of $\hat{E}$ and $\hat{h}$.

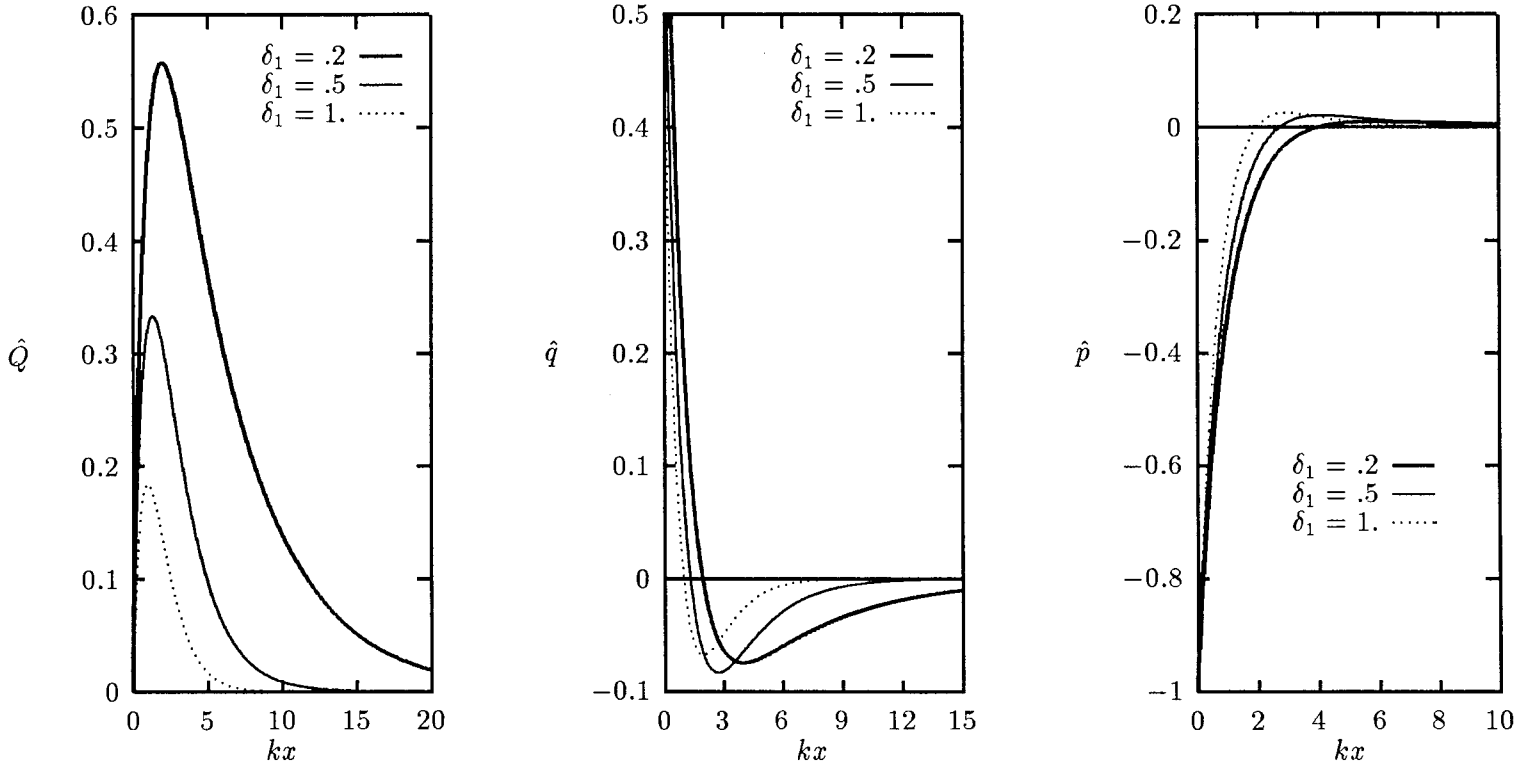

(a) Resultant Interlaminar Shearing Force

(b) Interlaminar Shearing Stress

(c) Interlaminar Normal Stresses

Figure 4.1 Nondimensional force and stresses, equations 4.11-4.13, with $T_1 = T_{01}e^{-\delta_1 kx}$ and $T_2 = 0$. Plotted for various values of δ_1, the temperature decay rate in strip 1.

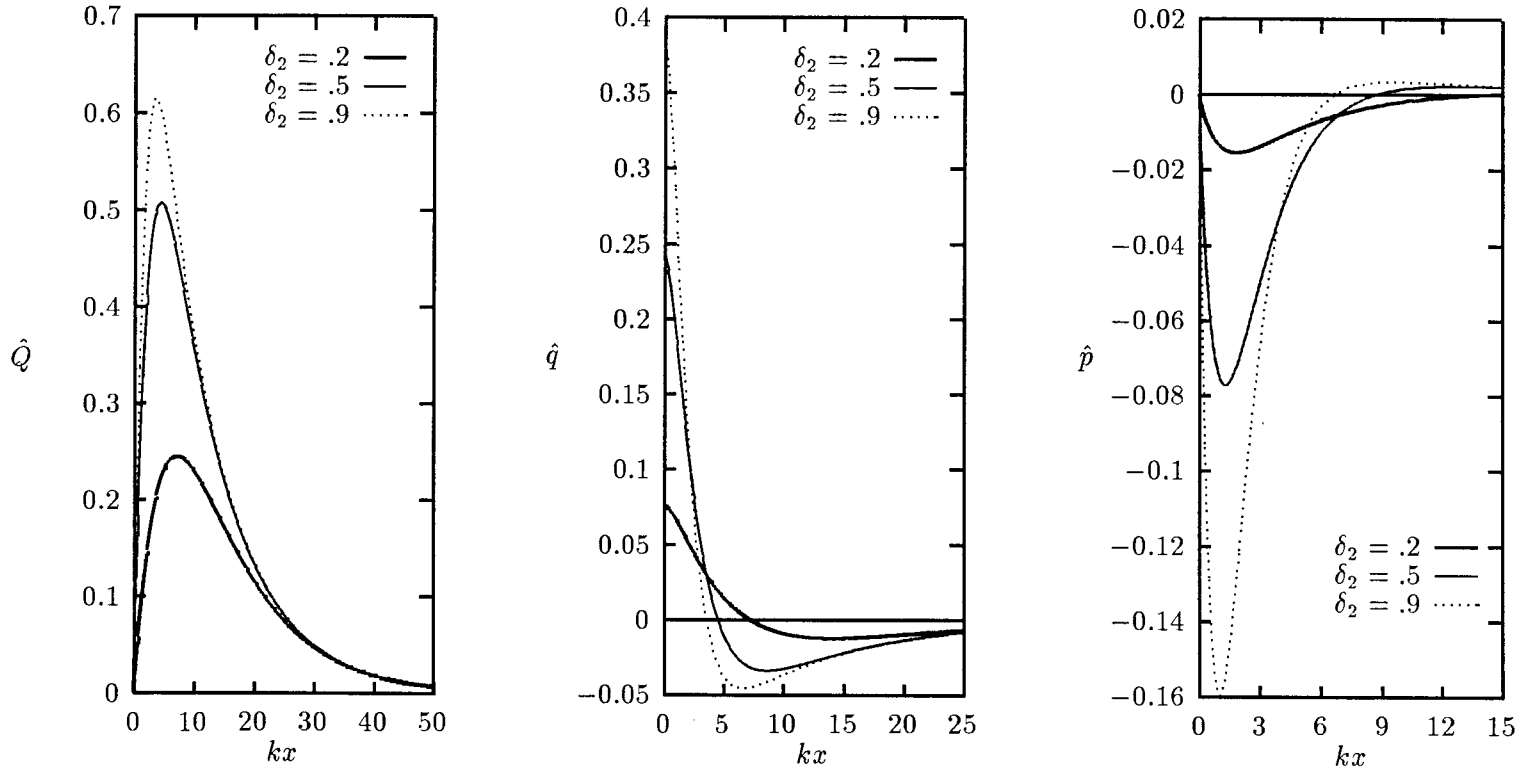

(a) Resultant Interlaminar Shearing Force

(b) Interlaminar Shearing Stress

(c) Interlaminar Normal Stresses

Figure 4.2 Nondimensional force and stresses, equations 4.11-4.13, with $T_1 = T_{01}e^{-\delta_1 kx}$, $T_2 = T_{02}e^{-\delta_2 kx}$. Plotted for $\hat{A} = 1, \delta_1 = .1$, and various values of δ_2, the temperature decay rate in strip 2. Note that $\hat{A} = 1$ implies that the two materials have the same αT at $x = 0$.

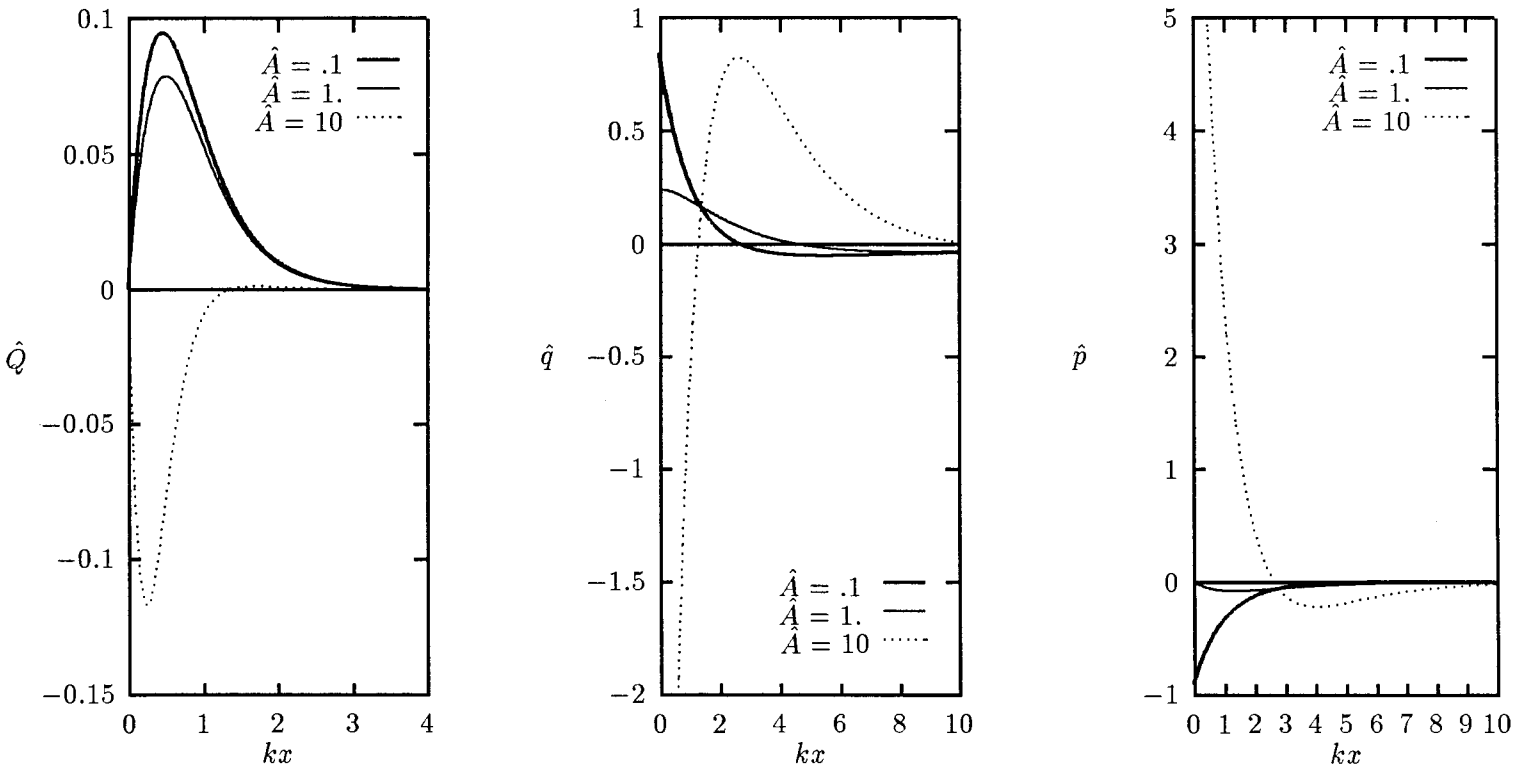

(a) Resultant Interlaminar Shearing Force

(b) Interlaminar Shearing Stress

(c) Interlaminar Normal Stresses

Figure 4.3 Nondimensional force and stresses, equations 4.11-4.13, with $T_1 = T_{01}e^{-\delta_1 kx}$, $T_2 = T_{02}e^{-\delta_2 kx}$. Plotted for various values of $\hat{A}$ with $\delta_1 = .1, \delta_2 = .5$.

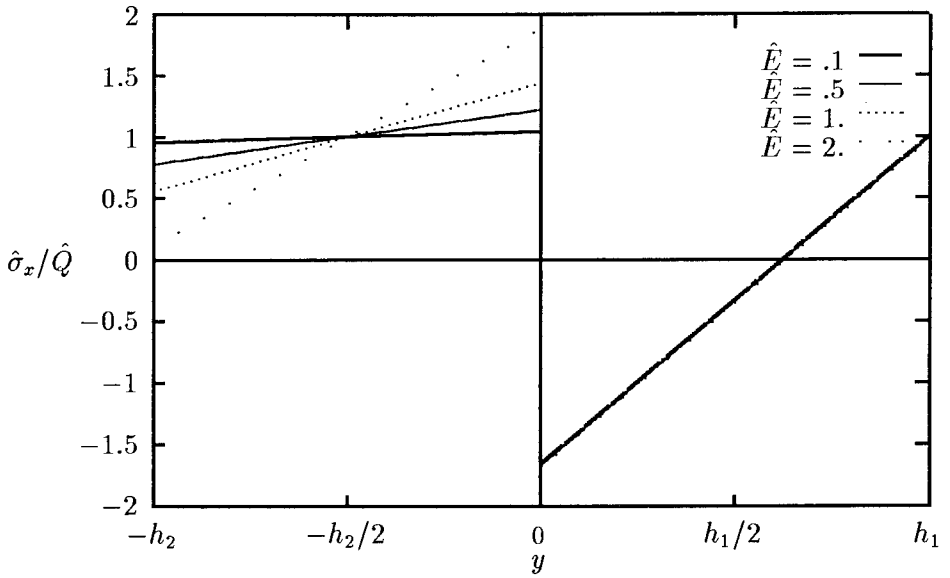

(a) Material with $\hat{h} = 1/3$

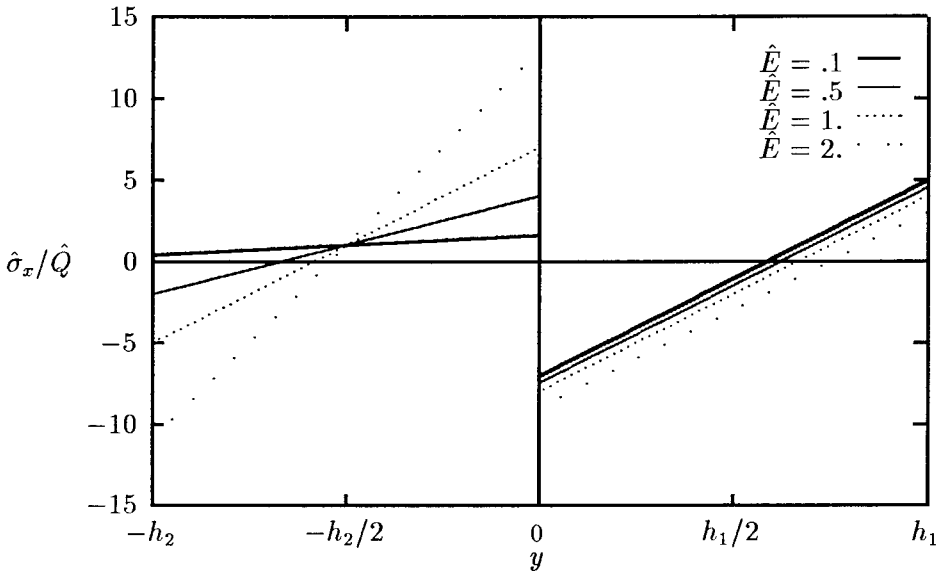

(b) Material with $\hat{h} = 1$

Figure 4.4 Nondimensional axial stress, equations 4.14 and 4.15, normalized to the resultant shearing force. Plotted through the thickness for various values of $\hat{E}$.

Figure 4.1 shows that, when one strip is heated and the other remains at constant temperature,[1] the resultant force due to interlaminar shear stress decreases as the temperature decay rate decreases. This is an indication of the fact that force is proportional to the total energy deposited in the strip. If the front surface temperature remains constant, the energy deposited in the strip decreases as the temperature decay rate in the strip increases. It may be shown from equation 4.17 that the interlaminar resultant force vanishes as the temperature decay rate goes to infinity. A decay rate of infinity corresponds to a constant temperature on the boundary[2] and zero temperature elsewhere. The interesting thing about this solution is that, while resultant force and interlaminar shear stress both approach zero, the interlaminar normal stress on the boundary approaches a definite limit as the decay rate goes to infinity. In fact, the nondimensional value of the limit is -1. With such a temperature distribution, the problem is essentially that of two rods, only one of which is heated. If the heated rod is allowed to freely expand and then is forced to assume its original position, a compressive nondimensional stress of magnitude -1 results. These results are encouraging and consistent with Timoshenko's solution. Figure 4.1 also shows that the slope of the stresses is steeper at higher temperature decay rates, a phenomenon which is certainly to be expected since stress is known to be proportional to the thermal gradient. A surprising result is that the interlaminar normal stress at the boundary is independent of temperature decay rate, as shown in Figure 4.1(c) and by Equation 4.19.

When both strips are heated, generalizing the results becomes more complicated, as illustrated in Figures 4.2 through 4.3. With all other parameters held constant, it appears from Figure 4.2 that a significant effect of increasing δ_2, the temperature decay rate in strip 2, is to increase the peak values of the interlaminar shearing force and both interlaminar stresses. Also, for the shearing force and peeling stress, the location of the peak values appears to approach the surface as δ_2 increases. Similar results would be obtained if δ_2 was held constant and δ_1 was varied. In either case, these effects are due to the fact that, as the temperature decay rate increases, the length over which the temperature must decrease to

[1]When only one of the strips is heated, $\hat{A} = 0$, and the results are nondimensionalized such that the independent coordinate is the nondimensional distance, kx, and the only parameter is the temperature decay rate of the heated strip.

[2]Boundary refers to the free edge at $x = 0$, while interface refers to the plane, $y = 0$.

zero becomes shorter, producing higher gradients in this region. The higher gradients, in turn, cause higher stresses. Figure 4.2 portrays an interesting phenomenon–namely, that the the peeling stress is zero at the corner point. This is apparently true for all values of δ_2. In fact, if $\hat{A} = 1$, we see from equation 4.13 that the corner peeling stress is zero for all values of both δ_1 and δ_2. When $\hat{A} = 1$ the product of front surface temperature and the thermal expansion coefficient is the same for the two materials. There is therefore no gradient in the interlaminar shear stress at that point, and this leads to a zero value of corner peeling stress. The peeling stress does, however, achieve its maximum value very near the free surface.

Figure 4.3 reflects an interesting feature when $\hat{A}$ changes from one to ten. Specifically, the shearing force and both interlaminar stresses experience a sign change in the region nearest the free surface. As shown in Figure 4.3(c), such a sign change may not occur throughout the beam, since the relative magnitudes of δ_1 and δ_2 determine the sign if $x \neq 0$. However, very close to the free edge, a sign change occurs and the physical reason for it is that the curvature of a bimaterial beam with $\alpha_1 T_{01} < \alpha_2 T_{02}$ must be opposite that of the same beam with $\alpha_1 T_{01} > \alpha_2 T_{02}$. Setting $x = 0$ in equation 4.12, we find the corner shearing stress changes signs at the following value of $\hat{A}$.

$$\hat{A}_0 = \frac{1 + \delta_2}{1 + \delta_1} \tag{4.20}$$

Now, $\hat{A}_0 = 1$ if and only if the temperature decay rates of both materials are identical. Equation 4.13 shows that the corner peeling stress changes sign for $\hat{A} = 1$ for all values of δ_1 and δ_2. This is significant since it implies that the corner peeling stress is compressive for $\hat{A} < 1$ and tensile for $\hat{A} > 1$, for the particular parameters used to generate Figure 4.3(c). Sufficiently large tensile peeling stresses could cause delamination to begin at the corner.

The concentrated corner force, $\hat{P}_0$, is given by equation 4.16 and is seen to depend on $\hat{A}$ and the two temperature decay rates, δ_1 and δ_2. Like the corner shear stress, it too experiences a sign change at $\hat{A} = \hat{A}_0$. As a matter of interest, the magnitude of P_0 is an indication of the strength of the apparent singularity at the corner.

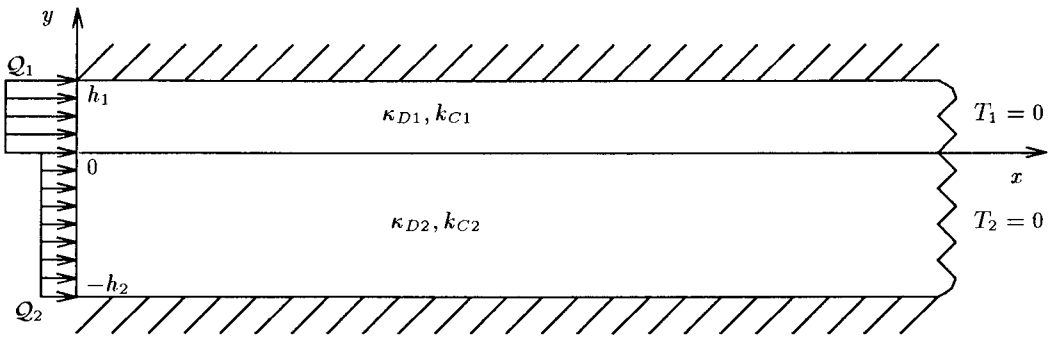

Figure 4.5 Flux Heated Bimaterial Semi-Infinite Beam

The magnitude of the peak values also increases significantly for the particular solutions depicted in Figure 4.3. The amount by which the magnitude of peak values changes is determined by the magnitude of $\hat{A}$. The plots are for a significant change in $\hat{A}$ and they show a significant change in stresses.

The results of the simple example problem are encouraging. A closed form solution was easily obtained for a layered beam with a nonuniform, decaying temperature distribution. While this success lends credence to the solution technique, the simple exponentially decaying temperature distribution is only qualitatively similar to the temperature in a semi-infinite medium subjected to uniform heat flux on the surface. We now attempt to solve the problem when the temperatures are more representative of what they would be in such a scenario.

4.2 A Semi-Infinite Beam with Constant End Flux

Consider a semi-infinite bimaterial beam, initially at zero temperature everywhere, which is subjected at time zero to the thermal boundary conditions depicted in Figure 4.5. The hash marks in the figure indicate insulated boundaries. Note that the interface is assumed to be an insulating layer, which causes T_1 and T_2 to be functions of x and t only, where t is time. The temperature distribution in this beam is given by the well-known

insulated rod solution:

$$T_1(x,t) = \frac{\mathcal{Q}_1 b}{k_{C1}}\left\{\frac{1}{\sqrt{\pi}}e^{-\hat{x}^2} - \hat{x}(1-\operatorname{erf}\hat{x})\right\} \tag{4.21}$$

$$T_2(x,t) = \frac{\mathcal{Q}_2 b\hat{b}}{k_{C2}}\left\{\frac{1}{\sqrt{\pi}}e^{-\tilde{x}^2} - \tilde{x}(1-\operatorname{erf}\tilde{x})\right\} \tag{4.22}$$

where

$$\hat{x} = \frac{x}{b}, \qquad \tilde{x} = \frac{\hat{x}}{\hat{b}}, \qquad b = 2\sqrt{\kappa_{D1}t}, \qquad \hat{b} = \sqrt{\frac{\kappa_{D2}}{\kappa_{D1}}}$$

$$\operatorname{erf} x = \frac{2}{\sqrt{\pi}}\int_0^x e^{-\eta^2}\,d\eta$$

and k_{Ci} and κ_{Di} are the thermal conductivity and thermal diffusivity, respectively, of the i^{th} layer. Note that b is the thermal diffusion length of layer 1 and that $\hat{b}$ is the ratio of the layer thermal diffusion lengths. Substituting equations 4.21 and 4.22 into equation 3.30, we obtain

$$\begin{aligned} Q''(x) - k^2 Q(x) &= \hat{b}bkA_2\left\{\frac{1}{\sqrt{\pi}}e^{-\tilde{x}^2} - \tilde{x}(1-\operatorname{erf}\tilde{x})\right\} - \\ &\quad bkA_1\left\{\frac{1}{\sqrt{\pi}}e^{-\hat{x}^2} - \hat{x}(1-\operatorname{erf}\hat{x})\right\} \end{aligned} \tag{4.23}$$

where $A_1 = \alpha_1\mathcal{Q}_1/(\kappa k_{C1}k)$ and $A_2 = \alpha_2\mathcal{Q}_2/(\kappa k_{C2}k)$. After applying the method of variation of parameters to this equation and enforcing the boundary conditions, the general solution to the problem is found to be:

$$\begin{aligned} \hat{Q}(\hat{x},\tilde{x}) &= \frac{1}{4}e^{2\phi\hat{x}}\left\{e^{\phi^2}\left[1-\operatorname{erf}(\hat{x}+\phi)\right] - \hat{A}e^{\hat{b}^2\phi^2}\left[1-\operatorname{erf}(\tilde{x}+\hat{b}\phi)\right]\right\} + \\ &\quad \frac{1}{4}e^{-2\phi\hat{x}}\left\{\begin{array}{l} 2\left[\operatorname{erf}\phi\, e^{\phi^2} - \hat{A}\operatorname{erf}\hat{b}\phi\, e^{\hat{b}^2\phi^2}\right] - e^{\phi^2}\left[1-\operatorname{erf}(\hat{x}-\phi)\right] + \\ \hat{A}e^{\hat{b}^2\phi^2}\left[1-\operatorname{erf}(\tilde{x}-\hat{b}\phi)\right] - 4\phi/\sqrt{\pi}\left(1-\hat{A}\hat{b}\right) \end{array}\right\} + \\ &\quad \phi\left\{\frac{1}{\sqrt{\pi}}\left[e^{-\hat{x}^2} - \hat{A}\hat{b}e^{-\tilde{x}^2}\right] - \left[\hat{x}(1-\operatorname{erf}\hat{x}) - \hat{A}\hat{b}\tilde{x}(1-\operatorname{erf}\tilde{x})\right]\right\} \\ \hat{q}(\hat{x},\tilde{x}) &= \frac{1}{4}e^{2\phi\hat{x}}\left\{e^{\phi^2}\left[1-\operatorname{erf}(\hat{x}+\phi)\right] - \hat{A}e^{\hat{b}^2\phi^2}\left[1-\operatorname{erf}(\tilde{x}+\hat{b}\phi)\right]\right\} - \\ &\quad \frac{1}{4}e^{-2\phi\hat{x}}\left\{\begin{array}{l} 2\left[\operatorname{erf}\phi\, e^{\phi^2} - \hat{A}\operatorname{erf}\hat{b}\phi\, e^{\hat{b}^2\phi^2}\right] - e^{\phi^2}\left[1-\operatorname{erf}(\hat{x}-\phi)\right] + \\ \hat{A}e^{\hat{b}^2\phi^2}\left[1-\operatorname{erf}(\tilde{x}-\hat{b}\phi)\right] - 4\phi/\sqrt{\pi}\left(1-\hat{A}\hat{b}\right) \end{array}\right\} - \end{aligned} \tag{4.24}$$

$$\frac{1}{2}\left[1-\operatorname{erf}\hat{x}-\hat{A}(1-\operatorname{erf}\tilde{x})\right] \tag{4.25}$$

$$\hat{p}(\hat{x},\tilde{x}) = \frac{1}{4}e^{2\phi\hat{x}}\left\{e^{\phi^2}\left[1-\operatorname{erf}(\hat{x}+\phi)\right]-\hat{A}e^{\hat{b}^2\phi^2}\left[1-\operatorname{erf}(\tilde{x}+\hat{b}\phi)\right]\right\}+$$
$$\frac{1}{4}e^{-2\phi\hat{x}}\left\{\begin{array}{l} 2\left[\operatorname{erf}\phi\, e^{\phi^2}-\hat{A}\operatorname{erf}\hat{b}\phi\, e^{\hat{b}^2\phi^2}\right]-e^{\phi^2}\left[1-\operatorname{erf}(\hat{x}-\phi)\right]+ \\ \hat{A}e^{\hat{b}^2\phi^2}\left[1-\operatorname{erf}(\tilde{x}-\hat{b}\phi)\right]-4\phi/\sqrt{\pi}\left(1-\hat{A}\hat{b}\right)\end{array}\right\} \tag{4.26}$$

$$\hat{P}_0 = \frac{-\phi}{\sqrt{\pi}}\left(1-\hat{A}\hat{b}\right)+\frac{1}{2}\left\{1-e^{\phi^2}\operatorname{erfc}\phi-\hat{A}(1-e^{\hat{b}^2\phi^2}\operatorname{erfc}\hat{b}\phi)\right\} \tag{4.27}$$

where

$$\begin{aligned}\hat{Q}(\hat{x},\tilde{x}) &= k^2Q(x)/(2A_1)\\ \hat{q}(\hat{x},\tilde{x}) &= kq(x)(2A_1)\\ \hat{p}(\hat{x},\tilde{x}) &= p(x)/(2A_1\varphi)\\ \hat{P}_0 &= k\int_0^\infty \hat{p}(\xi)\,d\xi\\ \operatorname{erfc}x &= 1-\operatorname{erf}x\\ \phi &= bk/2 = k\sqrt{\kappa_{D1}t}\end{aligned} \tag{4.28}$$

Equations 4.24, 4.25 and 4.26 are plotted in Figures 4.6 through 4.8 for various values of the parameters, $\hat{A}, \hat{b}$ and ϕ. Also, since the maximum values of $\hat{q}$ and $\hat{p}$ occur at $\hat{x} = \tilde{x} = 0$,[3] they are of special interest and are found from the above equations to be

$$\hat{q}_0 = \frac{1}{2}\left\{e^{\phi^2}\operatorname{erfc}\phi-\hat{A}e^{\hat{b}^2\phi^2}\operatorname{erfc}\hat{b}\phi-\left(1-\hat{A}\right)\right\}+\frac{\phi}{\sqrt{\pi}}\left(1-\hat{A}\hat{b}\right) \tag{4.29}$$

$$\hat{p}_0 = \frac{-\phi}{\sqrt{\pi}}\left(1-\hat{A}\hat{b}\right) \tag{4.30}$$

where $\hat{q}_0 = \hat{q}(0)$ and $\hat{p}_0 = \hat{p}(0)$. The nondimensional parameter, ϕ, is directly proportional to the square root of time, as shown in Equation 4.28. We see from equations 4.29 and 4.30 that the corner stresses are initially zero and become infinite as time goes to infinity. The solution (Equations 4.24-4.26) shows the stresses everywhere—not just at the corner,

[3] See (32) for a discussion of the maximum stresses.

to vanish at time zero and become infinite as time goes to infinity. This observation is not true at $x = \infty$ where all temperatures and stresses are required to be zero.

The ratio of the axial stresses, $\hat{\sigma}_1$ and $\hat{\sigma}_2$, to $\hat{Q}$ is independent of the particular form of temperature distribution. Therefore, the time-dependent solution currently under consideration yields ratios identical to those shown previously in Figure 4.4.

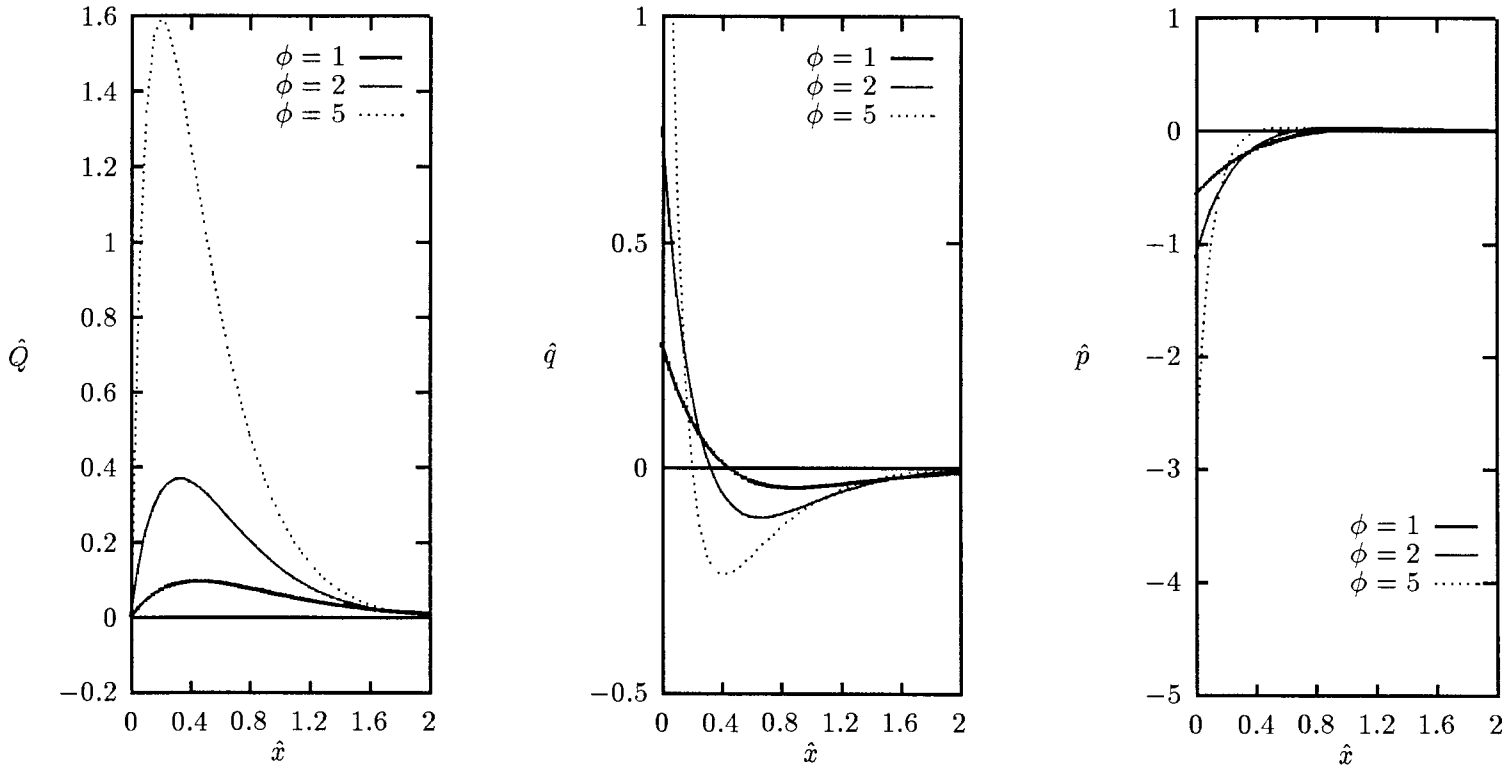

(a) Resultant Interlaminar Shearing Force

(b) Interlaminar Shearing Stress

(c) Interlaminar Normal Stresses

Figure 4.6 Nondimensional force and stresses, equations 4.24-4.26, with T_1 given by equation 4.21 and $T_2 = 0$. Plotted as a function of $\hat{x} = x/(2\sqrt{\kappa_{D1}t})$ for various values of the nondimensional time, $\phi = k\sqrt{\kappa_{D1}t}$.

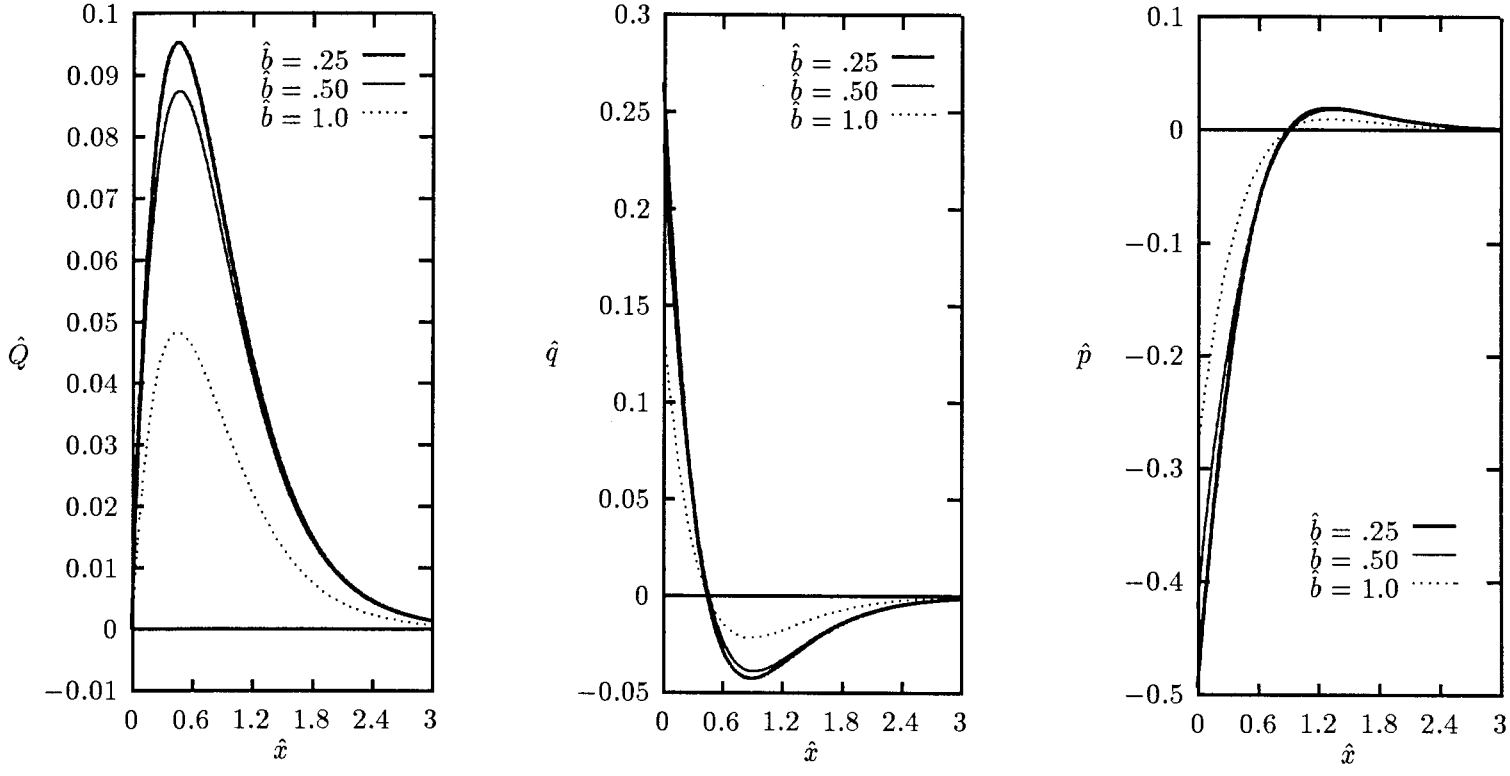

(a) Resultant Interlaminar Shearing Force

(b) Interlaminar Shearing Stress

(c) Interlaminar Normal Stresses

Figure 4.7 Nondimensional force and stresses, equations 4.24-4.26, with T_1 given by equation 4.21 and T_2 given by equation 4.22. Other constants are $\hat{A} = .5$ and $\phi = 1$. Plotted as a function of $\hat{x} = x/(2\sqrt{\kappa_{D1}t})$ for various values of the nondimensional ratio of thermal diffusivities, $\hat{b}$.

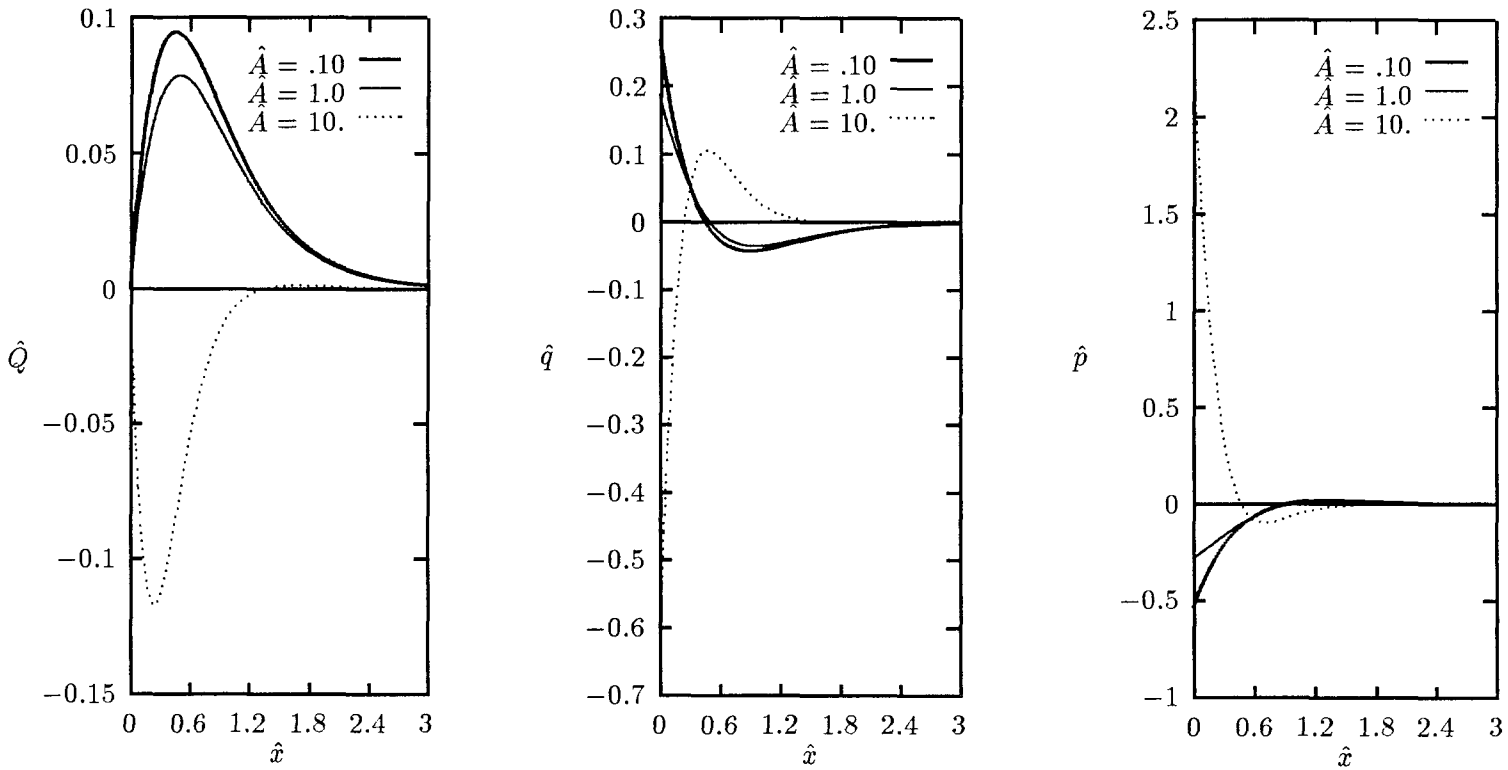

(a) Resultant Interlaminar Shearing Force

(b) Interlaminar Shearing Stress

(c) Interlaminar Normal Stresses

Figure 4.8 Nondimensional force and stresses, equations 4.24-4.26, with T_1 given by equation 4.21 and T_2 given by equation 4.22. Other constants are $\hat{b} = .5$ and $\phi = 1$. Plotted as a function of $\hat{x} = x/(2\sqrt{\kappa_{D1}t})$ for various values of the nondimensional parameter, $\hat{A}$.

The results for the temporal temperature distributions show trends similar to those discussed in Section 4.1. For example, Figure 4.6(a) shows that the peak resultant interlaminar shearing force, $\hat{Q}_{\max}$, increases as nondimensional time, ϕ, increases. The value of $\hat{x}$ at which this maximum occurs is the value of $\hat{x}$ where $\hat{q} = 0$. Let this value be denoted by $\hat{x}_M$ and let x_M be the dimensional distance represented by $\hat{x}_M$. Figure 4.6(b) shows that $\hat{x}_M$ decreases as ϕ increases. However, $\hat{x}$ is related to distance by the equation:

$$kx = 2\phi\hat{x} \tag{4.31}$$

Therefore, for the plots shown in Figure 4.6(b), kx_M increases as ϕ increases, implying that $\hat{Q}_{\max}$ occurs farther from the edge with increasing time. Similar trends in the interlaminar stresses are also apparent from the figure. These trends are to be expected because the temperature is proportional to the square root of time. Figure 4.8 indicates that the shearing force and both interlaminar stresses experience a sign change in the region nearest the free surface when $\hat{A}$ changes from one to ten. Interestingly, $\hat{A}_0$, the value of $\hat{A}$ at which the transition occurs, is time (ϕ) dependent for the corner shearing stress but independent of time for the corner peeling stress. Setting $\hat{q}(0) = 0$ in equation 4.25, we obtain

$$\hat{A}_0 = \frac{(2\phi/\sqrt{\pi})e^{\phi^2}\operatorname{erfc}\phi - 1}{(2\hat{b}\phi/\sqrt{\pi})e^{\hat{b}^2\phi^2}\operatorname{erfc}\hat{b}\phi - 1} \tag{4.32}$$

This equation shows that $\hat{A}_0 = 1$ for all time if and only if both materials have the same thermal diffusivity (i. e. $\hat{b} = 1$). Equation 4.30 shows that the corner interlaminar normal stress experiences the sign change at $\hat{A}_0 = 1/\hat{b}$ for all values of time. This is significant since it implies that the corner peeling stress is compressive for $\hat{A} < \hat{A}_0$ and tensile for $\hat{A} > \hat{A}_0$. Sufficiently large tensile peeling stresses could cause delamination to begin at the corner.

Although the temperature distribution addressed in Section 4.1 was not obtained from a heat transfer problem, it still represents a fundamental class of steady-state problems in which temperature falls from a constant value on one end of a long beam to zero on the other end. The solution in Section 4.2 represents a class of time-dependent problems

in which the heat flux (or dT/dx) is held constant on one end of a long beam while the temperature is kept at zero on the other end. Let us refer to these solutions as the fixed T and fixed T' solutions, respectively. The primary difference between these solutions is that the total energy transported into the fixed T system is constant whereas the energy transported into the fixed T' system increases linearly with time. In fact, it becomes infinite as time goes to infinity. Due to the principle of conservation of energy, the strain energy (and therefore, the stresses and strains) of the fixed T' solution exceed those of the fixed T solution at some point in time, and ultimately become infinite.

There are some similarities in the stress distributions resulting from the different temperature profiles. In the following comparisons it is helpful to recall that

$$T_1(x) = T_{01}e^{-\delta_1 kx} \tag{4.33}$$

$$T_2(x) = T_{02}e^{-\delta_2 kx} \tag{4.34}$$

for the fixed T problem and that kx of the fixed T problem is related to $\hat{x}$ of the fixed T' problem by equation 4.31. Comparing Figures 4.1(a) and 4.6(a), we see that $\hat{Q}$ (and therefore σ_x) has relatively large magnitude farther away from the edge when δ_1 decreases, and that the same trend exists in the time-dependent solution as time (or ϕ) increases. In a time-dependent fixed T problem, the temperature at a particular time can be approximated by an exponentially-decaying function. As time increases the decay rate in the approximate temperature decreases. Comparing Figures 4.1(b) and 4.1(c) with Figures 4.6(b) and 4.6(c), we see that the interlaminar stresses display the same similarity as $\hat{Q}$. Figure 4.2 shows the effect of varying δ_2 while holding all other parameters constant. Figure 4.7 shows the effect of varying $\hat{b}$ (κ_{D2}) while holding all other parameters constant. A comparison of these figures shows that all fixed T stresses increase as δ_2 increases while the fixed T' stresses increase as $\hat{b}$ decreases. When δ_2 is relatively large the temperature in layer 2 falls from its fixed boundary value to zero over a relatively short distance. This is the same type of behavior exemplified by a material with relatively low thermal diffusivity ($\hat{b}$). The thermal stresses are higher for problems where δ_2 is high (or $\hat{b}$ is low) due to the fact that the layerwise temperature difference is higher. Figures 4.3 and 4.8 show the effects

of varying $\hat{A}$ while holding all other parameters constant. A comparison of these figures reveals very similar behavior in both the fixed T and fixed T' solutions.

We have considered both fixed T and fixed T' problems for end-heated semi-infinite beams. However, in problems where heat flux is applied somewhere far from both ends of a very long beam, a more appropriate model might be an infinite beam with known flux at the origin, where the origin of coordinates is coincident with the center of the heated area. Fortunately the generic solution presented for semi-infinite beams is also applicable to infinite beams.

4.3 An Infinite Beam with Constant Flux at the Origin

Consider a layered beam of infinite length with a line source of constant heat flux applied along a line passing through the origin of coordinates and perpendicular to the longitudinal axis of the beam. If the temperature of such a beam is zero at infinity, the one-dimensional temperature distribution is given by the insulated rod solution and is symmetric about the origin:

$$T_1(x,t) = \frac{Q_1 b}{k_{C1}} \left\{ \frac{1}{\sqrt{\pi}} e^{-\hat{x}^2} - \mid \hat{x} \mid (1 - \text{erf} \mid \hat{x} \mid) \right\} \tag{4.35}$$

$$T_2(x,t) = \frac{Q_2 b \hat{b}}{k_{C2}} \left\{ \frac{1}{\sqrt{\pi}} e^{-\tilde{x}^2} - \mid \tilde{x} \mid (1 - \text{erf} \mid \tilde{x} \mid) \right\} \tag{4.36}$$

Due to the symmetry of the problem, the interlaminar shearing stress must be zero at the origin. The interlaminar shearing force, $Q(x)$, is governed by the same ordinary differential equation as in the semi-infinite problem:

$$Q''(x) - k^2 Q(x) = \frac{\alpha_2}{\kappa} T_2(x,t) - \frac{\alpha_1}{\kappa} T_1(x,t) \tag{4.37}$$

where

$$Q(x) = \int_{-\infty}^{x} q(\xi)\, d\xi \tag{4.38}$$

The general solution is the same as in the semi-infinite case, but the boundary conditions are different. Whereas before the boundary conditions were

$$Q(0) = \lim_{x \to \infty} Q(x) = 0 \tag{4.39}$$

the symmetry condition requires the following conditions for the infinite medium:

$$Q'(0) = \lim_{x \to \infty} Q(x) = 0 \tag{4.40}$$

The solution is found to be

$$\begin{aligned}
\hat{Q}(\hat{x},\tilde{x}) &= \frac{1}{4}e^{2\phi\hat{x}}\left\{e^{\phi^2}\operatorname{erfc}(\hat{x}+\phi) - \hat{A}e^{\hat{b}^2\phi^2}\operatorname{erfc}(\tilde{x}+\hat{b}\phi)\right\} + \\
&\quad \frac{1}{4}e^{-2\phi\hat{x}}\left\{e^{\phi^2}\operatorname{erfc}(\phi-\hat{x}) - \hat{A}e^{\hat{b}^2\phi^2}\operatorname{erfc}(\hat{b}\phi-\tilde{x}) + 2(\hat{A}-1)\right\} + \\
&\quad \phi\left\{\frac{1}{\sqrt{\pi}}\left[e^{-\hat{x}^2} - \hat{A}\hat{b}e^{-\tilde{x}^2}\right] - \left[\hat{x}(1-\operatorname{erf}\hat{x}) - \hat{A}\hat{b}\tilde{x}(1-\operatorname{erf}\tilde{x})\right]\right\} \qquad (4.41) \\
\hat{q}(\hat{x},\tilde{x}) &= \frac{1}{4}e^{2\phi\hat{x}}\left\{e^{\phi^2}\operatorname{erfc}(\hat{x}+\phi) - \hat{A}e^{\hat{b}^2\phi^2}\operatorname{erfc}(\tilde{x}+\hat{b}\phi)\right\} - \\
&\quad \frac{1}{4}e^{-2\phi\hat{x}}\left\{2(\hat{A}-1) + e^{\phi^2}\operatorname{erfc}(\phi-\hat{x}) - \hat{A}e^{\hat{b}^2\phi^2}\operatorname{erfc}(\hat{b}\phi-\tilde{x})\right\} - \\
&\quad \frac{1}{2}\left[\operatorname{erfc}\hat{x} - \hat{A}\operatorname{erfc}\tilde{x}\right] \qquad (4.42) \\
\hat{p}(\hat{x},\tilde{x}) &= \frac{1}{4}e^{2\phi\hat{x}}\left\{e^{\phi^2}\operatorname{erfc}(\hat{x}+\phi) - \hat{A}e^{\hat{b}^2\phi^2}\operatorname{erfc}(\tilde{x}+\hat{b}\phi)\right\} + \\
&\quad \frac{1}{4}e^{-2\phi\hat{x}}\left\{2(\hat{A}-1) + e^{\phi^2}\operatorname{erfc}(\phi-\hat{x}) - \hat{A}e^{\hat{b}^2\phi^2}\operatorname{erfc}(\hat{b}\phi-\tilde{x})\right\} \qquad (4.43)
\end{aligned}$$

There should be no concentrated corner force, P_0, in this problem because of symmetry and the fact that all stresses are zero at $x = \pm\infty$. This is easily confirmed by integrating equation 4.43 from $-\infty$ to ∞. The absence of the corner force is actually indicative of the fact that there is no corner in the infinite problem.

Equations 4.41 through 4.43 are plotted in Figure 4.9 for various values of the nondimensional time, ϕ, with $\hat{A} = 0$. The figures show that all forces and stresses increase with time and that the resultant force and interlaminar normal stress achieve their maximum values at the origin. The interlaminar shear stress undergoes a sign change at the origin

and its maximum slope occurs there as well. The figures imply and the equations confirm that these quantities become unbounded as time becomes infinite.

The figures indicate that material failure will occur at the origin at some time. This observation was confirmed experimentally by Camburn et. al. (43), who tested bimaterial beams made of a thin graphite epoxy layer laminated to a thick aluminum layer. In a typical experiment, a beam was loaded in uniform compression below the yield point of the graphite epoxy and the graphite epoxy side of the beam was subjected to laser irradiation at an intensity level below the ablation threshold. The graphite epoxy layer failed in compression at the center of the irradiated spot, which coincides with the origin in the present analysis. Failure stresses were much lower for the laser-heated beams than for baseline beams tested at room temperature.

It is interesting to compare the infinite and semi-infinite solutions. Figure 4.10 shows the two solutions for the largest possible layerwise temperature difference (i. e. $\hat{A} = 0.$) and for one specific value of the nondimensional time. The relative behavior of the two different solutions is independent of time. For example, the nondimensional resultant axial force, $\hat{Q}_\infty \gg \hat{Q}_{\infty/2}$ near $x = 0$, where the subscripts denote the solutions for the infinite and semi-infinite media. This is true for all values of time. Care must be taken when comparing these solutions, since all forces and stresses are nondimensionalized by a factor involving the heat flux, $\mathcal{Q}_1$, which must be below the material ablation threshold in order for the infinite model to apply and above the threshold for the semi-infinite model to apply. In typical problems, the two fluxes are likely to differ by about one order of magnitude. For example, in graphite epoxy laminates, thermal soak problems (infinite medium) are characterized by incident flux values in the tens of Watts per square centimeter, while ablation problems (semi-infinite medium) are characterized by flux values in the hundreds of Watts per square centimeter. Therefore, the dimensional values corresponding to the nondimensional values shown in Figure 4.10 differ by about an order of magnitude less than the nondimensional values shown in the figure.

The axial stresses are higher at the origin for the infinite beam than they are for the semi-infinite beam. This is due to the fact that the free thermal expansion of material at the origin of an end-heated semi-infinite beam is resisted by unheated material on only

one side of the heated end. The free expansion of the material at the origin of an infinite beam is resisted from unheated material on both sides of the heated area. Interestingly, Figure 4.10 shows the dimensional interlaminar stresses in the infinite beam to be small compared to those in the semi-infinite beam. This is because interlaminar stresses normally arise due to the presence of free edges, of which there are none in the infinite beam.

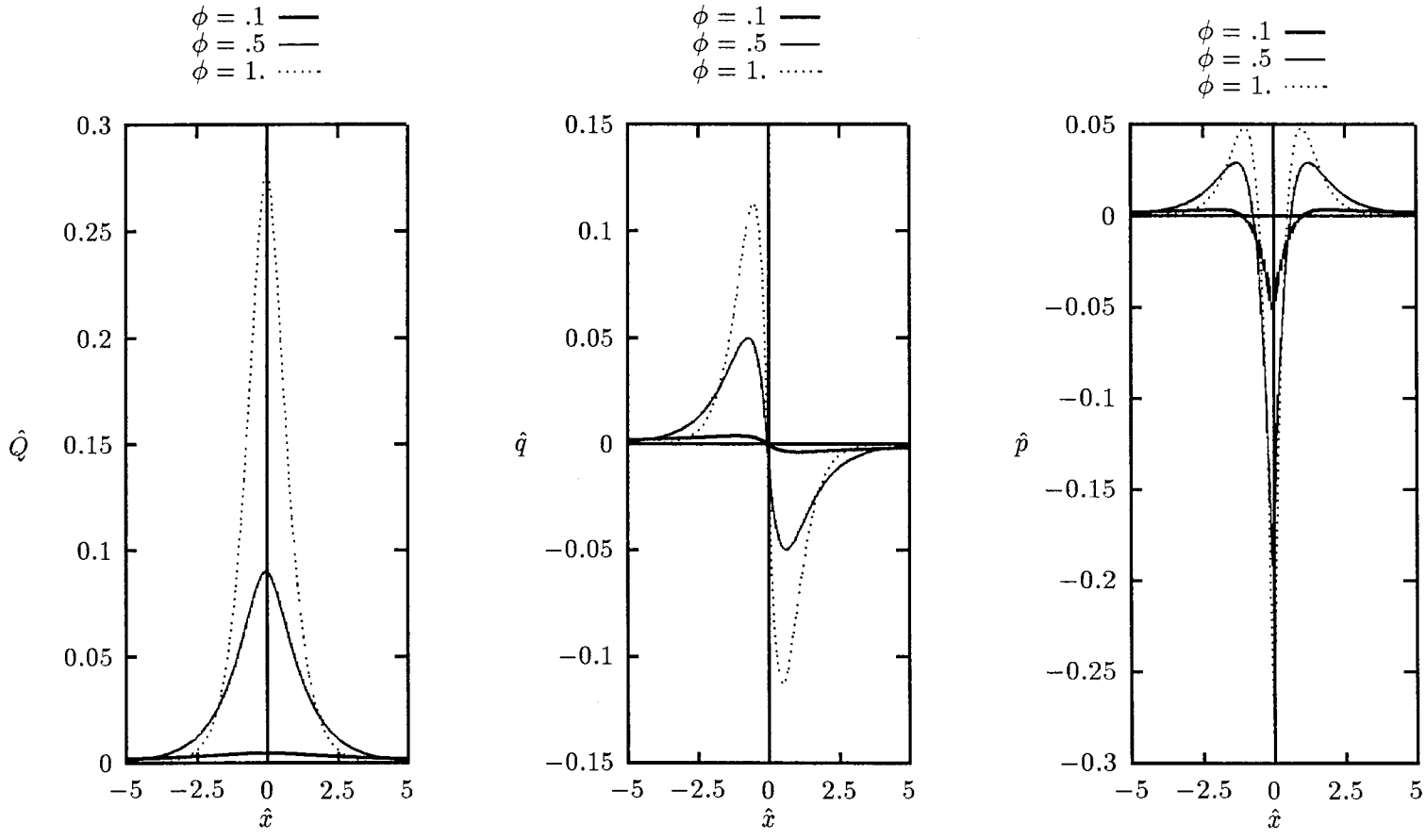

(a) Resultant Interlaminar Shearing Force

(b) Interlaminar Shearing Stress

(c) Interlaminar Normal Stresses

Figure 4.9 Nondimensional force and stresses, equations 4.41-4.43, with T_1 given by equation 4.21 and $T_2 = 0$. Plotted as a function of $\hat{x} = x/(2\sqrt{\kappa_{D1}t})$ for various values of the nondimensional time, $\phi = k\sqrt{\kappa_{D1}t}$.

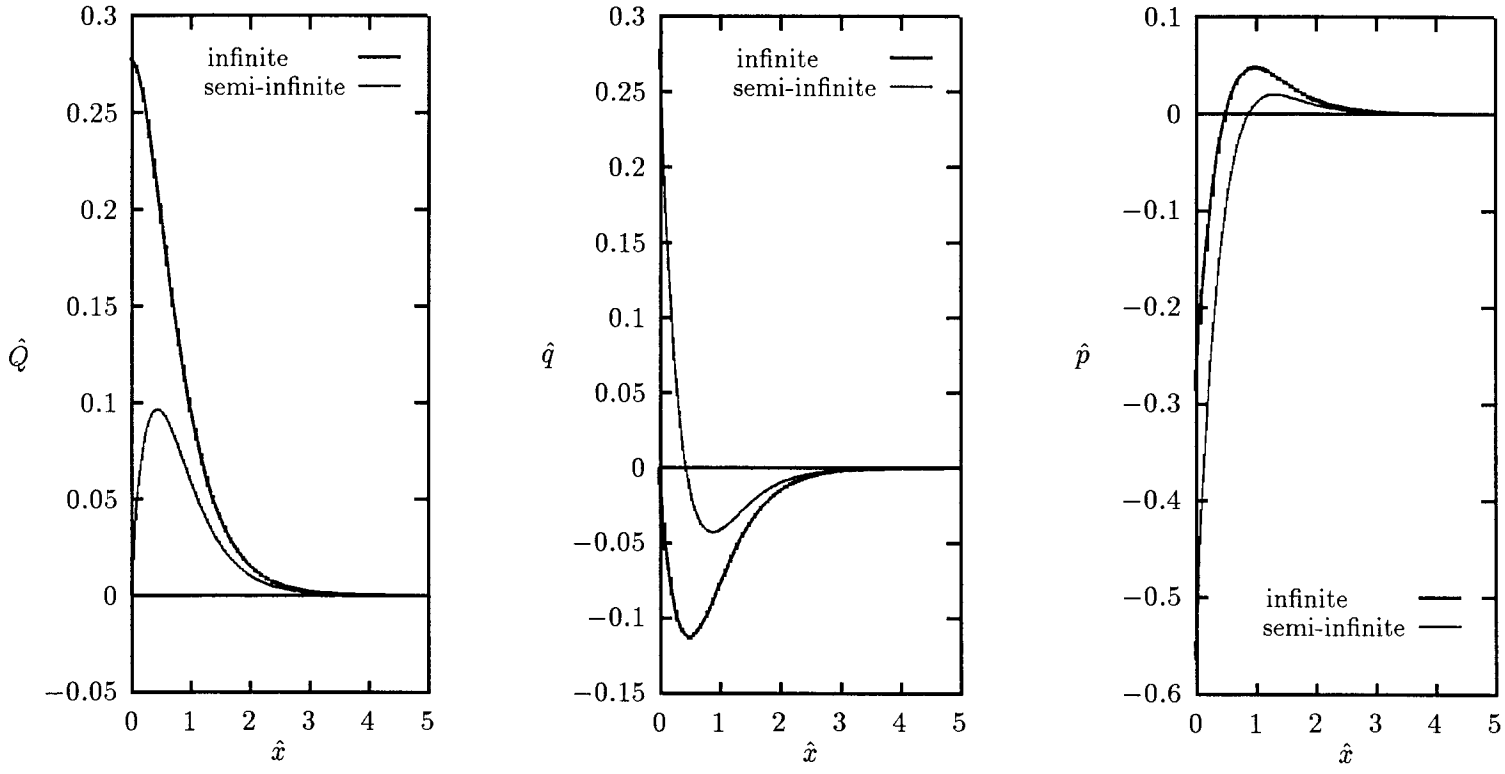

(a) Resultant Interlaminar Shearing Force

(b) Interlaminar Shearing Stress

(c) Interlaminar Normal Stresses

Figure 4.10 Comparison of the semi-infinite and infinite solutions. Nondimensional force and stresses, with T_1 given by equation 4.21 and $T_2 = 0$. Plotted as a function of $\hat{x} = x/(2\sqrt{\kappa_{D1} t})$ for nondimensional time, $\phi = 1$.

Let us consider a means by which the solutions given by equations 4.24-4.27 may be verified. As shown previously, Suhir's (32) solution is the foundation upon which the present solution is constructed. Therefore, it would be instructive to compare the two if possible. Suhir used his solution technique to analyze a molybdenum/aluminum bimetallic thermostat subjected to a temperature increase of $240°C$. (See Table 5.8 for a list of the material properties Suhir used.) Although Suhir's solution was presented for a bimetallic thermostat with uniform temperature increase, it is applicable to any finite-length bimetallic thermostat with a temperature variation symmetric about the midlength of the thermostat. For the purposes of our comparison, it is acceptable to consider a bimetallic beam with the temperature in one layer maintained at zero. Although this assumption is not physically probable, it has no bearing on the verification of equations 4.24-4.27, and it shortens the closed form solutions considerably because the parameter $\hat{A}$ is zero. It is noted, however, that this assumption prevents the verification of any terms in the solution which involve the parameter, $\hat{A}$.

Figure 4.11(a) shows the temperature in a semi-infinite molybdenum layer as a function of nondimensional distance and time. It is evident from the figure that $T_1 \approx 0$ for $\hat{x}$ greater than about 1.6 . Each of the temperature curves can be fitted very accurately using cubic polynomials. Equation 4.24 was used to determine the resultant interlaminar shearing force, $Q(x)$, due to the actual temperature distribution. Suhir's solution was then used to calculate $Q(x)$ due to the cubic approximations to the temperature distribution. Figure 4.11(b) shows the resulting force. Only one curve is shown for each time because the two solutions were indistinguishable.

Yet another verification of the solution may be obtained by comparing the fixed end temperature solution (equations 4.11-4.16) to the exact transient solution (equations 4.24-4.27) at discrete values of time. This is possible because, at a fixed point in time, the insulated rod temperature solution (equations 4.21 and 4.22) is approximated reasonably well by a simple exponentially decaying function. Figure 4.12 shows the results of such a comparison and indicates excellent agreement between the different solutions.

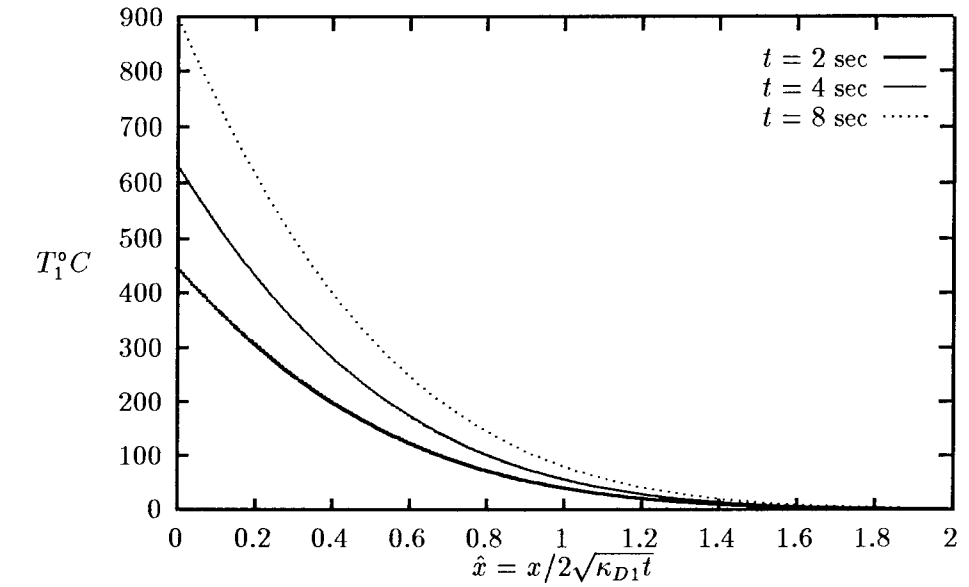

(a) Temperature in a semi-∞ end-heated Molybdenum beam.

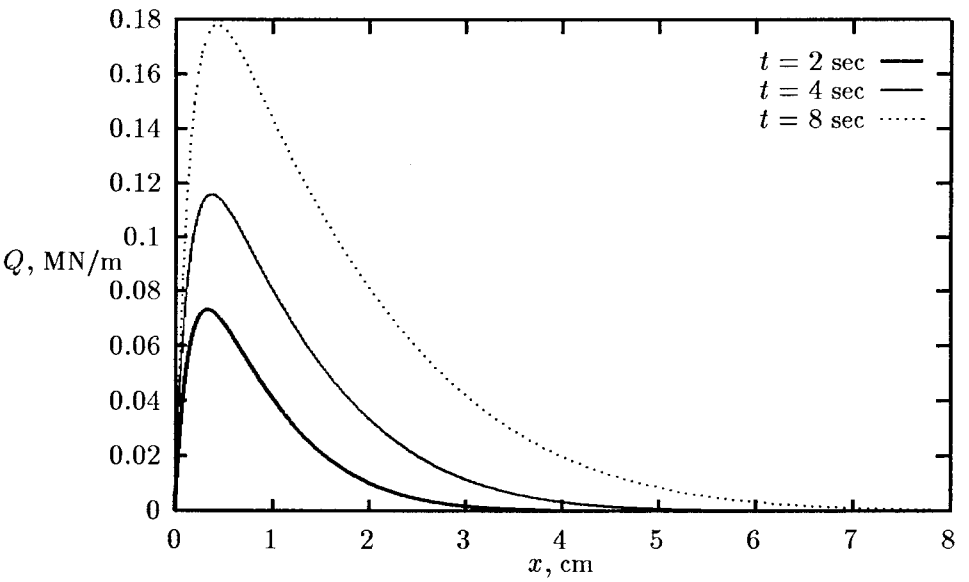

(b) Resultant interlaminar shearing force.

Figure 4.11 Temperature and resultant shearing force in a molybdenum/aluminum beam where the aluminum is kept at zero temperature.

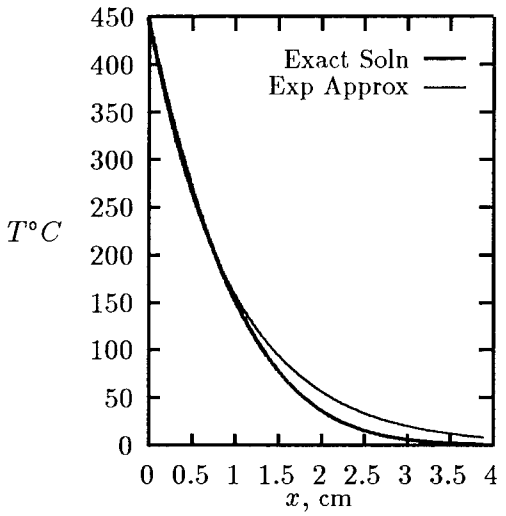

(a) Temperature at $t = 2$ seconds.

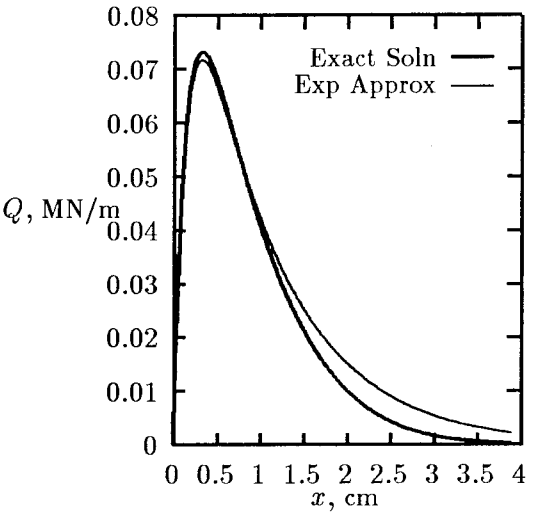

(b) Resultant interlaminar shearing force at $t = 2$ seconds.

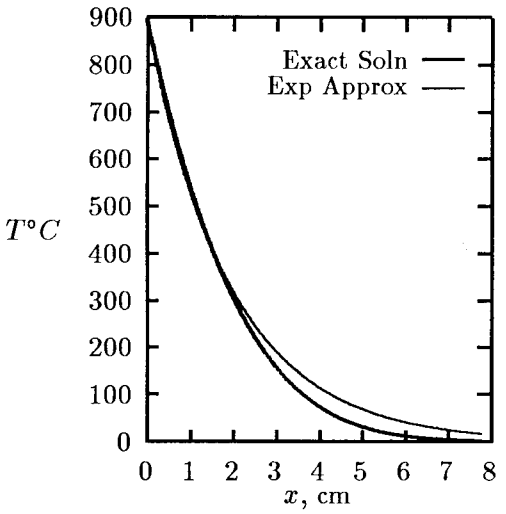

(c) Temperature at $t = 8$ seconds.

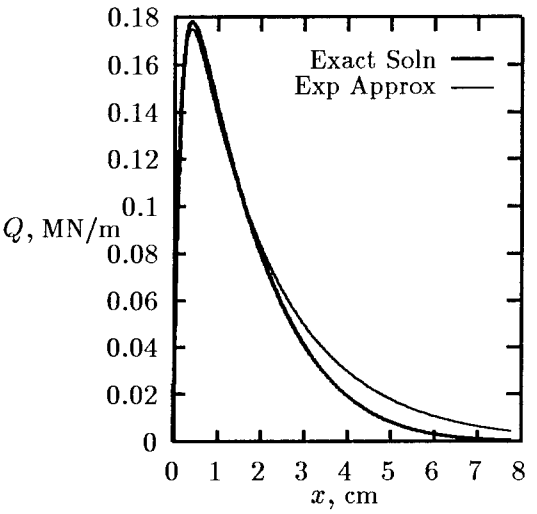

(d) Resultant interlaminar shearing force at $t = 8$ seconds.

Figure 4.12 Temperature and resultant interlaminar shearing force in a heated molybdenum/aluminum beam with the aluminum temperature maintained at zero. Comparison of the exact transient solution to the fixed-end temperature solution at two different values of time.

4.4 Summary

A simple strength of materials solution has been modified and shown to develop a closed form solution for thermal stresses in infinite and semi-infinite bimaterial beams with nonuniform temperature distributions. The solution technique was applied for an exponentially decaying temperature distribution and found to produce physically explainable and believable results. It was then applied for the more complicated temperatures found in the insulated rod exposed to uniform flux on one end and constant temperature at infinity. A closed form solution to the governing differential equation was obtained using the method of variation of parameters. Once again the results were both explainable and believable. All of the solutions presented herein were derived from Bernoulli-Euler beam theory, which is known to be inaccurate very near the ends of a beam. We now establish the domain of applicability of the present solution and provide several numerical examples to illustrate how the solution may be used in a failure analysis.

V. Applicability of the Solution

Since the present solution is derived from Bernoulli-Euler beam theory, it inherits all the strengths and weaknesses of the beam theory. In particular, and of utmost importance to the semi-infinite solution, beam theory is known to be inaccurate in the neighborhood of discontinuities and free surfaces. The length of this region, often referred to as a St Venant boundary layer, has been taken to be on the order of the beam thickness for homogeneous beams and was shown by Kuo(35) to be less than three times the thickness of the thinner layer for bimaterial beams.

In transient heat transfer problems, the thermal diffusion length, $b = 2\sqrt{\kappa_{D1} t}$, is a measure of the distance over which conduction heat transfer has occured at time t. Let ζ be the nondimensional length given by

$$\zeta = \frac{h}{b} \tag{5.1}$$

where h is the total beam thickness. If ζ is a large number, this means that heat has not diffused very far into the St Venant boundary layer. Consequently, if ζ is large, it is unlikely that significant stresses exist outside of the boundary layer. On the other hand, if ζ is a small number, heat has diffused into the material beyond the boundary layer and it is much more likely that significant stresses exist outside of the boundary layer. We now determine whether our solution predicts stresses of sufficient magnitude to cause material failure inside the domain of applicability (i. e. outside the St Venant boundary layer).

5.1 Applications

All of the results, equations, and plots presented thus far have been in nondimensional form. The most obvious benefit of this approach is that it greatly reduces the number of parametric analyses and plots needed to characterize a problem. One of the most obvious drawbacks of this approach is that it is sometimes difficult to look at nondimensional results and have a comfortable understanding of what real-world problems they represent. It is important to consider a few examples with dimensionalized quantities in order to assess the potential applicability of the solution to real problems. This is especially true for the

semi-infinite beam problem since the results are not believed to be accurate within about one beam thickness of the free edge. For the sake of brevity the following examples assume T_2 to be zero unless otherwise stated.

EXAMPLE 1: Let us consider first the problem of a good thermal conductor bonded to a poor thermal conductor of similar stiffness. For example, suppose we have a copper/porcelain beam with the material properties shown in Table 5.1. Figure 5.1 shows the interlaminar resultant shearing force, the interlaminar shearing stress and the maximum normal stresses in the two layers. The maximum normal stresses occur at the top and bottom of the layers. In the current context, the word maximum is meant to imply the largest values of tensile and compressive stress, sign notwithstanding. In the event all the normal stresses are of the same sign, the maximum and minimum values are plotted. The interlaminar normal stress is not presented in the figure because it is identically zero in the current model when the two layers have the same Young's modulus and thickness. As shown in Table 5.1, the layer thicknesses are equal and the Young's moduli are very nearly equal. Consequently, the resulting interlaminar normal stresses are negligible. The magnitude of the interlaminar shearing stress is relatively small except near $x = 0$. The St Venant boundary layer addressed earlier extends one beam thickness into the beam. Therefore, we are primarily interested in the stress values outside of this boundary layer (i. e. for $x \geq .508$ cm). In this region failure due to interlaminar shear does not seem likely.

Figure 5.1 suggests that the most likely cause of failure for this type of material configuration would be either tensile or compressive failure of one of the layers due to

Table 5.1 Example 1 Material Properties (Ref. 44-46)

MATERIAL	E MPa	ν	h cm	α cm/cm/° C	k_C W/(cm ° C)	κ_D cm^2/sec	$\mathcal{Q}$ W/cm^2
1, Copper	1.22 X 10^5	.33	.254	17.7 X 10^{-6}	3.86	1.12	1000
2, Porcelain	1.11 X 10^5	.33	.254	5.5 X 10^{-6}	.05	.013	0

excessive normal stresses. In the present context, failure is assumed to occur in a layer if the stresses in the layer exceed its strength. The strength of the porcelain in this example is 72 MPa in tension and -550 Mpa in compression. The strength of copper is 225 Mpa and is assumed to be the same in both tension and compression. Figure 5.2(b) shows that the first region of this bimaterial beam to experience failure will be the top surface of the porcelain layer. For this example the top surface of the porcelain coincides with the bimaterial interface. The failure is in tension and occurs at $t \approx .48$ seconds. Figure 5.2(a) shows that, if it was possible for the porcelain layer to survive, the copper layer would eventually fail in compression at the bottom surface (i. e. along the bimaterial interface) at $t \approx 3.45$ seconds.

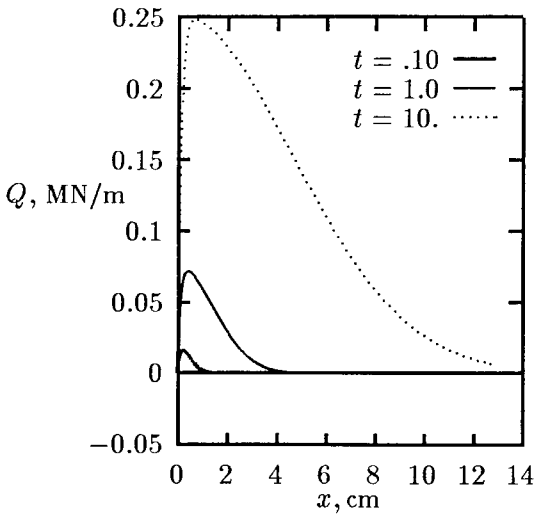

(a) Resultant Interlaminar Shearing Force

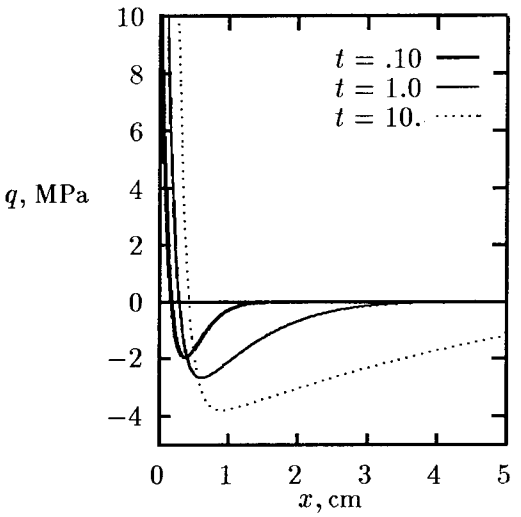

(b) Interlaminar Shearing Stress

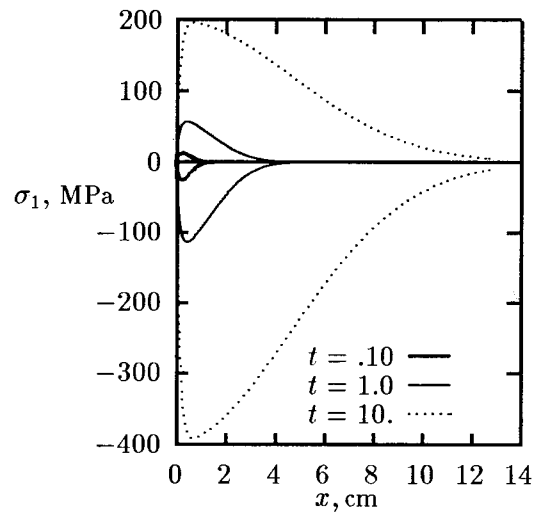

(c) Layer 1 (Copper) Maximum Normal Stresses. The positive stresses are at the top surface and the the negative stresses are at the interface.

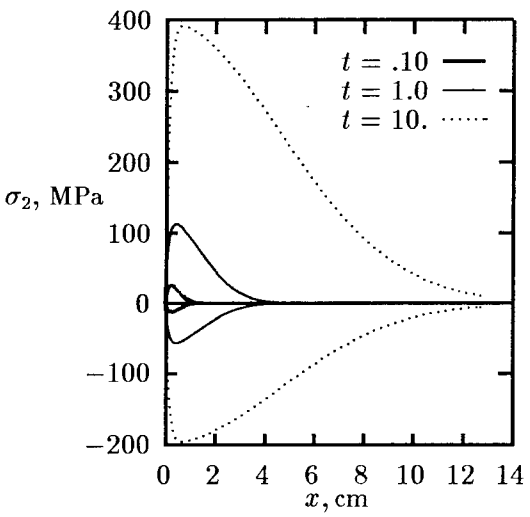

(d) Layer 2 (Porcelain) Maximum Normal Stresses. The positive stresses are at the interface and the negative stresses are at the bottom surface.

Figure 5.1 Resultant interlaminar force and stresses for Example 1. Plotted as a function of distance for various values of time. This example represents a good conductor bonded to a poor conductor of similar modulus. See Table 5.1 for the material properties used to generate the plots.

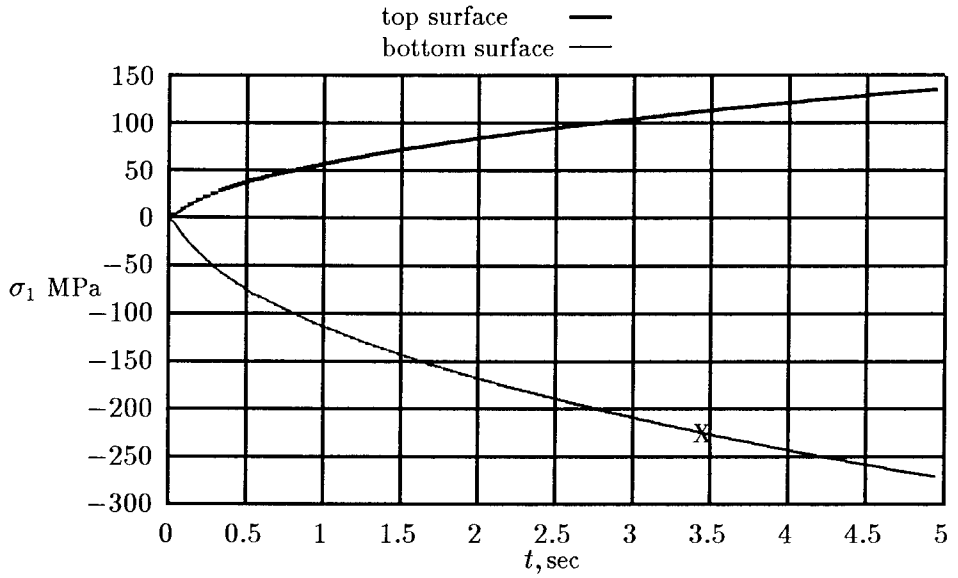

(a) Layer 1 (Copper) Peak Normal Stresses

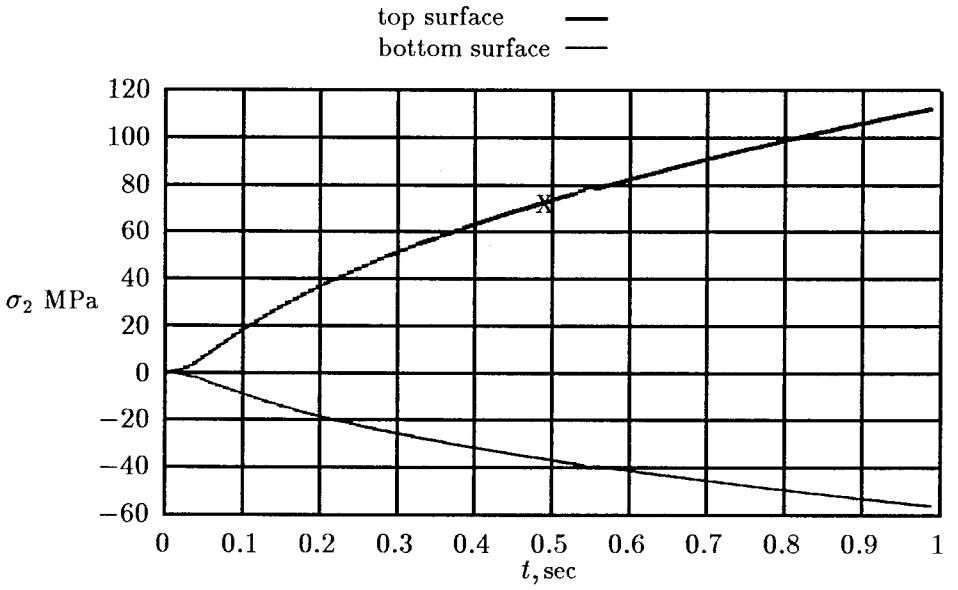

(b) Layer 2 (Porcelain) Peak Normal Stresses

Figure 5.2 Peak normal stresses at the edge of the St Venant boundary layer for Example 1. Plotted as a function of time. Strength values denoted by X.

Table 5.2 Example 2 Material Properties (Ref. 44-46)

MATERIAL	E MPa	ν	h cm	α cm/cm/° C	k_C W/(cm ° C)	κ_D cm^2/sec	Q W/cm^2
1, Copper	1.22 X 10^5	.33	.339	17.7 X 10^{-6}	3.86	1.12	1000
2, Porcelain	1.11 X 10^5	.33	.169	5.5 X 10^{-6}	.05	.013	0

EXAMPLE 2: Let us now consider the effect of the ratio of material thicknesses, $\hat{h}$, on the stresses. All material properties, including the total beam thickness, remain the same as in Example 1. The only changes to Table 5.1 are the individual layer thicknesses. Changing $\hat{h}$ from 1 to 1/2 results in the stresses shown in Figure 5.3. All of the stresses increase with time and, just as in Example 1, the layer axial stresses are much higher than the interlaminar stresses. The peak interlaminar shearing stress does increase by about a factor of 2. The interlaminar normal stress appears to be negligible in the region where $x > h$. It is interesting to note that the porcelain layer is entirely in tension, whereas the bottom of it was in compression in Example 1. It may easily be verified that $\sigma_{x2}(-h_2) \equiv 0$ by substituting the Table 5.2 properties into equation 3.53. Figure 5.4(b) shows the first failure to be in tension at the top of the porcelain layer, and will occur at $t \approx .58$ seconds. Figure 5.4(a) shows that, if it was possible for the porcelain layer to survive, the copper layer would fail in compression at the bottom surface at $t \approx 2.85$ seconds. Comparing Examples 1 and 2 indicates that the effect of decreasing the ratio of porcelain to copper thickness, while keeping the total thickness constant, is to extend the life of the porcelain layer while shortening the life of the copper layer.

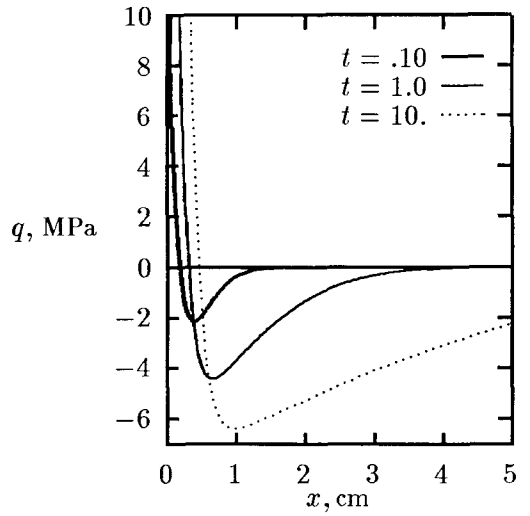

(a) Interlaminar Shearing Stress

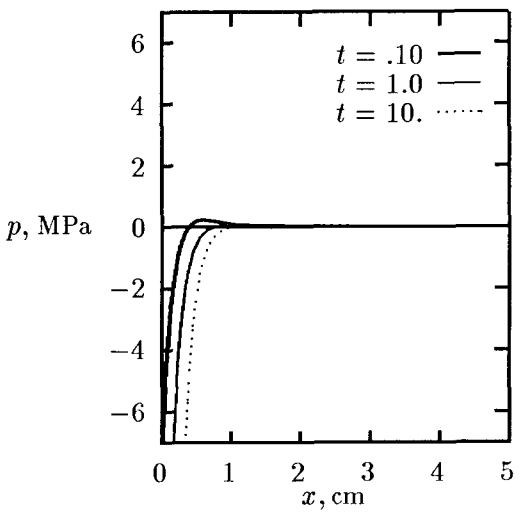

(b) Interlaminar Normal Stress

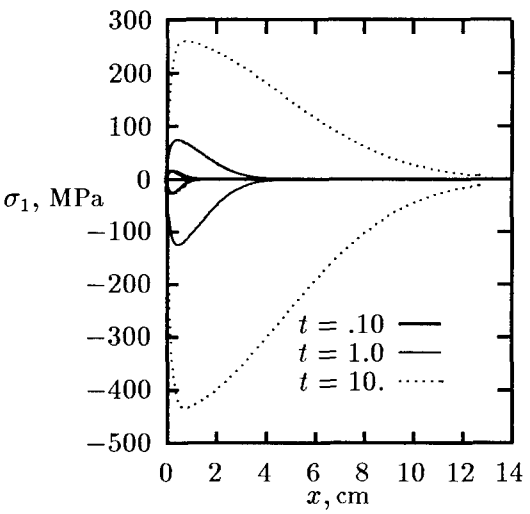

(c) Layer 1 (Copper) Maximum Normal Stresses. The positive stresses are at the top surface and the negative stresses are at the interface.

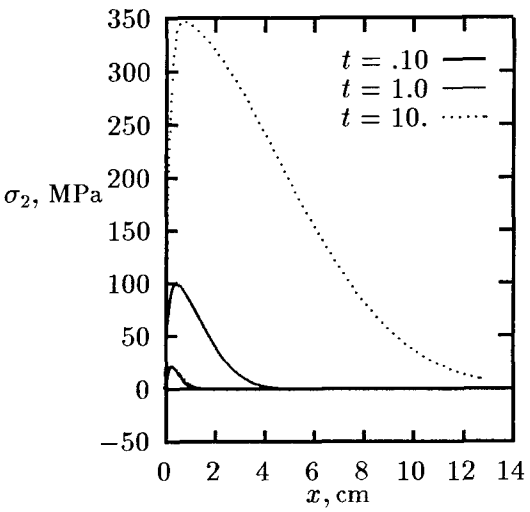

(d) Layer 2 (Porcelain) Maximum Normal Stresses. The positive stresses are at the interface and the negative stresses are at the bottom surface.

Figure 5.3 Interlaminar stresses and maximum normal stresses for Example 2. Plotted as a function of distance for various values of time. This example is identical to Example 1, except that the ratio of thicknesses, $\hat{h}$, is now 1/2. See Table 5.2 for a list of the material properties used to generate the plots.

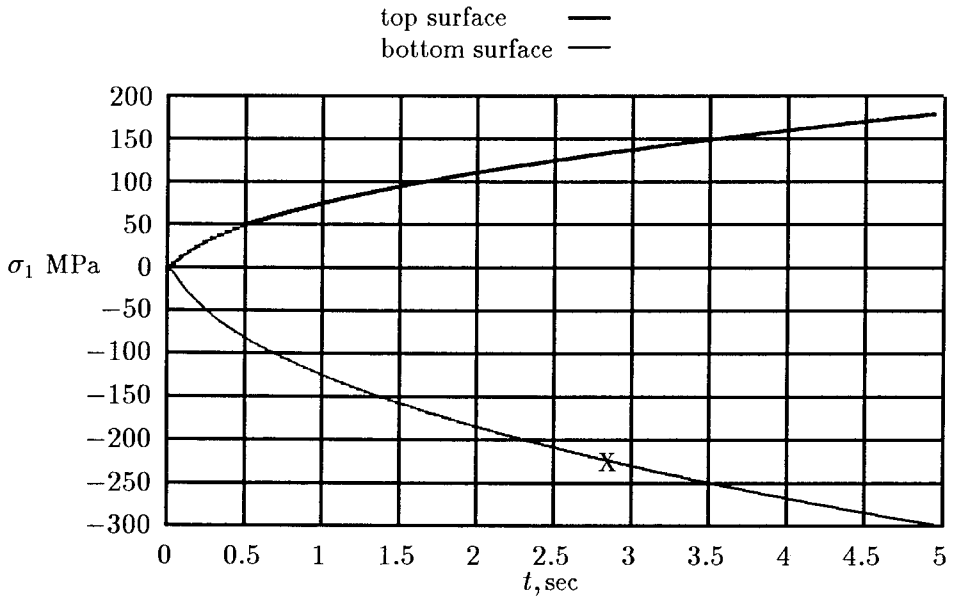

(a) Layer 1 (Copper) Peak Normal Stresses

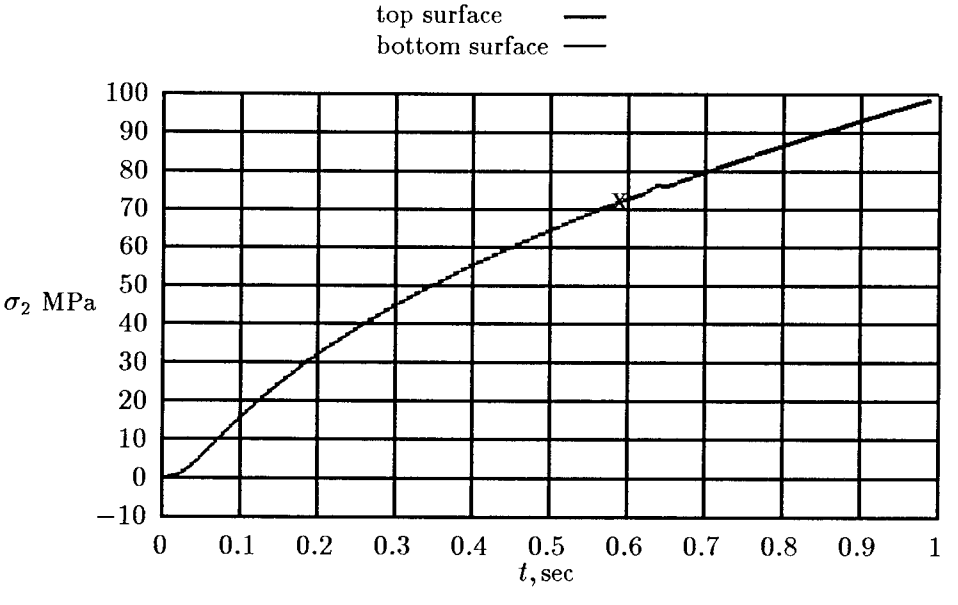

(b) Layer 2 (Porcelain) Peak Normal Stresses

Figure 5.4 Peak normal stresses at the edge of the St Venant boundary layer for Example 2. Plotted as a function of time. Strength values denoted by X.

There are obviously an infinite number of examples one could consider. Having just investigated the effect of changing only one material parameter, it seems appropriate to assess the effect of the various properties on the resultant interlaminar shearing force and the stresses. From equations 4.28 we have

$$\begin{aligned} \hat{Q}(\hat{x},\tilde{x}) &= Q(x)\left(\frac{k^2}{2A_1}\right) \\ \hat{q}(\hat{x},\tilde{x}) &= q(x)\left(\frac{k}{2A_1}\right) \\ \hat{p}(\hat{x},\tilde{x}) &= p(x)\left(\frac{1}{2A_1\varphi}\right) \end{aligned} \tag{5.2}$$

where $A_1 = \alpha_1 \mathcal{Q}_1/(\kappa k_{C1} k)$. Making the substitution and introducing new notation, we obtain

$$\begin{aligned} Q &= Q_f \hat{Q} \\ q &= q_f \hat{q} \\ p &= p_f \hat{p} \end{aligned} \tag{5.3}$$

where

$$\begin{aligned} Q_f &= \frac{2\alpha_1 \mathcal{Q}_1}{k_{C1}(\kappa k^3)} \\ q_f &= \frac{2\alpha_1 \mathcal{Q}_1}{k_{C1}(\kappa k^2)} \\ p_f &= \frac{2\alpha_1 \mathcal{Q}_1 \varphi}{k_{C1}(\kappa k)} \end{aligned} \tag{5.4}$$

If the material Poisson's ratios are approximately equal, equation 3.31 may be written as follows:

$$k^2 = \frac{3}{2h_1^2}\bar{k}^2 \tag{5.5}$$

where

$$\bar{k}^2 = \frac{(1-\nu)(1+\hat{h})^2}{1+B\hat{h}^2}\left[\frac{(B+1)(1+B\hat{h}^2)+3B(1+\hat{h})^2}{B+\hat{h}^2}\right] \tag{5.6}$$

The interfacial compliance coefficient, κ, may also be simplified when the Poisson's ratios are approximately equal. Assuming equality, we have

$$\kappa = \frac{2h}{3E_1(1-\nu)}\bar{\kappa} \tag{5.7}$$

where

$$\bar{\kappa} = \frac{\hat{E}+\hat{h}}{\hat{E}(1+\hat{h})} \tag{5.8}$$

The load and stress scale factors (equations 5.4) may now be written in the following manner:

$$\begin{aligned} Q_f &= \frac{\alpha_1 \mathcal{Q}_1}{k_{C1}} E_1(1-\nu)\left(2\sqrt{\frac{2}{3}}\right) \quad h^2 \quad \frac{1}{\bar{\kappa}\bar{k}^3} \\ q_f &= \frac{\alpha_1 \mathcal{Q}_1}{k_{C1}} E_1(1-\nu)(2) \quad h \quad \frac{1}{\bar{\kappa}\bar{k}^2} \\ p_f &= \frac{\alpha_1 \mathcal{Q}_1}{k_{C1}} E_1(1-\nu)\left(\sqrt{\frac{3}{2}}\right) \quad h \quad \left(\frac{1}{1+\hat{E}\hat{h}^3} - \frac{1}{1+\hat{h}}\right)\frac{1}{\bar{\kappa}\bar{k}} \end{aligned} \tag{5.9}$$

With the scale factors written in this form, the effect of several parameters on the stresses and loads is evident. For example, all three factors are linearly proportional to the magnitude of the coefficient of thermal expansion, the heat flux at $x = 0$, and the Young's modulus of layer 1. They are inversely proportional to the thermal conductivity of layer 1. The interlaminar stresses are directly proportional to the total beam thickness. The layer normal stresses are proportional to Q/h, and are therefore also proportional to the total beam thickness. The effects of variations in $\hat{E}$ and $\hat{h}$ on the loads and stresses may be determined by analyzing the following functions:

$$\begin{aligned} \bar{Q}_f &= \frac{1}{\bar{\kappa}\bar{k}^3} \\ \bar{q}_f &= \frac{1}{\bar{\kappa}\bar{k}^2} \\ \bar{p}_f &= \frac{1}{\bar{\kappa}\bar{k}}\left(\frac{1}{1+\hat{E}\hat{h}^3} - \frac{1}{1+\hat{h}}\right) \end{aligned} \tag{5.10}$$

The nondimensional loads and stresses given by equations 4.24 through 4.26 were previously shown to increase as the nondimensional time, ϕ, increases. As defined, ϕ is proportional to

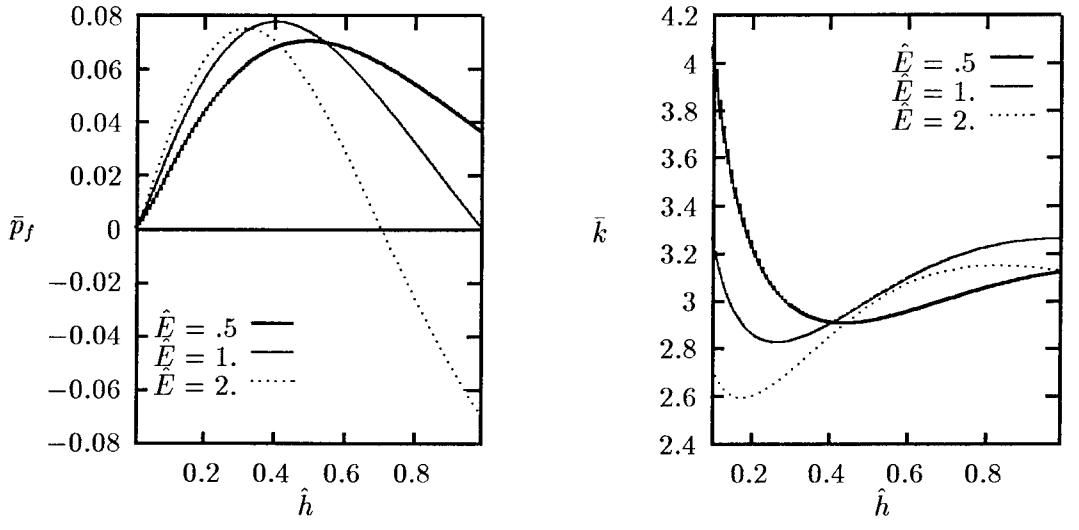

(a) Scale Factor for $p(x)$

(b) Dimensionless Material Parameter, $\bar{k}$

Figure 5.5 Scale factor for the interlaminar normal stress and dimensionless material parameter, $\bar{k}$. Plotted as a function of the ratio of thicknesses, $\hat{h}$, for various values of the ratio of Young's moduli, $\hat{E}$.

the material parameter, k. Therefore, the effect of variations in $\hat{E}$ and $\hat{h}$ must be predicted. Figures 5.5 and 5.6 show the factors of interest as functions of $\hat{E}$ and $\hat{h}$. Figure 5.6 suggests that variations in $\hat{h}$ have little effect on the magnitude of Q and q for $0 \leq \hat{E} \leq 2$. It appears that these magnitudes increase by no more than about a factor of 2, as $\hat{h}$ increases by a factor of 10, for all values of $\hat{E}$ considered. Figure 5.6 suggests that the magnitude of p and k are relatively sensitive to changes in $\hat{h}$ for $0 \leq \hat{E} \leq 2$. Figure 5.5 shows $\bar{p}_f$ and $\bar{k}$ as functions of $\hat{h}$ with $\hat{E}$ as a parameter.

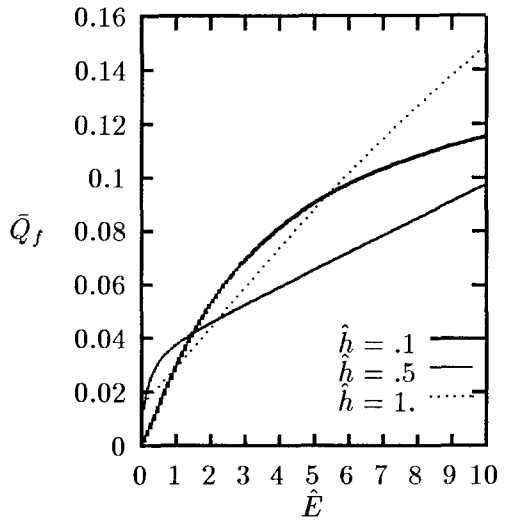

(a) Scale Factor for $Q(x)$

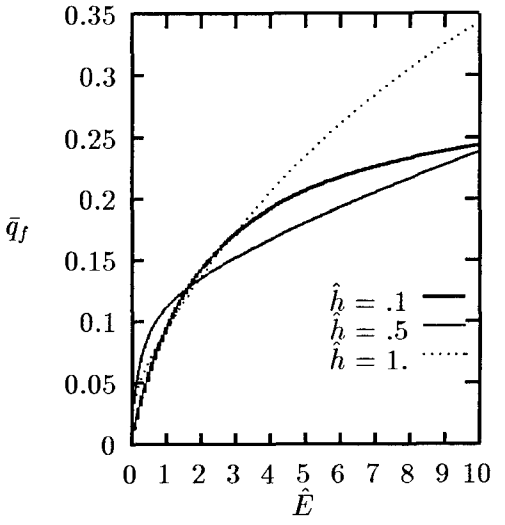

(b) Scale Factor for $q(x)$

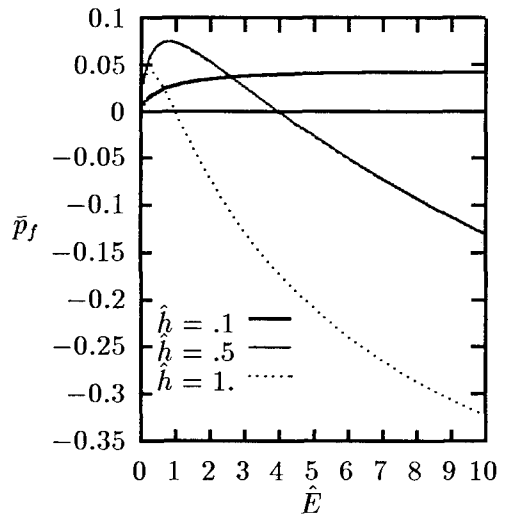

(c) Scale Factor for $p(x)$

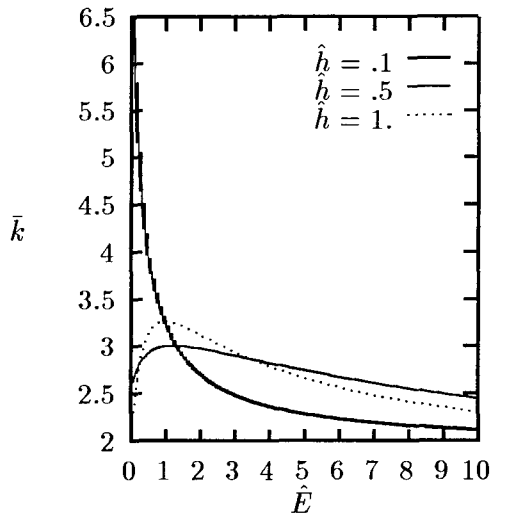

(d) Dimensionless Material Parameter, $\bar{k}$

Figure 5.6 Scale factors for the dimensionless interlaminar resultant force and interlaminar stresses, and the dimensionless material property, $\bar{k}$. Plotted as a function of the ratio of Young's moduli, $\hat{E}$, for various values of the ratio of thicknesses, $\hat{h}$.

EXAMPLE 3: The first two example problems considered a good conductor bonded to a poor conductor with approximately the same Young's modulus. Let us now consider the same conductor bonded to a poor conductor of much lower modulus. This might be the case when metal strips are bonded using certain epoxy adhesives. Table 5.3 lists the material properties and Figure 5.7 shows the resulting stresses. Comparing Figures 5.1 and 5.7, one sees that the stresses are lower for the "softer" adhesive. Of particular interest are the interlaminar shearing stress and the normal stress in the adhesive layer. The interlaminar shearing stress is much lower than for the *stiffer* adhesive of Example 1 and the normal stresses in the adhesive layer are nowhere compressive.

Figure 5.7 suggests that the most likely cause of failure in this example would be excessive normal stresses (σ_1, σ_2) in one of the layers. However, the magnitude of these stresses is significantly below the material strength values (225 MPa for the copper and 70 MPa for the epoxy) after 10 seconds of heating. For the incident heat flux given in Table 5.3, the heated end of the copper layer will melt in about 12 seconds. We therefore conclude that, for this example, the bimaterial beam will become inelastic and succomb to thermal failure (via melting and/or ablation) before it fails due to thermal stresses.

Table 5.3 Example 3 Material Properties (Ref. 45-48)

MATERIAL	E MPa	ν	h cm	α cm/cm/° C	k_C W/(cm ° C)	κ_D cm^2/sec	Q W/cm^2
1, Copper	1.22×10^5	.33	.254	17.7×10^{-6}	3.86	1.12	1000
2, Epoxy	3.59×10^3	.33	.254	65×10^{-6}	.002	.001	0

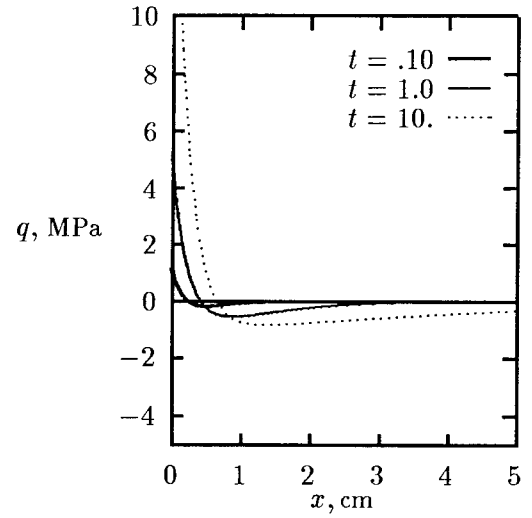

(a) Interlaminar Shearing Stress

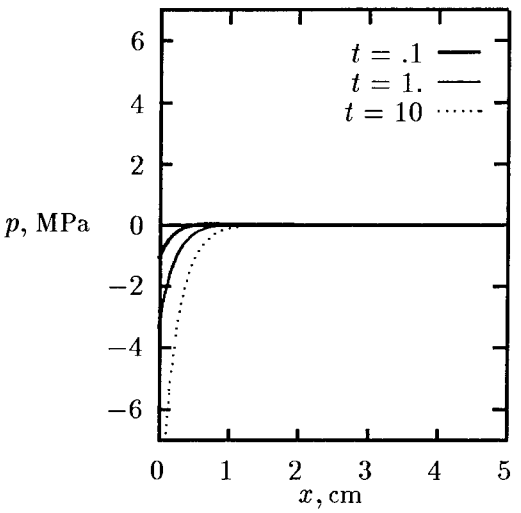

(b) Interlaminar Normal Stress

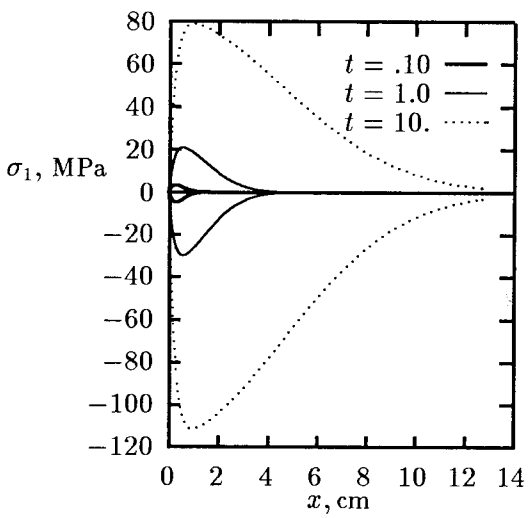

(c) Layer 1 (Copper) Maximum Normal Stresses. The positive stresses are at the top surface and the negative stresses are at the interface.

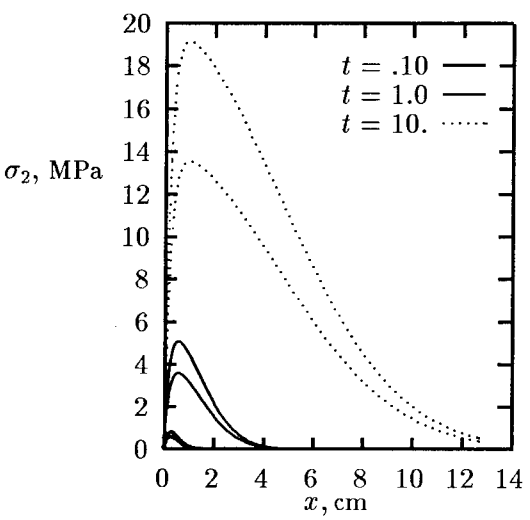

(d) Layer 2 (Epoxy) Maximum Normal Stresses. The higher stresses are at the interface and the lower stresses are at the interface.

Figure 5.7 Interlaminar stresses and peak normal stresses for Example 3. Plotted as a function of distance for various values of time. This example represents a good conductor bonded to a poor conductor with much lower modulus. See Table 5.3 for the material properties used to generate the plots.

Comparing the results of Examples 1 and 3, it is evident that the principal reason for the different failure possibilities is the significant difference in Young's moduli of the poor conductor (layer 2 in each example). While it is true that the thermal properties of the two poor conductors are quite different, this does not affect the stresses because no heat is conducted into the poorly conducting layers in both examples (i. e. $q_2 = 0$). These results suggest that, for a good conductor with Young's modulus E_1, there is some value of $\hat{E} = E_2/E_1$ below which failure due to elastic thermal stresses is not probable. Figure 5.8 shows the time to failure as a function of $\hat{E}$ for both a copper/epoxy and an aluminum/epoxy bimaterial beam. The figure indicates that, as $\hat{E}$ becomes small, the time to failure exceeds the time at which the heated end of the metal layer reaches the melting temperature.

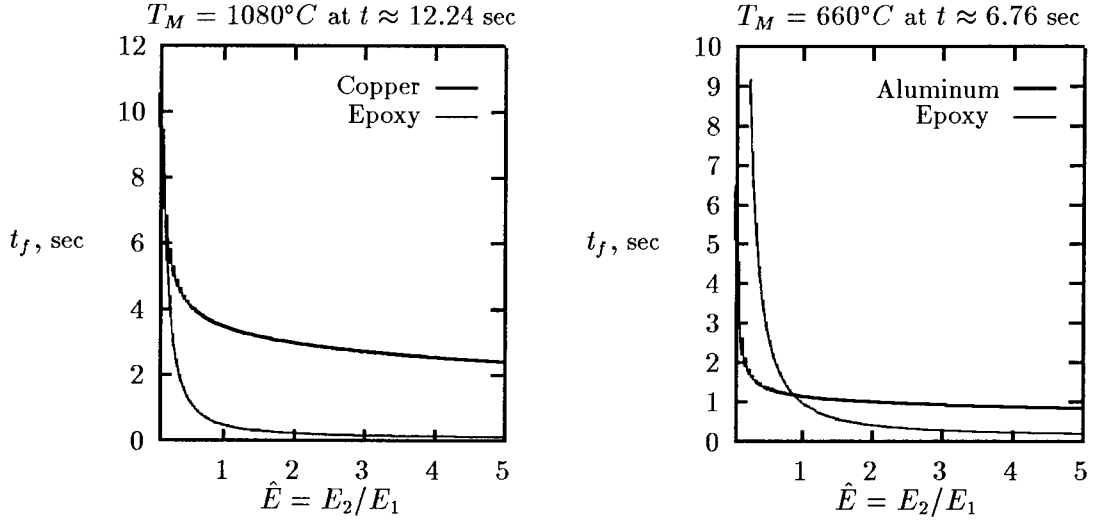

(a) Copper/Epoxy Beam

(b) Aluminum/Epoxy Beam

Figure 5.8 Time-to-failure for two metal/epoxy bimaterial beams. Plotted as a function of the ratio of Young's moduli, $\hat{E}$, of the epoxy to the metal.

EXAMPLE 4: Thus far we have not addressed the effect of thermal properties on the stresses. In particular, the thermal diffusivity and thermal conductivity are very important in the development of thermal-induced stresses. These properties are not completely independent, but it is nevertheless instructive to vary them independently to assess their relative roles in the development of stresses. We first consider the thermal diffusivity. This property does not appear in any of the stress scale factors, but, for the semi-infinite beam, it is hidden in the nondimensional length variable, $\hat{x}$. Table 5.4 shows the material properties used for this example. Note that material 1 is identified as a hypothetical solid because it would be difficult to find a single material capable of having such diverse values of thermal diffusivity as the entries in the table. Figure 5.9 shows the resultant shearing force and the stresses (at $t = 10$ seconds) as a function of distance with thermal diffusivity as a parameter. The figure suggests that all stresses increase as the diffusivity increases. Furthermore, the extent of a certain stress level into the material increases with increased diffusivity. These results are due to the fact that a good diffuser will allow for more rapid thermal transport than a poor diffuser. This will cause a larger volume of material to undergo a temperature increase. The heated material will then expand, causing higher stresses to persist further from the edge than if the heated material was a poor diffuser.

Table 5.4 Example 4 Material Properties (Ref. 44-46)

MATERIAL	E MPa	ν	h cm	α cm/cm/° C	k_C W/(cm°C)	κ_D cm^2/sec	$\mathcal{Q}$ W/cm^2
1, Solid (Hypothetical)	1.22 X 10^5	.33	.254	17.7 X 10^{-6}	3.86	.1,.5,1	1000
2, Porcelain	1.11 X 10^5	.33	.254	5.5 X 10^{-6}	.05	.013	0

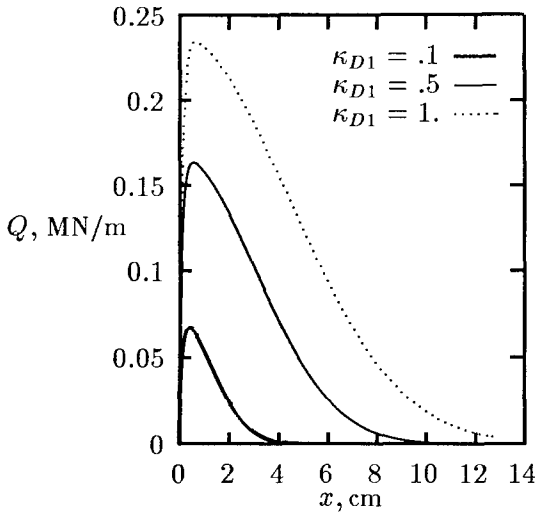

(a) Resultant Interlaminar Shearing Force

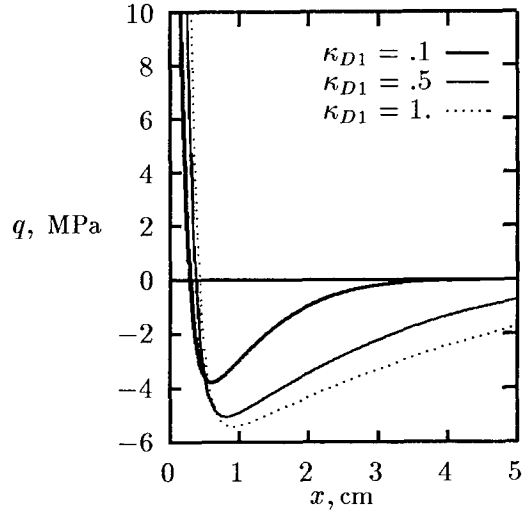

(b) Interlaminar Shearing Stress

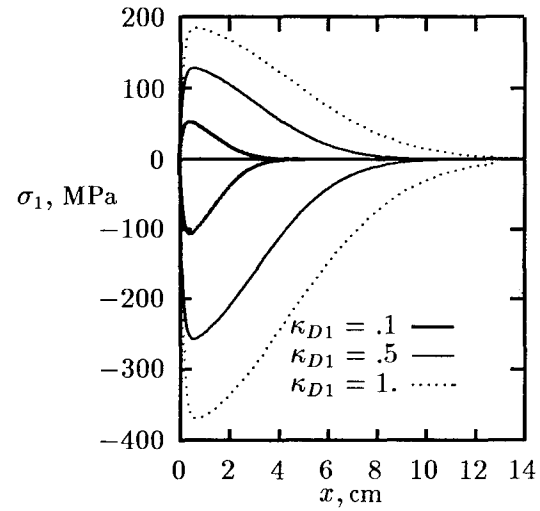

(c) Layer 1 (Solid) Maximum Normal Stresses. The positive stresses are at the top surface and the negative stresses are at the interface.

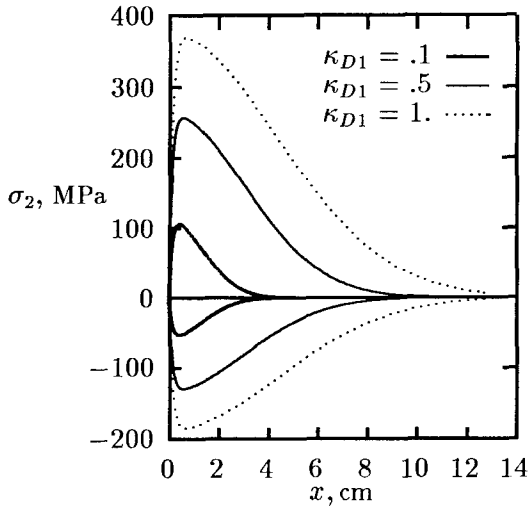

(d) Layer 2 (Porcelain) Maximum Normal Stresses. The positive stresses are at the interface and the negative stresses are at the bottom surface.

Figure 5.9 Resultant interlaminar shearing force, interlaminar shearing stress and peak normal stresses for Example 4. Plotted as function of distance (at $t = 10$ seconds) for various values of the thermal diffusivity of the heated layer. See Table 5.4 for a list of material values used to generate the plots.

EXAMPLE 5: It appears evident from the previous examples that thermal diffusivity and thermal conductivity are critical players in determining both the magnitude of stresses and whether or not significant stresses occur outside the St Venant boundary layer region. The results of Example 4 showed that increasing the thermal diffusivity caused both the peak stresses and their extent into the material to increase. It was not clear that thermal diffusivity affected one of these factors more than the other. The thermal conductivity in Example 4 was quite high. Therefore, let us now consider the effects of varying the thermal conductivity for a poor diffuser. Figure 5.10 shows the stresses for the material properties listed in Table 5.5. The plots reveal that stresses are very high when both thermal conductivity and thermal diffusivity are low. Also, it appears from the figure that the extent of significant stresses into the material increases very little with significant variations in conductivity. This observation, coupled with those made earlier for Example 4, suggests that thermal diffusivity is the driving factor in determining how far beyond the boundary layer significant stresses may be expected.

Table 5.5 Example 5 Material Properties (Ref. 44)

MATERIAL	E MPa	ν	h cm	α cm/cm/° C	k_C W/(cm°C)	κ_D cm^2/sec	Q W/cm^2
1, Solid (Hypothetical)	1.22 X 10^5	.33	.254	17.7 X 10^{-6}	.05,.1,.5	.1	100
2, Porcelain	1.11 X 10^5	.33	.254	5.5 X 10^{-6}	.05	.013	0

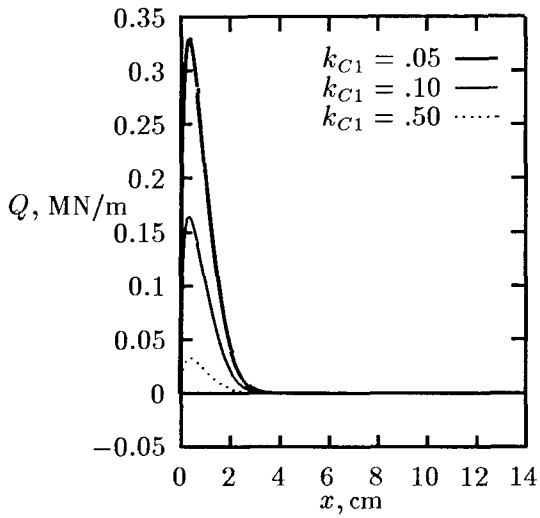

(a) Resultant Interlaminar Shearing Force

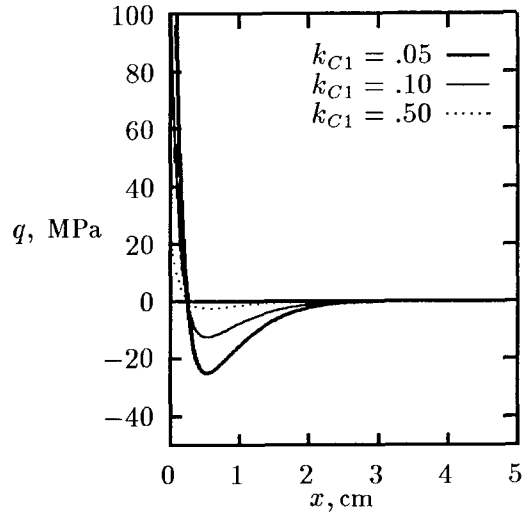

(b) Interlaminar Shearing Stress

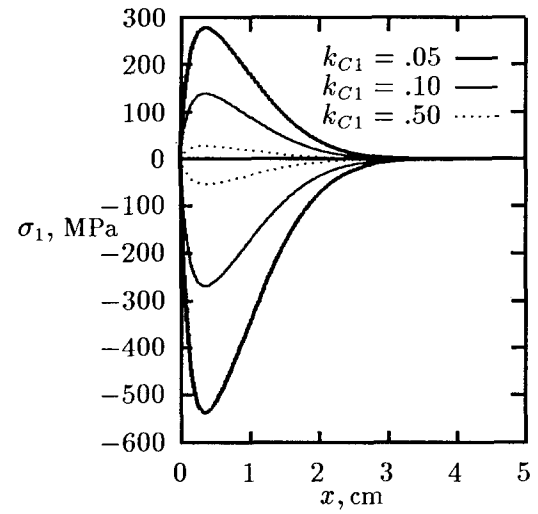

(c) Layer 1 (Solid) Maximum Normal Stresses. The positive stresses are at the top surface and the negative stresses are at the interface.

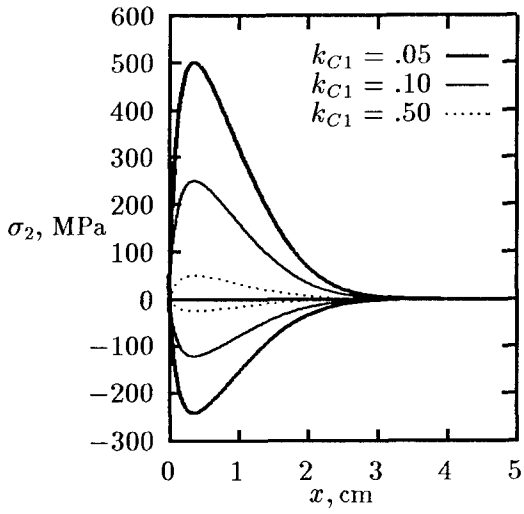

(d) Layer 2 (Porcelain) Maximum Normal Stresses. The positive stresses are at the interface and the negative stresses are at the bottom surface.

Figure 5.10 Resultant interlaminar shearing force, interlaminar shearing stress, and peak normal stresses for Example 5. Plotted as a function of distance (at $t = 5$ seconds) for various values of the thermal conductivity of the heated layer. In this example, the heated layer has a low diffusivity. See Table 5.5 for a list of material values used to generate the plots.

EXAMPLE 6: Let us now consider the effect of thermal conductivity on the stresses in a good diffuser. Table 5.6 lists the properties for our example and Figure 5.11 shows the resulting stresses. Comparing Figures 5.10 and 5.11, we see that the higher thermal diffusivity indeed results in extending the region of significant stresses into the material. Increasing the thermal conductivity seems to be the primary contributor to increases in the stress magnitude.

Table 5.6 Example 6 Material Properties (Ref. 44)

MATERIAL	E MPa	ν	h cm	α cm/cm/° C	k_C W/(cm°C)	κ_D cm^2/sec	$\mathcal{Q}$ W/cm^2
1, Solid (Hypothetical)	1.22 X 10^5	.33	.254	17.7 X 10^{-6}	.05,.1,.5	1.12	100
2, Porcelain	1.11 X 10^5	.33	.254	5.5 X 10^{-6}	.05	.013	0

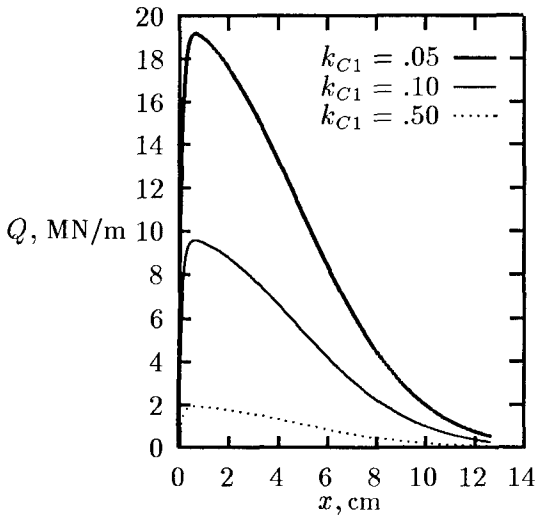

(a) Resultant Interlaminar Shearing Force

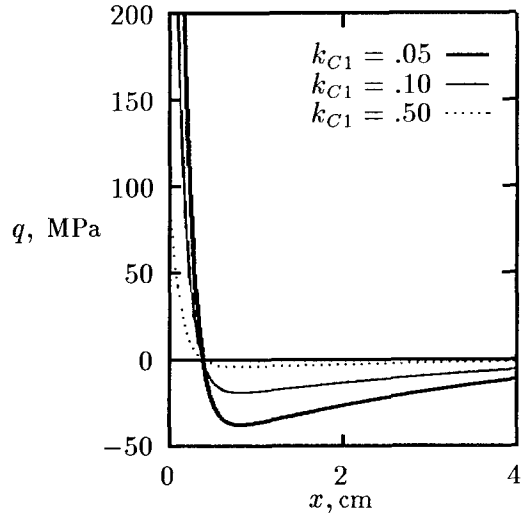

(b) Interlaminar Shearing Stress

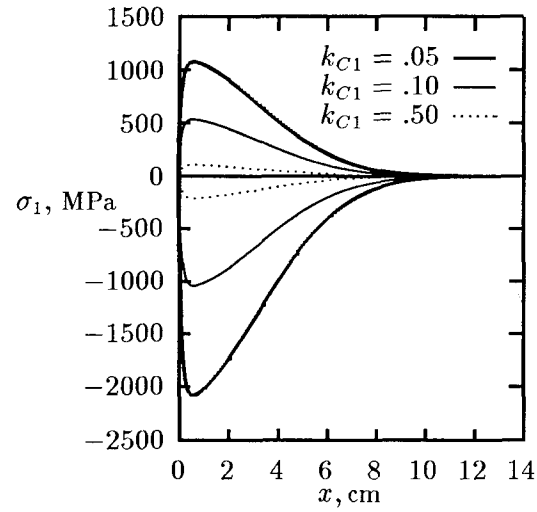

(c) Layer 1 (Solid) Maximum Normal Stresses. The positive stresses are at the top surface and the negative stresses are at the interface.

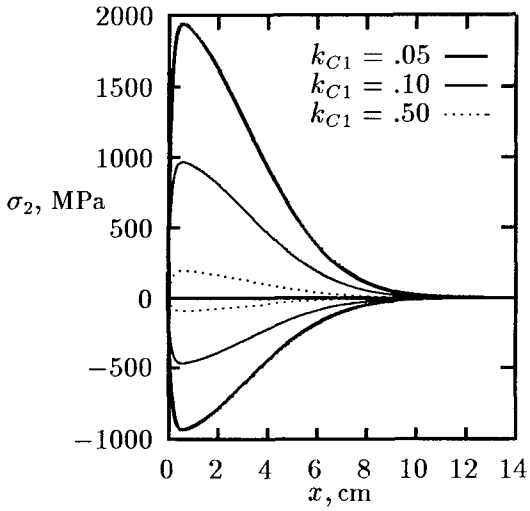

(d) Layer 2 (Porcelain) Maximum Normal Stresses. The positive stresses are at the interface and the negative stresses are at the lower surface.

Figure 5.11 Resultant interlaminar shearing force, interlaminar shearing stress, and peak normal stresses for Example 6. Plotted as a function of distance (at $t = 5$ seconds) for various values of the thermal conductivity of the heated layer. In this example, the heated layer has a high diffusivity. See Table 5.6 for a list of material values used to generate the plots.

EXAMPLE 7: In the last few examples we have examined the effect of varying either the thermal conductivity or thermal diffusivity while holding the other constant. In reality this is probably not possible because the two properties are related by the definition

$$\kappa_{D1} = \frac{k_{C1}}{\rho_1 c_{p1}} \tag{5.11}$$

where c_{p1} is the specific heat at constant pressure. While it is not expected that κ_{D1} will scale linearly with k_{C1} as one considers different materials, the two properties are certainly proportional if the variation in the product of density and specific heat is not great. For the sake of making our examples a bit more realistic, let us consider an example in which the ratio of thermal conductivity to thermal diffusivity remains constant. Table 5.7 lists the material properties and Figure 5.12 shows the resulting stresses.

Table 5.7 Example 7 Material Properties (Ref. 44)

MATERIAL	E MPa	ν	h cm	α cm/cm/° C	k_C W/(cm°C)	κ_D cm^2/sec	Q W/cm^2
1, Solid (Hypothetical)	1.22 X 10^5	.33	.254	17.7 X 10^{-6}	.05,.1,.5	.1,.2,1	100
2, Porcelain	1.11 X 10^5	.33	.254	5.5 X 10^{-6}	.05	.013	0

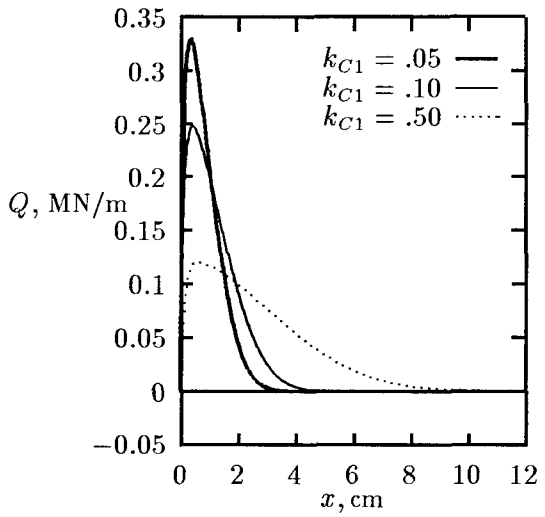

(a) Resultant Interlaminar Shearing Force

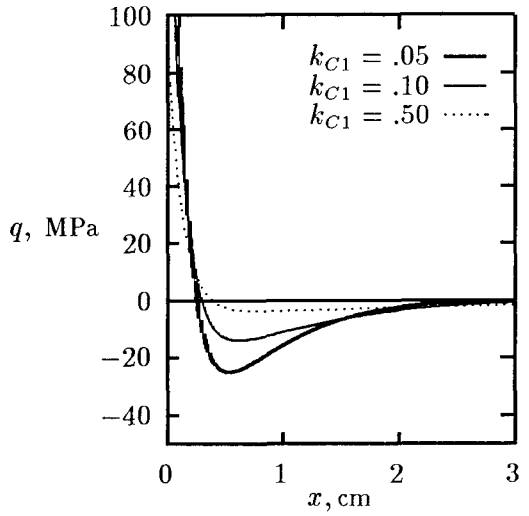

(b) Interlaminar Shearing Stress

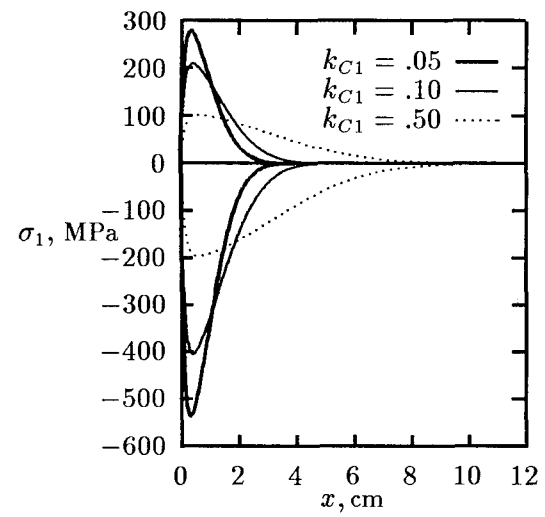

(c) Layer 1 (Solid) Maximum Normal Stresses. The positive stresses are at top surface and the negative stresses are at the interface.

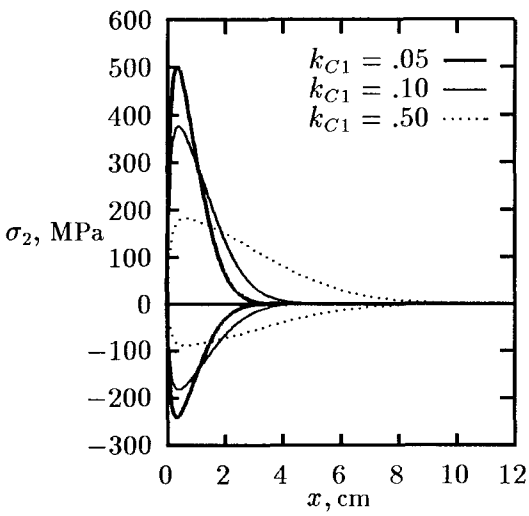

(d) Layer 2 (Porcelain) Maximum Normal Stresses. The positive stresses are at the interface and the negative stresses are at the bottom surface.

Figure 5.12 Resultant interlaminar shearing force, interlaminar shearing stress, and peak normal stresses for Example 7. Plotted as a function of distance (at $t = 5$ seconds) for various values of the thermal conductivity of the heated layer. In this example, the ratio of thermal diffusivity to thermal conductivity is held constant. See Table 5.6 for a list of material values used to generate the plots.

EXAMPLE 8: As a final example, let us consider the stresses in a bimetallic beam where both metals are reasonably good conductors and $T_2 \neq 0$. We consider the molybdenum/aluminum beam addressed by Suhir (32), except that his analysis was for a finite beam with uniform temperature increase. Table 5.8 lists the material properties and Figure 5.13 shows the peak normal stresses. The interlaminar stresses are not plotted because they are large in the boundary layer region only and are negligible compared to the normal stresses outside this region. The material strength values are taken in this example to be 78 MPa (45:page 715) and 689 MPa (49), respectively, and it is assumed that they are the same in tension and compression. Figure 5.13(d) shows that the first failure in this beam will be in compression at the top of the aluminum layer (i. e. along the interface), and will occur at $t \approx 2.67$ seconds. At the time of failure, the end temperature of the molybdenum layer is about $520°C$, which is well below the melting temperature of molybdenum ($2610°C$). The end temperature and the melting temperatures of the aluminum layer are $415°C$ and $660°C$, respectively. Thus, while it is likely both metals are still elastic at the predicted failure time, very little additional heating would have to be applied to cause the temperature of the aluminum layer to exceed the value at which it ceases to behave elastically.

Table 5.8 Example 8 Material Properties (Ref. 32)

MATERIAL	E MPa	ν	h cm	α cm/cm/° C	k_C W/(cm°C)	κ_D cm^2/sec	Q W/cm^2
1, Molybdenum	3.25 X 10^5	.33	.254	4.9 X 10^{-6}	1.23	.479	500
2, Aluminum	7.038 X 10^4	.33	.254	23.6 X 10^{-6}	2.04	.842	500

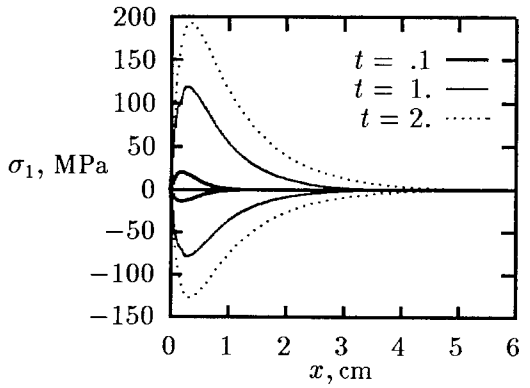

(a) Layer 1 (Molybdenum) Maximum Normal Stresses. Plotted as a function of distance with time as parameter.

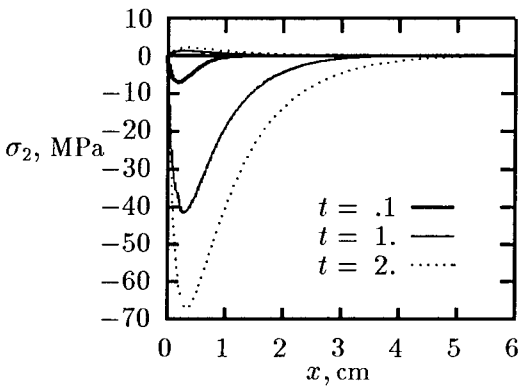

(b) Layer 2 (Aluminum) Maximum Normal Stresses. Plotted as a function of distance with time as parameter.

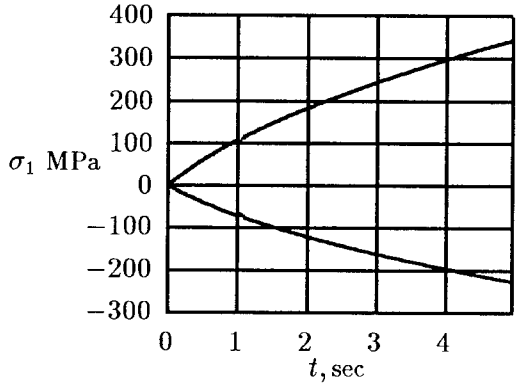

(c) Layer 1 (Molybdenum) Peak Normal Stresses. Plotted as a function of time at the edge of the St Venant boundary layer.

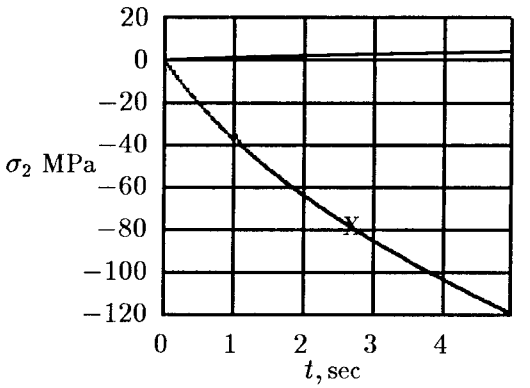

(d) Layer 2 (Aluminum) Peak Normal Stresses. Plotted as a function of time at the edge of the St Venant boundary layer. Strength denoted by X.

Figure 5.13 Peak normal stresses for Example 8. In subfigures (a) and (c) the positive stresses are at the interface and the negative stresses are at the top surface. In subfigures (b) and (d) the negative stresses are at the interface and the positive stresses are at the bottom surface.

5.2 Summary

The preceding examples show that the simple strength of materials solution predicts significant axial thermal stresses outside of the St Venant boundary layer for bimaterial beams where at least one of the layers is a relatively good thermal conductor. If both layers are poor conductors, very high stresses result, but they are near the edge in the region where the solution is not applicable. For all combinations of materials considered the interlaminar stresses were relatively small in the domain of applicability of the solution.

An attractive feature of the solution technique presented in Chapter III is that it can readily be applied to problems where temperature varies in both the lengthwise and thickness directions. The problems considered thus far have been for bimaterial beams with a thermally insulated interface. In reality, thermal conduction in a bimaterial beam heated on the end will be two-dimensional. It is reasonable to assume that the effect of two-dimensional heat conduction would be to lower the point-by-point temperature difference in a bimaterial beam, when compared to the same beam with one-dimensional heat conduction. In our model, the resultant interlaminar shearing force is driven by the difference, $\alpha_1 T_1(x,t) - \alpha_2 T_2(x,t)$, as shown in equation 3.30. The interlaminar stresses are related to the derivatives of this difference. Therefore, the thermal stresses in a bimaterial beam with an insulated interface will certainly differ from those in the same beam with a conducting interface.

Another attractive feature of the solution technique is that it is readily applied to layered beams with more than two layers. If one were to model a nonhomogeneous material of finite thickness as a discrete number of homogeneous layers, it is reasonable to assume that the thickness of these layers would affect the magnitude of the thermal stresses. We now attempt to quantify what effects two-dimensional heat transfer and layer thicknesses have on our solution.

VI. Two-Dimensional Heat Transfer and Multiple-Layered Beams

As noted in the previous chapter, the strength of materials solutions derived and presented thus far are applicable to bimaterial beams with one-dimensional heat transfer in the lengthwise direction. We now attempt to determine the effects of two-dimensional heat transfer and multiple material layers on the magnitude of the thermal stresses calculated using our solution.

6.1 Two-Dimensional Heat Transfer

In an attempt to quantify the effects of two-dimensional heat transfer on thermal stresses, we now study the effects of thermal transport in the y-direction on stresses in the finite bimaterial beam shown in Figure 6.1. The beam is relatively thin, with insulated top and bottom faces. The temperature distribution in the beam is obtained by solving the following system of equations:

$$\frac{\partial^2 T_1}{\partial x^2} + \frac{\partial^2 T_1}{\partial y^2} = \frac{1}{\kappa_{D1}} \frac{\partial T_1}{\partial t} \tag{6.1}$$

$$\frac{\partial^2 T_2}{\partial x^2} + \frac{\partial^2 T_2}{\partial y^2} = \frac{1}{\kappa_{D2}} \frac{\partial T_2}{\partial t} \tag{6.2}$$

The initial and boundary conditions for the problem are

$$T_1(x, y, 0) = T_2(x, y, 0) = 0$$

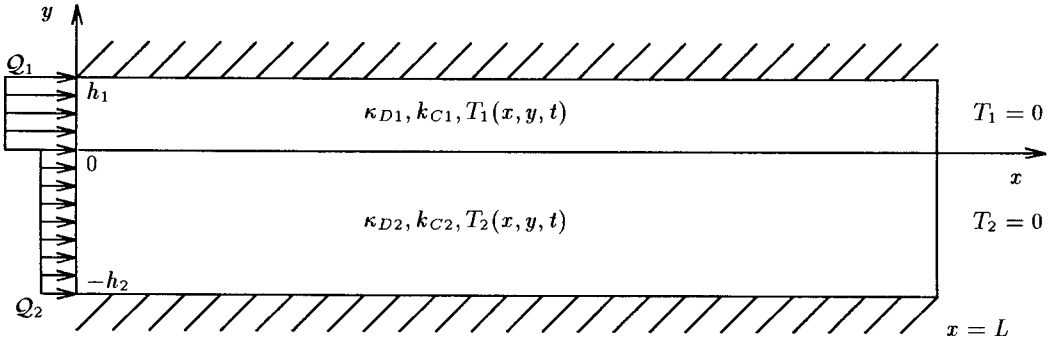

Figure 6.1 Flux Heated Bimaterial Long Beam

$$
\begin{aligned}
\frac{\partial T_1}{\partial x}(0,y,t) &= -\frac{\mathcal{Q}_1}{k_{C1}}, \quad 0 < y \leq h_1 \\
\frac{\partial T_2}{\partial x}(0,y,t) &= -\frac{\mathcal{Q}_2}{k_{C2}}, \quad 0 > y \geq -h_2 \\
T_1(L,y,t) &= 0, \quad 0 < y \leq h_1 \\
T_2(L,y,t) &= 0, \quad 0 > y \geq -h_2 \\
\frac{\partial T_1}{\partial y}(x,h_1,t) &= 0 \\
\frac{\partial T_2}{\partial y}(x,-h_2,t) &= 0 \\
T_1(x,0,t) &= T_2(x,0,t) \\
k_{C1}\frac{\partial T_1}{\partial y}(x,0,t) &= k_{C2}\frac{\partial T_2}{\partial y}(x,0,t)
\end{aligned}
$$

The last two boundary conditions will be referred to as matching conditions. Continuity of both temperature and flux implies perfect thermal contact along the interface between the two materials.

Özişik (50) provides an exact solution to this problem using integral transforms. The author has derived this solution using a slightly different approach. However, the resulting temperature distributions are given in terms of double Fourier series. For each eigenvalue in the x-direction, there are an infinite number of eigenvalues in the y-direction, a substantial number of which are small in magnitude. What this means is that large numbers of terms must be retained for accuracy, leading to numerical convergence difficulties. Numerous attempts were made to formulate approximate solutions based on characteristics observed from the exact solution. These attempts were successful only for steady state solutions (i. e. long time) and were dismissed. A different approach is therefore sought to provide meaningful insight into the role of transverse conduction in alleviating thermal stresses in bonded materials.

It is possible to formulate a one-dimensional solution which preserves the *flavor* of transverse conduction in the two-dimensional problem. This is accomplished by approximating the conduction heat transfer along the interface by some equivalent convection heat transfer. In other words, it is assumed that temperature is a function of x only, but with one medium losing heat to the other. The amount of heat lost to the other medium is

also assumed to be a function of x only. Thus, an apparent effect of transverse conduction is preserved. The convection heat transfer coefficient is approximated by the reciprocal of the thermal resistance of the layered medium (46:page 25). The approximate problem to be solved is described by the following equations:

$$\frac{\partial^2 \tilde{T}_1}{\partial \hat{x}^2} - \omega^2(\tilde{T}_1 - \tilde{T}_2) = \frac{\partial \tilde{T}_1}{\partial \hat{t}} \tag{6.3}$$

$$\frac{\partial^2 \tilde{T}_2}{\partial \hat{x}^2} + \frac{\omega^2}{\hat{h}\hat{k}_C}(\tilde{T}_1 - \tilde{T}_2) = \frac{1}{b^2}\frac{\partial \tilde{T}_2}{\partial \hat{t}} \tag{6.4}$$

$$\tilde{T}_1(\hat{x}, 0) = 0 \tag{6.5}$$

$$\tilde{T}_2(\hat{x}, 0) = 0 \tag{6.6}$$

$$\tilde{T}_1(1, \hat{t}) = 0 \tag{6.7}$$

$$\tilde{T}_2(1, \hat{t}) = 0 \tag{6.8}$$

$$\frac{\partial \tilde{T}_1}{\partial \hat{x}}(0, \hat{t}) = -1 \tag{6.9}$$

$$\frac{\partial \tilde{T}_2}{\partial \hat{x}}(0, \hat{t}) = -\frac{\hat{Q}}{\hat{k}_C} \tag{6.10}$$

where H, the effective convection heat transfer coefficient, is given by

$$H = \frac{k_{C2}}{h_2}\left(\frac{1}{1 + \hat{k}_C/\hat{h}}\right) = \frac{k_{C1}}{h_1}\left(\frac{1}{1 + \hat{h}/\hat{k}_C}\right) \tag{6.11}$$

and

$$\hat{x} = x/L \qquad \hat{t} = \kappa_{D1} t/L^2$$

$$\tilde{T}_1 = k_{C1} T_1/(\mathcal{Q}_1 L) \qquad \tilde{T}_2 = k_{C1} T_2/(\mathcal{Q}_1 L)$$

$$\omega^2 = HL^2/(h_1 k_{C1}) \qquad b^2 = \kappa_{D2}/\kappa_{D1}$$

We resort to the finite Fourier cosine transform to solve this problem. Let

$$\overline{T}_i(\gamma_m, \hat{t}) = \sqrt{2L}\int_0^1 \tilde{T}_i(\hat{x}, \hat{t}) \cos \gamma_m \hat{x}\, d\hat{x} \tag{6.12}$$

$$\tilde{T}_i(\hat{x}, \hat{t}) = \sqrt{\frac{2}{L}}\sum_{m=1}^{\infty} \overline{T}_i(\gamma_m, \hat{t}) \cos \gamma_m \hat{x} \tag{6.13}$$

where $\gamma_m = (2m-1)\pi/2$. Using this transformation, equations 6.3 and 6.4 reduce to

$$\frac{d\overline{T}_1}{d\hat{t}} = \sqrt{2L} + \omega^2\overline{T}_2 - (\omega^2 + \gamma_m^2)\overline{T}_1 \tag{6.14}$$

$$\frac{d\overline{T}_2}{d\hat{t}} = \frac{b^2\hat{Q}}{\hat{k}_C}\sqrt{2L} + \frac{b^2\omega^2}{\hat{h}\hat{k}_C}\overline{T}_1 - (\frac{b^2\omega^2}{\hat{h}\hat{k}_C} + b^2\gamma_m^2)\overline{T}_2 \tag{6.15}$$

Equations 6.14 and 6.15 are easily decoupled and solved subject to the initial conditions (equations 6.5 and 6.6). An equally valid approach is to write equations 6.14 and 6.15 as a first order system and solve the system using the matrix method for ordinary differential equations. Decoupling of the equations produces two second order equations which require initial values of both the transformed temperatures and their first derivatives. The derivatives are not specified in the original problem but are easily derived from equations 6.14 and 6.15. Going through this process, we find the temperatures to be given by

$$\tilde{T}_1(\hat{x},\hat{t}) = 2\sum_{m=1}^{\infty}\left[C_{1m}e^{\psi_{1m}\hat{t}} + C_{2m}e^{\psi_{2m}\hat{t}} + \frac{d_m}{c_m}\right]\cos\gamma_m\hat{x} \tag{6.16}$$

$$\tilde{T}_2(\hat{x},\hat{t}) = \frac{2}{\omega^2}\sum_{m=1}^{\infty}\left[D_{1m}e^{\psi_{1m}\hat{t}} + D_{2m}e^{\psi_{2m}\hat{t}} + \frac{d_m}{c_m}(\omega^2+\gamma_m^2) - 1\right]\cos\gamma_m\hat{x} \tag{6.17}$$

where ψ_{1m} and ψ_{2m} are roots of the characteristic equation

$$\psi_m^2 + b_m\psi_m + c_m = 0$$

and

$$b_m = \omega^2\left(1 + \frac{b^2}{\hat{h}\hat{k}_C}\right) + \gamma_m^2(1+b^2)$$

$$c_m = b^2\left\{\left(\frac{\omega^2}{\hat{h}\hat{k}_C} + \gamma_m^2\right)(\omega^2+\gamma_m^2) - \frac{\omega^4}{\hat{h}\hat{k}_C}\right\}$$

$$d_m = b^2\left\{\frac{\omega^2\hat{Q}}{\hat{k}_C} + \frac{\omega^2}{\hat{h}\hat{k}_C} + \gamma_m^2\right\}$$

$$C_{1m} = \frac{d_m\psi_{2m} + c_m}{c_m(\psi_{1m} - \psi_{2m})}$$

$$C_{2m} = -\frac{d_m\psi_{1m} + c_m}{c_m(\psi_{1m} - \psi_{2m})}$$

$$D_{1m} = C_{1m}[\psi_{1m} + \omega^2 + \gamma_m^2]$$

$$D_{2m} = C_{2m}[\psi_{2m} + \omega^2 + \gamma_m^2]$$

The convergence of these series solutions was verified by comparing the limit as $\hat{t} \to \infty$ with the analytical steady-state solution to equations 6.3 and 6.4, which is given by

$$\tilde{T}_1(\hat{x},\infty) = \left(\frac{\hat{Q}}{\hat{k}_C} - 1\right)\left[\frac{1}{R^2}\right]\left\{\frac{\sinh\,(\omega R(\hat{x}-1))}{\omega R\cosh\omega R} - (\hat{x}-1)\right\} - (\hat{x}-1) \tag{6.18}$$

$$\tilde{T}_2(\hat{x},\infty) = \left(\frac{\hat{Q}}{\hat{k}_C} - 1\right)\left[\frac{1}{\hat{h}\hat{k}_C R^2}\right]\left\{-\frac{\sinh\,(\omega R(\hat{x}-1))}{\omega R\cosh\omega R} + (\hat{x}-1)\right\} - \frac{\hat{Q}}{\hat{k}_C}(\hat{x}-1) \tag{6.19}$$

where $R = 1 + 1/(\hat{h}\hat{k}_C)$.

If the interface is insulated (i. e. $\omega = 0$), the resulting temperature distribution is one-dimensional and is given by

$$\tilde{T}_1(\hat{x},\hat{t}) = 2\sum_{m=1}^{\infty}\frac{1-e^{-\gamma_m^2\hat{t}}}{\gamma_m^2}\cos\gamma_m\hat{x} \tag{6.20}$$

$$\tilde{T}_2(\hat{x},\hat{t}) = 2\frac{\hat{Q}}{\hat{k}_C}\sum_{m=1}^{\infty}\frac{1-e^{-b^2\gamma_m^2\hat{t}}}{\gamma_m^2}\cos\gamma_m\hat{x} \tag{6.21}$$

Note that equations 6.20 and 6.21 are the solutions to equations 6.3 and 6.4, respectively, with $\omega = 0$. Although the series

$$\sum_{m=1}^{\infty}\frac{1}{\gamma_m^2}\cos\gamma_m\hat{x} \tag{6.22}$$

is not twice differentiable term-by-term, it may be shown that

$$\sum_{m=1}^{\infty}\frac{1}{\gamma_m^2}\cos\gamma_m\hat{x} = \frac{1}{2}(1-\hat{x}) \tag{6.23}$$

Therefore, the insulated interface temperature distribution may also be written in the following manner:

$$\tilde{T}_1(\hat{x},\hat{t}) = -(\hat{x}-1) - 2\sum_{m=1}^{\infty}\frac{e^{-\gamma_m^2\hat{t}}}{\gamma_m^2}\cos\gamma_m\hat{x} \tag{6.24}$$

$$\tilde{T}_2(\hat{x},\hat{t}) \;=\; -\frac{\hat{Q}}{\hat{k}_C}(\hat{x}-1) - 2\frac{\hat{Q}}{\hat{k}_C}\sum_{m=1}^{\infty}\frac{e^{-b^2\gamma_m^2\hat{t}}}{\gamma_m^2}\cos\gamma_m\hat{x} \qquad (6.25)$$

The time-independent portions of these functions are the steady-state solutions to the insulated interface problem. Convergence to the steady-state solution is easily verified by taking the limit of equations 6.24 and 6.25 as $\hat{t} \rightarrow \infty$. Figure 6.2 shows the layer-wise temperature difference in the layers of a bimaterial beam with a convection interface condition and an insulated interface condition.

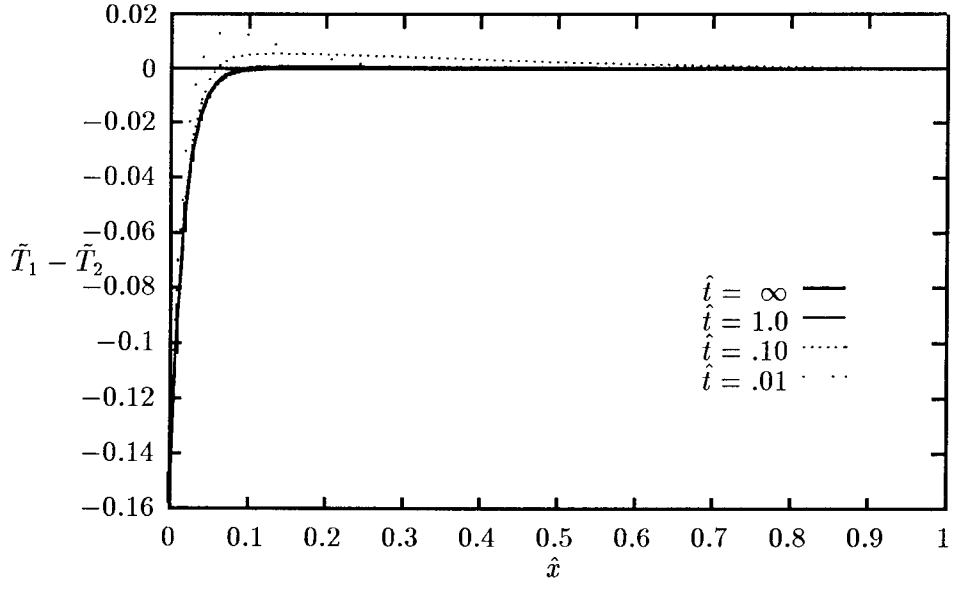

(a) Convection Along the Interface: $b^2 = .1, \omega^2 = 100, \hat{h}\hat{k}_C = .1/3, \hat{h}\hat{Q} = 1/3.$

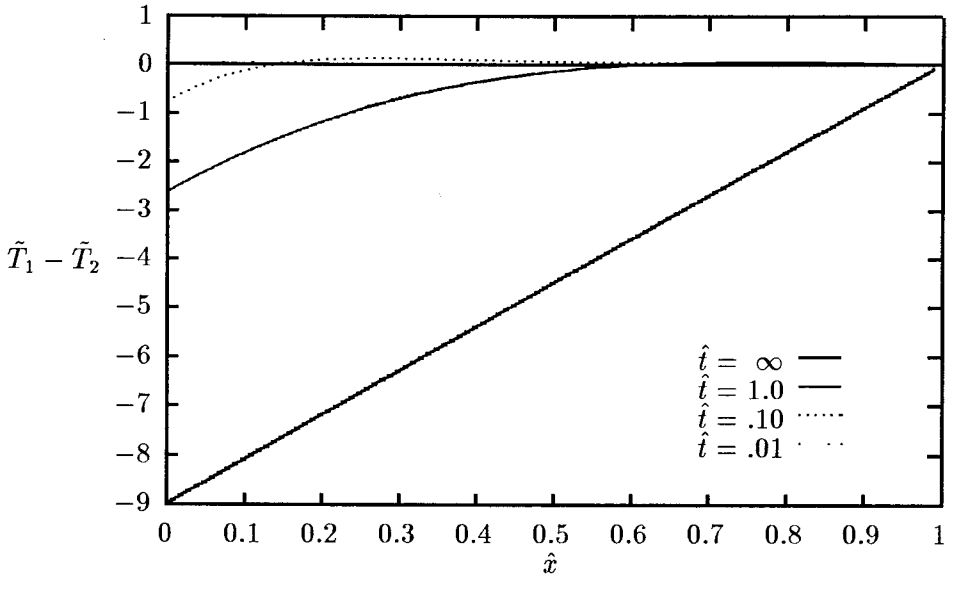

(b) Insulated Interface: $\omega^2 = 0.$

Figure 6.2 Temperature difference, $\tilde{T}_1 - \tilde{T}_2$, between layers of a finite bimaterial beam, with and without transverse conduction heat transfer along the interface. Plotted as a function of $\hat{x} = x/L$, with nondimensional time, $\hat{t}$, as a parameter. Note that $\hat{t} = \infty$ corresponds to the steady-state solution.

As stated earlier, it is reasonable to assume that the point-by-point temperature difference ($\Delta T(x)$) in a bimaterial beam with transverse conduction along the interface is lower than $\Delta T(x)$ of the same beam with an insulated interface. This assumption can be proven for the steady-state problem. Let $\Delta\tilde{T}_{\omega=0}$ and $\Delta\tilde{T}_{\omega\neq 0}$ represent the layerwise temperature difference $(\tilde{T}_1 - \tilde{T}_2)$ for the insulated and conducting interface problems, respectively. Subtracting the steady-state components of equations 6.20 and 6.21, we obtain

$$\Delta\tilde{T}_{\omega=0} = -2\left(\frac{\hat{Q}}{\hat{k}_C} - 1\right)\sum_{m=1}^{\infty}\frac{\cos\gamma_m\hat{x}}{\gamma_m^2} \tag{6.26}$$

Subtracting equation 6.19 from equation 6.18 and expanding the resulting function into a Fourier cosine series, we obtain

$$\Delta\tilde{T}_{\omega\neq 0} = -2\left(\frac{\hat{Q}}{\hat{k}_C} - 1\right)\sum_{m=1}^{\infty}\frac{\cos\gamma_m\hat{x}}{\gamma_m^2 + \omega^2\left(1 + 1/(\hat{h}\hat{k}_C)\right)} \tag{6.27}$$

Comparing equations 6.26 and 6.27, we see that

$$\Delta\tilde{T}_{\omega=0}(\hat{x}) < \Delta\tilde{T}_{\omega\neq 0}(\hat{x}) \tag{6.28}$$

for all nonzero values of ω.

Figure 6.2 suggests that similar behavior occurs in the transient problem. For example, the maximum temperature in both beams is at $x = 0$ and $t = \infty$. Figure 6.2(a) shows that $\Delta\tilde{T}(0,\infty) \approx -0.16$ for a bimaterial beam with transverse conduction along the interface. Figure 6.2(b) shows that $\Delta\tilde{T}(0,\infty) = -9.0$ for the same beam with an insulated interface. (These plots are both on the same scale.) We see therefore that two-dimensional heat transfer lowers the maximum layerwise temperature difference by about ninety-eight percent! Figure 6.2(a) also suggests that thermal equilibrium is achieved near the heated end of the beam with interface conduction. In other words, $\Delta\tilde{T} \approx 0$ over most of the length of this beam.

As we have just shown, the layer-wise temperature distribution in a heated bimaterial beam with interface conduction (modeled as equivalent convection) is easily obtained for a beam of finite length using the Fourier cosine transformation. Attempts to obtain a closed

form solution for the temperature distribution in a semi-infinite bimaterial beam with the same interface conditions were unsuccessful. However, if it were somehow possible to model the semi-infinite *bimaterial* beam as an equivalent *homogeneous* beam, the temperature distribution is the well-known insulated rod solution.

The example problem suggested that $\tilde{T}_1 \approx \tilde{T}_2$ over most of the length of a finite bimaterial beam with conduction along the interface. If this is true for finite beams, it should also hold for semi-infinite beams. Therefore, it is proposed that the temperature distribution in the semi-infinite beam be determined by analyzing an equivalent homogeneous beam where $T_1 = T_2$. Note that the equivalent homogeneous model is used only to obtain a closed form expression for the temperature distribution. When calculating the stresses due to this temperature distribution, the beam is analyzed as a bimaterial beam. This approximation allows us to obtain a closed form solution for the thermal stresses, from which we are able to estimate the error in the stress distribution when two-dimensional heat conduction is ignored. The thermally equivalent problem is formulated by taking the flux, conductivity and product of density and specific heat to be weighted averages, with layer thickness being the weight factor:

$$\begin{aligned} \overline{Q} &= Q_1 \frac{1+\hat{Q}\hat{h}}{1+\hat{h}} \\ \overline{k}_C &= k_{C1} \frac{1+\hat{k}_C\hat{h}}{1+\hat{h}} \\ \overline{\rho C_p} &= \rho_1 C_{p1} \frac{1+\hat{\rho}\hat{C}_p\hat{h}}{1+\hat{h}} \end{aligned}$$

The equivalent thermal diffusivity is then given by

$$\overline{\kappa}_D = \overline{k}_C / (\overline{\rho C_p}) = \kappa_{D1} \left(\frac{1+\hat{k}_C\hat{h}}{1+\hat{\kappa}_D\hat{h}/\hat{k}_C} \right) \tag{6.29}$$

Using these equivalent thermal properties, the average temperature distribution in a finite beam may be written as

$$\hat{T} = 2 \frac{1+\hat{Q}\hat{h}}{1+\hat{k}_C\hat{h}} \sum_{m=1}^{\infty} \frac{1-e^{-K\gamma_m^2\hat{t}}}{\gamma_m^2} \cos\gamma_m\hat{x} \tag{6.30}$$

where $\hat{T} = k_{C1}T/(Q_1 L)$ and $K = \overline{\kappa}_D/\kappa_{D1}$. Once the average temperature distribution is obtained in this manner, the stresses may then be calculated using the solution technique given in Chapter III.

The temperature distribution in a semi-infinite layered beam with an insulated interface is given by equations 4.21 and 4.22. Using the weighted average concept discussed above, we may write the average temperature distribution as

$$\bar{T}(x,t) = \sqrt{K}\frac{1+\hat{h}\hat{Q}}{1+\hat{h}}\frac{Q_1 b}{k_{C1}}\left\{\frac{1}{\sqrt{\pi}}e^{-\bar{x}^2} - \bar{x}\ \text{erfc}\ \bar{x}\right\} \tag{6.31}$$

where $\bar{x} = x/(b\sqrt{K})$. The interlaminar shearing force is calculated by substituting equation 6.31 into equation 3.30. After making the substitution and going through the algebra, we arrive at the following result:

$$\hat{Q}_{\text{cond}} = \left\{\left[1 - \frac{\hat{A}\hat{k}_C}{\hat{Q}}\right] K^{3/2}\frac{1+\hat{h}\hat{Q}}{1+\hat{h}\hat{k}_C}\right\}\hat{Q}_{\text{ins}} \tag{6.32}$$

In this equation, the subscripts on $\hat{Q}$ denote the solutions with interface conduction (modeled as equivalent convection) and with no interface conduction. The forces and stresses for the insulated interface condition are given by equations 4.24-4.27. In order to calculate the corresponding quantities when interface conduction is considered, we need only multiply the insulated interface quantities by the scale factor given in equation 6.32. The magnitude of this scale factor is determined by the values of the parameters, $K, \hat{k}_C, \hat{Q}$, and $\hat{A}$.

Suppose we were using the current approach to assess the magnitude of thermal-induced stresses in graphite/epoxy laminates subjected to 10.6μ laser radiation. The ratio of boundary heat fluxes is determined by the ratio of the different coefficients of absorption of the constituent materials. In this case the constituent materials are graphite fibers and epoxy, both of which are very good absorbers at 10.6μ. Therefore, for most problems involving graphite/epoxy or other commonly used structural composites, very little error is introduced by prescribing $\hat{Q}$ to be unity. In fact, this assumption could be made with confidence for most nonmetallic composites provided the incident laser beam is infrared. If the volume fraction of the graphite/epoxy laminate is .75, it can be shown that $\hat{h} = 1/3$.

With these values of $\hat{Q}$ and $\hat{h}$, equation 6.32 becomes

$$\hat{Q}_{\text{cond}} = \frac{1}{2}(1 - \hat{A}\hat{k}_C)\sqrt{3 + \hat{k}_C}\,\hat{Q}_{\text{ins}} \tag{6.33}$$

Graphite fibers are much better conductors than epoxy, implying that $\hat{k}_C$ is very small for graphite/epoxy laminates. In the event that $\hat{k}_C$ is negligible, we have

$$\hat{Q}_{\text{cond}} \approx \frac{\sqrt{3}}{2}\,\hat{Q}_{\text{ins}} \tag{6.34}$$

Through this analysis we have seen that the insulated interface solutions presented in Chapter IV overestimate the actual solutions (incorporating the effects of transverse conduction) by something on the order of twenty percent for one specified set of material properties.

6.2 Multiple-Layered Beams

We now consider a semi-infinite composite beam of finite thickness consisting of N discrete layers of material, each of which is made up by a layer of fiber material embedded between two layers of matrix material. The total thickness of the beam is $h = h_1 + h_2$, where h_1 and h_2 are the total fiber and matrix thicknesses. We propose to study what effect N has on the thermal stresses. Note that as N is varied, the total beam thickness remains constant. Therefore, N is inversely proportional to the thickness of the fiber and matrix sublayers.

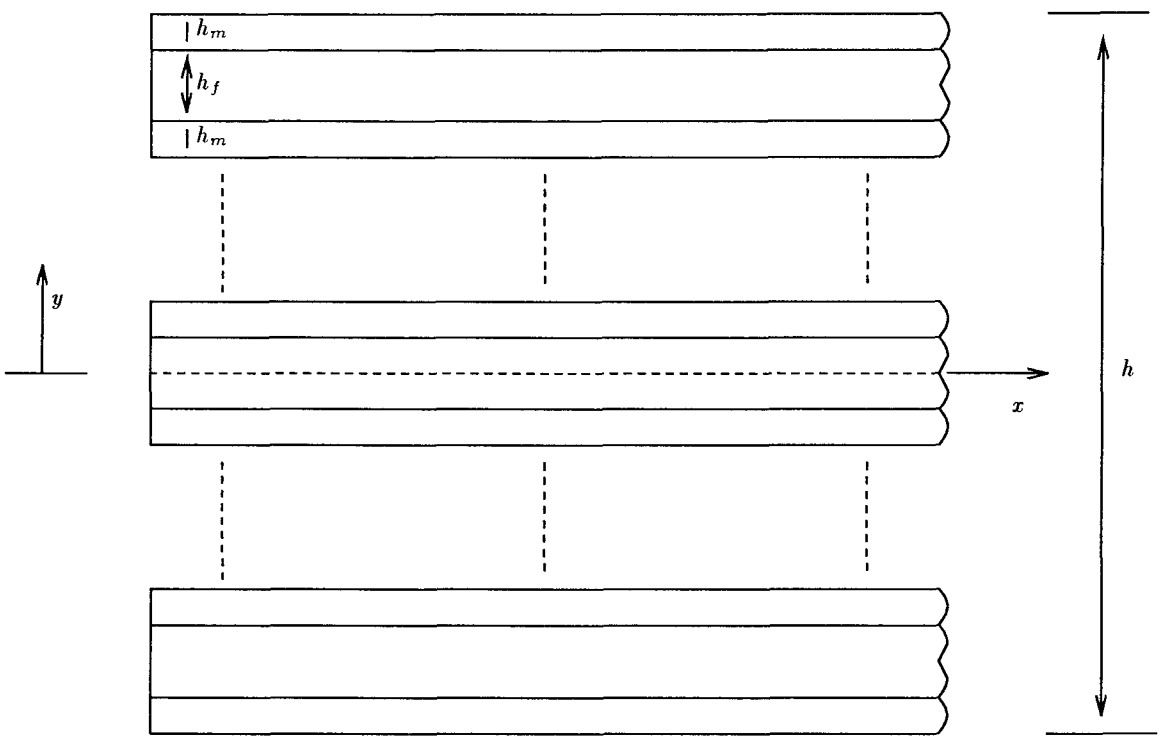

Figure 6.3 A unidirectional composite beam with an alternating stack of matrix and fiber material. There is a total of N layers in the stack, where N is an odd integer.

For the present analysis, it suffices to consider a simple temperature distribution in which the temperature in the fiber layers decays exponentially while the temperature in the matrix layers remains constant. The reference temperature will be taken to be zero for convenience. Given a value for N, the various thicknesses in the model are related by

$$\begin{aligned} h_m &= \frac{2h_2}{N+1} \\ h_f &= \frac{2h_1}{N-1} \end{aligned}$$

The governing differential equation for the interlaminar shear force is given by equation 3.30:

$$Q_N''(x) - k_N^2 Q_N(x) = \frac{N+1}{N-1}[\alpha_1 T_1(x,t) - \alpha_2 T_2(x,t)] \tag{6.35}$$

where Q_N is the resultant interlaminar shearing force in any fiber layer when there are N total layers of material, and

$$k_N^2 = \frac{N+1}{N-1}\frac{\Lambda_N}{\kappa_N} \tag{6.36}$$

$$\Lambda_N = \frac{N-1}{2}\left(\frac{1}{h_1 E_1} + \frac{1}{h_2 E_2}\right) \tag{6.37}$$

$$\kappa_N = \frac{4}{3}\left(\frac{h_2}{(N+1)E_2} + \frac{h_1}{2(N-1)E_1}\right) \tag{6.38}$$

If Q_m denotes the resultant interlaminar shearing force in any matrix layer, then

$$Q_m = \frac{N-1}{N+1} Q_N \tag{6.39}$$

As before, the force and resulting interlaminar stresses are time dependent only in the sense that the temperatures are allowed to be time dependent. To apply this solution to a problem, we look at the problem where the temperature in the fibers decays exponentially while the matrix temperature remains at zero. Let $T_1 = T_{01}e^{-\eta x}$ and $T_2 = 0$. The interlaminar shear force, interlaminar stresses and the concentrated corner forces are given by

$$\hat{Q}_N = \frac{N+1}{N-1}\frac{\kappa_3}{\kappa_N}\left[\frac{1}{\delta_1^2 - (k_N/k_3)^2}\right]\left[e^{-\delta_1 \hat{x}} - e^{-(k_N/k_3)\hat{x}}\right] \tag{6.40}$$

$$\hat{q}_N = \frac{\kappa_3}{\kappa_N}\left[\frac{1}{\delta_1^2-(k_N/k_3)^2}\right]\left[-\delta_1 e^{-\delta_1\hat{x}}+\frac{k_N}{k_3}e^{-(k_N/k_3)\hat{x}}\right] \tag{6.41}$$

$$\hat{p}_N = \frac{1}{N+1}\frac{\kappa_3}{\kappa_N}\left[\frac{1}{\delta_1^2-(k_N/k_3)^2}\right]\left[-\delta_1^2 e^{-\delta_1\hat{x}}+\left(\frac{k_N}{k_3}\right)^2 e^{-(k_N/k_3)\hat{x}}\right] \tag{6.42}$$

$$\hat{P}_{N_0} = -\frac{1}{N+1}\frac{\kappa_3}{\kappa_N}\left[\frac{1}{\delta_1+k_N/k_3}\right] \tag{6.43}$$

where

$$\begin{aligned} A_1 &= \frac{\alpha_1 T_{01}}{\kappa_3} \\ \hat{Q}_N &= \frac{k_3^2}{A_1}Q_N \\ \hat{q}_N &= \frac{k_3}{A_1}q_N \\ \hat{p}_N &= \frac{1}{h_2 A_1}p_N \\ \hat{x} &= k_3 x \end{aligned}$$

and the various quantities are nondimensionalized with respect to the 3–layer solution. The κ and k ratios in the above equations may be written in terms of $N, B = \hat{E}\hat{h}$ and $\hat{h}$. The result is

$$\frac{\kappa_3}{\kappa_N} = \frac{(B+\hat{h}^2)(N^2-1)}{2B(N+1)+4(N-1)\hat{h}^2} \tag{6.44}$$

$$\frac{k_N}{k_3} = \frac{1}{2}\sqrt{\frac{(N+1)(N-1)^2(B+\hat{h}^2)}{B(N+1)+2(N-1)\hat{h}^2}} \tag{6.45}$$

It may easily be shown that

$$\lim_{N\to\infty}\frac{\kappa_3}{\kappa_N}\left[\frac{1}{\delta_1^2-(k_N/k_3)^2}\right] = 0 \tag{6.46}$$

Therefore, $\hat{Q}_N$ vanishes everywhere as N becomes infinite, as suggested by Figure 6.4. The interlaminar stresses, on the other hand, go to zero everywhere except at the corner as N becomes infinite. Taking the limit of the corner shear stress as N goes to infinity, we obtain

$$\lim_{N\to\infty}\hat{q}_N(0) = -\sqrt{\frac{B+\hat{h}^2}{B+2\hat{h}^2}} \tag{6.47}$$

which is easily seen to be about -1 for most values of B and $\hat{h}$. The greatest value it can reach is $-1/\sqrt{2}$ when $B = 0$. Taking the limit of the corner peeling stress as N goes to infinity, we obtain

$$\lim_{N\to\infty} \hat{p}_N(0) = -\frac{1}{2} \tag{6.48}$$

Equations 6.40 through 6.43 are plotted in Figures 6.4 through 6.7.

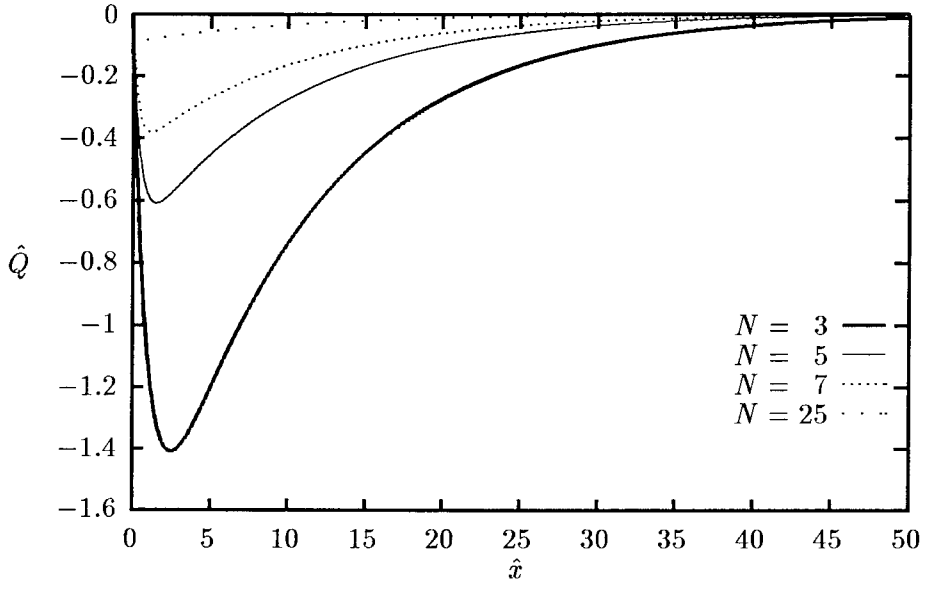

(a) $\delta_1 = .1$

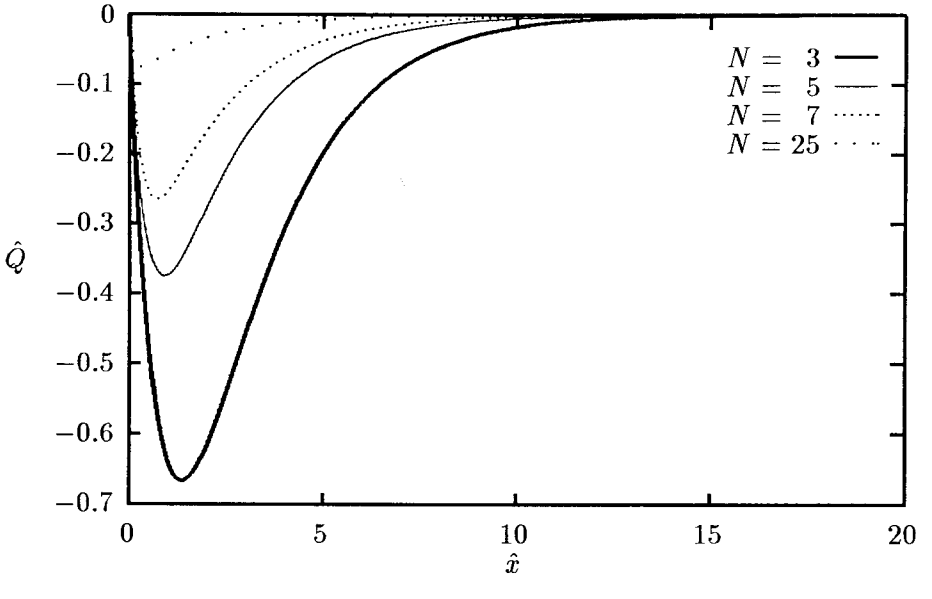

(b) $\delta_1 = .5$

Figure 6.4 Nondimensional resultant axial force, equation 6.40, with $T_1 = T_{01}e^{-\delta_1 k_3 x}$, $T_2 = 0$. Plotted for various values of N, the number of layers in the model, with δ_1 being the temperature decay rate in the fiber layers.

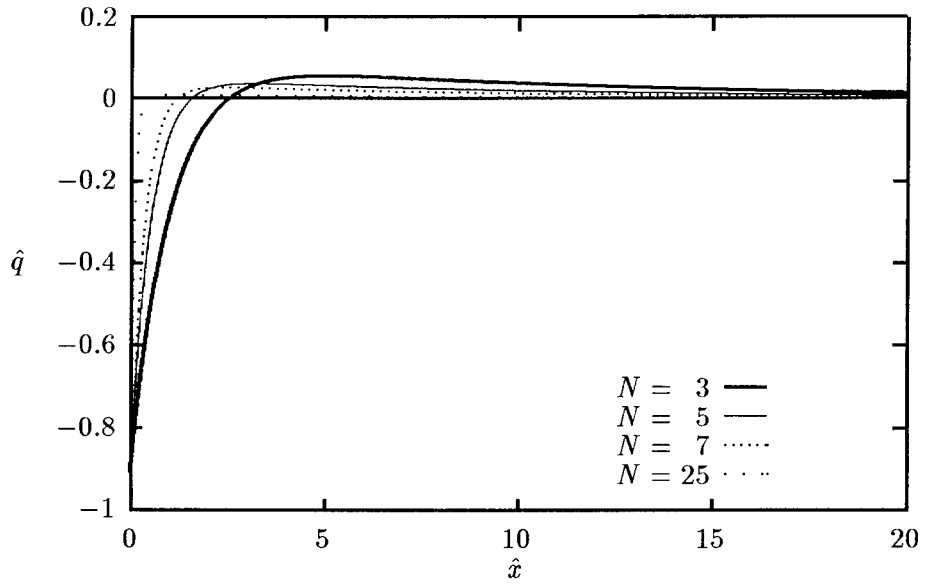

(a) $\delta_1 = .1$

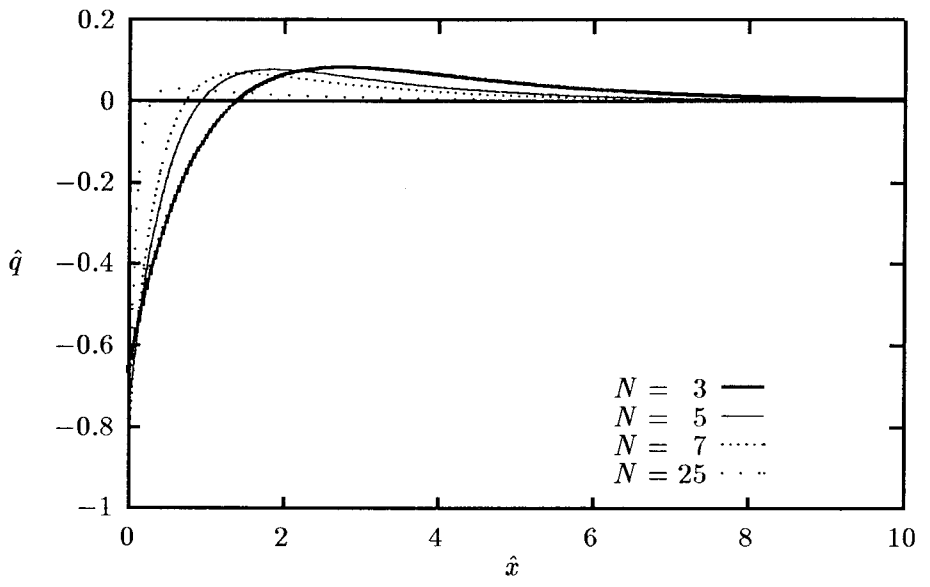

(b) $\delta_1 = .5$

Figure 6.5 Nondimensional interlaminar shear stress, equation 6.41, with $T_1 = T_{01}e^{-\delta_1 k_3 x}$, $T_2 = 0$. Plotted for various values of N, the number of layers in the model, with δ_1 being the temperature decay rate in the fiber layers.

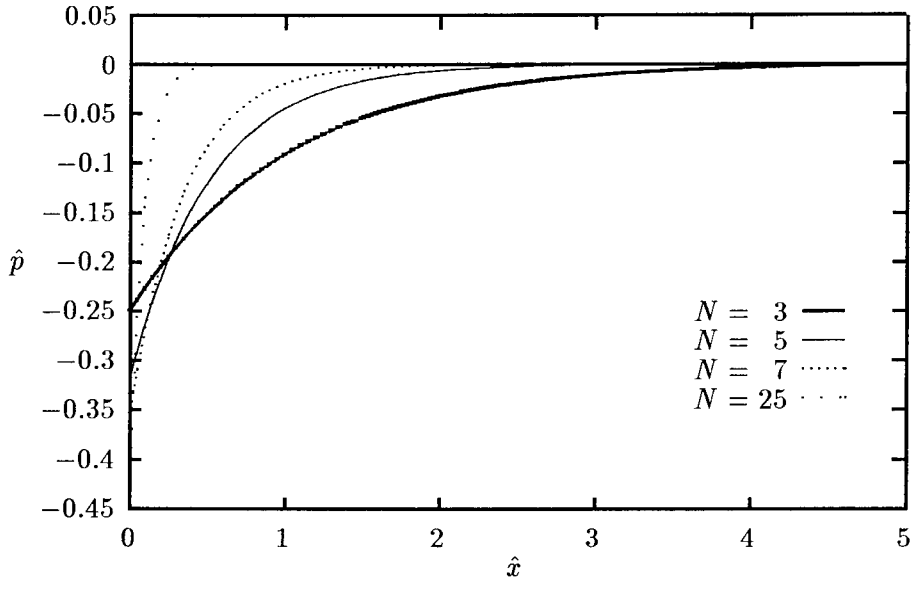

(a) $\delta_1 = .1$

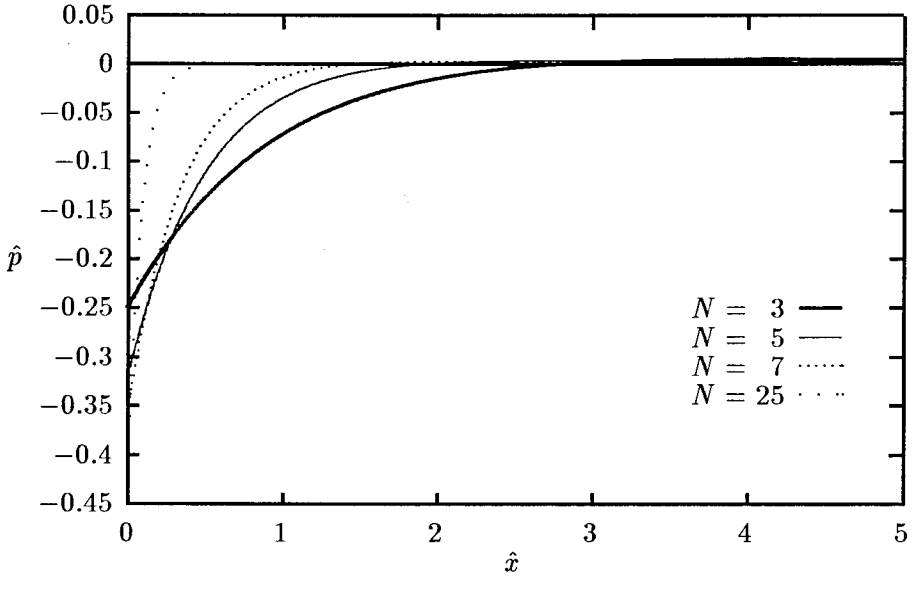

(b) $\delta_1 = .5$

Figure 6.6 Nondimensional interlaminar normal stress, equation 6.42, with $T_1 = T_{01}e^{-\delta_1 k_3 x}$, $T_2 = 0$. Plotted for various values of N, the number of layers in the model, with δ_1 being the temperature decay rate in the fiber layers.

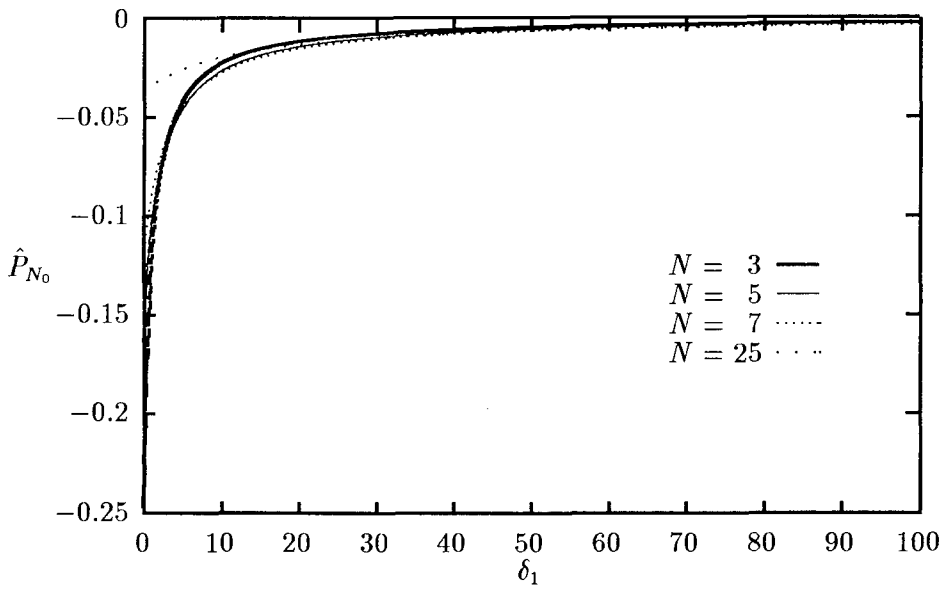

Figure 6.7 Nondimensional concentrated corner force, equation 6.7, with $T_1 = T_{01}e^{-\delta_1 k_3 x}, T_2 = 0$. Plotted as a function of δ_1, the temperature decay rate in the fiber layers, for various values of N, the number of layers in the model.

As shown both in the above figures and in the analysis of the equations, the interlaminar shearing force and the interlaminar stresses approach zero as the number of layers increases. This is true everywhere for the shearing force and it is true for the stresses everywhere but at the corner point. The predicted interlaminar stresses should diminish as N increases, as illustrated by the following simple argument. As N increases, the total amount of fiber and matrix material doesn't change, but the number of interlaminar interfaces increases. The total amount of thermal energy in the system remains constant throughout the analysis. If $N = 3$ we have one layer of fiber material embedded between two matrix layers. Suppose this fiber layer were allowed to freely expand. The amount of force required to compress it back to its original length is given by

$$F = h_f E \alpha T \tag{6.49}$$

where h_f is the total fiber thickness. If the material is then divided up into N layers, there are $(N-1)$ interfaces between the two constituents. The total force given by equation 6.49 must be resisted by interlaminar shearing stresses distributed over all of the interfaces. The interlaminar shearing stress, τ, is then given by

$$\tau = \frac{h_f E \alpha T}{(N-1)L} \tag{6.50}$$

which vanishes as N goes to infinity. Typically, the diameter of fibers in a fiber-reinforced composite laminate is very small compared to the laminate thickness. If, in our multiple layer model, the thickness of the fiber sublayers was chosen to be about one fiber diameter, this would equate to a large value for N. Correspondingly, our analysis shows that the thermal stresses would be negligible except very near the edge where the solution is not applicable.

6.3 Summary

As suspected, the inclusion of two-dimensional heat transfer and multiple layers into our model has a definite impact on the magnitude of thermal stresses calculated using the model. In particular, it was shown that the thermal stresses in one specific bimaterial beam with an insulated interface are on the order of twenty percent higher that those in the same beam with two-dimensional conduction across the interface. It was shown that the number of discrete layers used to model a nonhomogeneous beam of finite thickness had a much more pronounced impact on the magnitude of the thermal stresses. In fact, the stresses were shown to approach zero (everywhere except at the end of the beam) as the number of layers in the model became large. The implications of this finding on the utility of our solution are discussed in the concluding chapter.

VII. Concluding Comments

7.1 Review

This work began as a result of the author's research into potential mechanisms responsible for the failure of composite pressure vessels subjected to high energy laser irradiation. Various researchers analyzed the overall problem, but none of them addressed the role of thermal transport in the fiber direction and the ensuing thermal stresses. The present author worked with many of the same researchers on materials characterization programs, in which it was observed that heat conducted away from the irradiated area was substantial. So much, in fact, that material heats of ablation (Q^*) calculated from experimental data were falsely inflated when heat loss from the irradiated area by conduction into the surrounding material was not accounted for. For example, it was not uncommon for the experimental data to predict Q^* values of 100 (kJ/gm) for carbon based composites, whereas the actual value was known to be about 30 (kJ/gm). Since the coupon experiments showed heat loss via conduction away from the heated area to be significant, and the large-scale failure analyses ignored this phenomenon, it was decided to pursue a solution capable of assisting researchers in determining the effects of thermal stresses in such problems. The problem of thermal stresses in end-heated layered beams was proposed as a suitable model for providing meaningful insight into the outcome of the more complicated problem.

A literature review was then conducted to assess the current state-of-the-art knowledge of thermal stresses in layered beams. The results of the review were documented in Chapter II, and they show that surprisingly little work has been done in the area of obtaining simple closed-form solutions to layered composite beams subjected to the type of temperature distribution found in typical laser interaction problems. In particular, no solutions were found in the literature for the thermal stresses in semi-infinite (or very long) layered beams with decaying temperature distributions. There was one solution, however, the one due to Suhir (32), which appeared to be applicable to the current problem provided certain assumptions could be made. By incorporating the concept of interfacial compliance, Suhir was able to extend Timoshenko's classical bimetallic thermostat solution to account for prescribed normal stresses on the ends and for the presence of interlaminar stresses

near the ends. Suhir's solution was limited, however, to bimetallic strips (or beams) of finite length subjected to a uniform temperature change.

Suhir's solution technique was presented in Chapter III and was extended to apply to semi-infinite beams with nonuniform temperature distributions. The only limitations on the temperature distribution are that it be differentiable and decay to zero at infinity. It was shown that Suhir's *interfacial shear compliance coefficient* was applicable to semi-infinite strips and beams with stress-free end loads if the temperature was of a decaying nature and vanished at infinity. It is important to note that the semi-infinite beam with a uniform temperature distribution is not a special case of the solution and cannot be treated using Suhir's interfacial compliance coefficient. Using the extended technique, it was possible to write the resultant interlaminar shearing force as the solution to a second order ordinary differential equation with prescribed boundary conditions. Closed-form solutions for the thermal stresses could then be obtained for any temperature distribution for which a particular solution to the governing differential equation was available in closed form. The solutions presented in Chapter III were all written in terms of a generic particular solution.

The extended solution technique presented in Chapter III was applied to problems with specified temperature distributions in Chapter IV. At first a very simple problem with exponentially decaying, steady state temperatures was solved. The results of this exercise were very encouraging since a closed form solution to the governing differential equation was easily obtained. The solution technique was then applied to a layered beam in which the temperature in each layer was given by the time-dependent insulated rod solution, a much more complicated function than the simple exponentially decaying function considered earlier. By using the method of variation of parameters, a closed-form solution was found for complicated temperature distributions of this type. Finally, the method was applied to a beam of infinite length with a heat source at the origin. All the results presented in Chapter IV were nondimensional and were therefore applicable to any combination of materials meeting the underlying assumptions.

While the nondimensional solutions of Chapter IV covered a multitude of material combinations and heat loads, they were insufficient for making failure predictions due to the

presence of St Venant boundary layer effects. Since the solutions were based on Bernoulli-Euler beam theory which is inaccurate within about one beam thickness of the ends, it was not clear from the nondimensional results whether or not stresses of sufficient magnitude to cause failure existed anywhere outside of the boundary layer. Several numerical examples were then considered to determine the solution's utility in making failure predictions.

From these examples, it was concluded that significant normal (i. e. axial and bending) stresses occur in layered beams outside the St Venant boundary layer if at least one of the layers is a good thermal conductor. Thermal diffusivity was shown to be the key parameter in establishing how far into the beam significant stresses exist at a specific point in time. Thermal conductivity was shown to contribute more to the magnitude of stresses than to their extent into the beam. It was also concluded from the example problems that the solution is not very useful in the analysis of layered beams if all the layers are poor diffusers. In such a problem, very high stresses develop, but they are limited to the St Venant boundary layer region of the beam, where the present strength of materials solution technique is not applicable. In all of the example problems, the interlaminar stresses were found to be insignificant outside the boundary layer region when compared to the axial stresses. In every example where mechanical failure was deemed likely, it was predicted to be via tension or compression in one of the constituent layers. A very simple strength of materials failure criterion was employed. If the axial stress was found to exceed the strength (in compression or tension) in either of the constituent layers, it was then concluded that failure occurred in that layer.

It was determined from the example problems that the thermal stresses are of sufficient magnitude to cause failure outside of the St Venant boundary layer in a bimaterial beam made of a good conductor bonded to a poor conductor of similar stiffness. For the specific examples considered, it was concluded that the poor conductor would fail long before the good conductor. However, it was shown that the stresses would be lower (and the predicted time-to-failure longer) in the poor conductor if its thickness is decreased while the total beam thickness is held constant. The effects of this thickness variation were just the opposite in the good conductor. That is, as the thickness of the poor conductor was decreased, the stresses were found to be higher (and the time-to-failure shorter) in the good

conductor. It was shown that, if the stiffnesses of the constituent layers differed greatly, the end temperature of the materials would reach the melting or ablation temperature before stresses sufficient of causing failure developed outside the boundary layer. In such cases the failure was referred to as *thermal failure* as opposed to *mechanical failure.*

Two simplifying assumptions were addressed in Chapter VI in an attempt to understand the extent of their effect on the thermal stresses: the role of two-dimensional heat transfer in thin bonded layers, and the effect of the number of discrete layers used to model a laminate of fixed thickness. It was shown for a specific example that the thermal stresses in a bimaterial beam with two-dimensional heat transfer along the interface were about twenty percent lower than the stresses in an identical beam with an insulated interface. These results were obtained by performing a pseudo two-dimensional analysis in which transverse conduction was modeled as equivalent convection. It was concluded from this analysis that the temperature distribution in a long, thin bimaterial beam (or strip) with the prescribed thermal boundary conditions is accurately approximated by the solution to another problem in which a single-layered beam with the appropriate average thermal properties is subjected to the same thermal conditions. This approximation was shown to be very good everywhere except at the heated end of the beam, and especially good outside of the St Venant boundary layer. These findings suggest the presence of a sort of *thermal* St Venant boundary layer and that its length is shorter than that of the *mechanical* St Venant boundary layer.

The stresses were shown in Chapter VI to be inversely proportional to the number of discrete layers used to model a composite beam of fixed thickness. This finding suggests that the solution is not suitable for use in micromechanical models of unidirectional fiber-reinforced composite materials. The reason is that the thickness of fiber sublayers must approach individual fiber diameters in such a model. Typical fibers are relatively small in diameter, implying that the discrete layer model of a lamina may contain many layers.

7.2 Validity of the Solution

As noted earlier, very few solutions were found in the literature dealing with thermal stresses in layered beams subjected to the types of temperature variations considered in

the present work. The solution is based on the work by Suhir (32), which is in turn based on Timoshenko's classical bimetallic thermostat solution. The validity of Suhir's solution outside of the St Venant boundary layer was established by Suhir in (32) and was later confirmed numerically by Kuo's finite element solution (35). Therefore, one means of establishing the validity of the present solution is to show agreement with Suhir's solution.

Although Suhir published his solution for uniform temperature distributions, the key idea in his solution is that of using an interfacial compliance coefficient to provide a *correction factor* to the equation for the interfacial strain in a layered beam with a nonuniform interlaminar shearing stress distribution. The interfacial compliance coefficient is derived from an exact solution in elasticity, the Ribière solution, which is applicable to a strip of finite length loaded in shear on one face with the shear load being symmetric about the midlength of the strip. The layered beam subjected to uniform temperature change is a special case of this problem. The concept, however, is applicable to a beam with nonuniform temperature change if the temperature distribution is symmetric about the midlength of the beam.

The present solution was shown in Chapter IV to be in excellent agreement with Suhir's solution for both cubic and exponential temperature distributions (see Figures 4.11 and 4.12). Also, it is known that the temperature distribution in a semi-infinite rod at early time is the same as that in a sufficiently long rod of finite length at the same value of time. The solution to the governing differential equation (equation 3.30) is, however, easier to obtain in the finite problem because the temperature in the finite problem is available as a Fourier series. This is in contrast to the semi-infinite problem which requires the evaluation of complicated integrals required by the method of variation of parameters. The present solution (equations 4.24-4.27) was compared to the Fourier series solution at several points in time, and was found to be in excellent agreement.

The similarities and differences in the behavior of the solution for fixed end temperature (equations 4.11-4.16) and fixed end flux (equations 4.24-4.27) boundary conditions in the semi-infinite beam suggest that the solution is valid. For example, a comparison of Figures 4.1(a) and 4.6(a) reveals that $\hat{Q}$ (and therefore σ_x) has relatively large magnitude farther away from the edge when δ_1 decreases, and that the same trend exists in the time-

dependent solution as time (or ϕ) increases. Comparing Figures 4.1(b) and 4.1(c) with Figures 4.6(b) and 4.6(c), we see that the interlaminar stresses display the same similarity as $\hat{Q}$. These observations are meaningful because, although the thermal boundary conditions in the two cases are different, similarities exist in the temperature distributions and in the amount of thermal energy deposited into the layered beam. There are no applied mechanical loads, implying that all stresses must be a result of the heating. Therefore, similar temperature distributions should lead to similar stress distributions, and this is suggested by comparisons such as the one addressed above.

Another indication of the solution validity is that it satisfies both the governing differential equation and the boundary conditions. As shown in Chapter III, the interlaminar shearing stress, $q(x)$, is the first derivative of the resultant interlaminar shearing force, $Q(x)$, and the peeling stress is a multiple of the second derivative of $Q(x)$. The plots included in Chapter IV confirm these relationships. Figures 4.1-4.3 and 4.6-4.8 show, for example, that $q(x) = 0$ at the same location in the beam where $Q(x)$ achieves its absolute extreme value. Since the layered beams under consideration in the present study are subjected to no mechanical loads, the interlaminar shearing stress must be self-equilibrating over the length of the beam. The solution exhibits this behavior.

7.3 Potential Solution Applications

Unless otherwise stated in the suggested applications that follow, the present solution can be used with confidence to calculate the stresses in end-heated layered media outside of the St Venant boundary layer and is to be used with caution within the boundary layer.

Perhaps the most obvious application of the present solution is in the design and analysis of bimetallic beams or plates exposed to nonuniform temperature environments. The solution may be used in such problems to determine the axial and interlaminar stresses. The potential for failure due to excessive thermal stresses can be addressed using this solution, and, although deflection was not specifically addressed in the present work, the tip deflection is easily determined from the stresses calculated using the present solution. In a transient thermal environment, the solution can be used to predict the time at which yielding or failure of one or both of the components is expected. The present solution

could be used as part of an iterative design approach in which the stresses and deflection are calculated, and modifications are made in the design until acceptable performance is predicted. The analysis given is directly applicable to a simple structure such as a thermostat. With the appropriate change in elastic constants, the solution can be used to perform these analyses in any bimetallic strip, beam or plate.

The present solution is grounded in beam theory. Therefore, it may be used in any application where beam theory is used and with the same degree of confidence. The resulting quantities of interest include bending stresses, bending moments, deflection, etc. The advantage of this solution is that it may be used for layered beam theory analyses in other than uniform temperature environments. For example, the solution can be used with confidence to determine the bending stresses and tip deflection of a bimetallic cantilever beam where the beam is mounted to a very large hot or cold mass and protrudes into a time-dependent temperature field. In this case, however, the beam would experience lengthwise heating (or cooling) which is not directly addressed in the present analysis. Assuming the thermal problem is solved first, the present analysis is then applicable for the determination of stresses. It is noted that, although beam theory is an approximate theory, it has been used extensively in engineering design and analysis and yields the exact solution in many cases (see Rivello (51:page 142)).

The solution is useful in the analysis of end-heated composite laminates with laminae consisting of fibers which are good conductors embedded in matrix material which is a poor conductor, provided the layup is not unidirectional. For example, the solution is applicable to a [0/90/0/90] graphite epoxy laminate because the effective thermal conductivity in the fiber direction of the 0° layers is dominated by the fiber conductivity (which is high) while that of the 90° layers is dominated by the matrix conductivity (which is low). The present solution can be used to calculate the bending and interlaminar stresses in such laminates. This information could be used to make failure predictions outside of the boundary layer or it could be used to design an appropriate laminate for a particular thermal application.

The solution is applicable to certain classes of problems where layered composite or dissimilar materials are heated by a laser or other intense heating source. An example of this type of problem is the laser-heated graphite-epoxy/aluminum beams studied by

Camburn, Lippert and Maddux (43). In order to satisfy the assumptions inherent in the present solution, the heat source must span the entire heated area in one dimension and must cover a very small area in the other dimension. For example, the diameter of the laser spot in the experiments documented in (43) was very small relative to the length of the beams and larger than the width of the beams. Other applications of this nature are when a composite laminate is heated by a long, thin laser heat source or when layered dissimilar materials used in hypersonic flight are subjected to intense aerodynamic heating by line shocks. In these applications, the solution may be used to calculate bending and interlaminar stresses in the materials at least one laminate thickness away from any exposed free edges. The solution is not recommended for complex problems such as the laser-heated composite bottles discussed in Chapter I.

The governing differential equation for the present solution, equation 3.30, can be used to calculate the length of the St Venant boundary layer in a layered beam with a prescribed self-equilibrating (but nonzero) normal stress distribution on the end. The effects of any of the material parameters considered in the present problem on the length of the St Venant boundary layer could be determined using the present solution. For example, the solution may be used to determine the effect of layer stiffnesses on the boundary layer length.

Finally, although it was not proven, there is reason to believe that the present simplified solution can be used to establish an upper bound on the depth of damage into layered dissimilar materials due to end heating. Most of the simplifying assumptions inherent in the present solution tend to cause the stresses to be overestimated. For example, the present solution assumes that mechanical properties exhibit no temperature dependence. In actuality, many engineering materials are known to become more compliant (i. e. the stiffness decreases) as temperature increases. The thermal stresses in a bimaterial beam decrease as the stiffness of the constituents decrease. Therefore, one effect of ignoring the temperature dependence of the stiffness is that the resulting stresses are overestimated. Another reason the present solution overestimates the stresses is that it ignores the mechanism of yielding which is known to relieve stresses in nonbrittle materials. It is therefore reasonable to postulate that, if the simple solution fails to predict damage, yielding, or

failure, the actual state of stress and displacement in the material will be less damaging. It is therefore possible to use this solution as an aid in determining whether failure due to thermal stresses will or will not occur in a particular situation. Bear in mind that the original problem is inherently quite complex. The strength of materials solution presented herein has in no way been presented as an accurate solution to the complex problem. Nevertheless, it provides a quick and simple estimate of thermal stresses in certain types of composite materials.

7.4 Summary

A simple engineering technique was developed to obtain closed-form solutions to layered beam problems subjected to quite arbitrary temperature distributions. The most important contribution of this research is the extension of Suhir's simple solution technique to apply to problems with nonuniform, transient temperature distributions. The solution is based on Bernoulli-Euler beam theory which allows an engineer to make rapid calculations which are quite accurate throughout the vast majority of the beam. It is proposed that the solution obtained in this research provides a suitable engineering approximation to thermal stress problems in certain structures with complicated nonuniform temperature distributions.

In the author's estimation the biggest limitation of the present solution is that it cannot be used to address the problem of free-edge delamination. In most of the cases considered, the free-edge peeling stress was compressive, tending to prevent delamination. In some cases, however, it was tensile and therefore could cause delamination to occur. In any event, the beam theory solutions do not apply within a *boundary layer* thickness of the free edge. In this region, the thickness of which is on the order of the beam thickness, the stresses are not believed to be reliable. Both the magnitude and sign of stresses in this small region may be incorrect. In spite of these shortcomings, the solution is still useful in determining the depth to which material failure may be expected to occur. Assume, for example, that we use the proposed solution technique to analyze a beam and the resulting interlaminar shear stress turns out to exceed the matrix material strength. If the distance over which the excessive stress exists is shorter than the boundary layer thickness, we

can really say nothing at all, for the solution is unreliable within this boundary layer. If, on the other hand, the distance is N boundary layer thicknesses, we can conclude with confidence that failure will not occur beyond N boundary layer thicknesses into the material. The present solution would predict failure in the region between one and N boundary layer thicknesses thick. The overestimating nature of the solution means that stresses are probably lower than predicted and the failure would actually occur over a shorter region, if at all.

The current simplified analysis provides an inexpensive and attractive means by which potential *problem areas* can be identified in aerospace structures subject to high heating loads. Given a design concept, simple analyses such as the one presented in this dissertation can be used quickly to identify areas of concern in large structures. The solution is presented as a means by which engineers and researchers can quickly obtain estimates of the thermal stresses in high-temperature composite and dissimilar material configurations.

Bibliography

1. J. W. Cardinal, et al. **Structural Failure Analyses of Filament Wound Pressurized Cylinders Subject to Continuous Wave Laser Irradiation.** Technical Report AFWL-TR-87-48, Air Force Weapons Laboratory, Kirtland Air Force Base, New Mexico, June 1988.

2. M. A. Tamm, August 10, 1988. **NRL Memorandum Report 6248: Composite Bottle Failure by Elongated Spot CW Laser Irradiation LTH-1 Lethality Enhancement Study.**

3. W. F. Bozich, A. D. Straw, D. Bell, R. Farahmand and E. M. Olsen. **Space-Based Laser (SBL) Liquid Booster Vulnerability Program. Volume 4. Vulnerability Assessment (U).** Technical Report AFWL-TR-89-64-VOL-4, Air Force Weapons Laboratory, Kirtland Air Force Base, New Mexico, September 1990, **(SECRET).**

4. E. M. Olsen and T. J. Keliher. **Solid Booster Vulnerability Program. Volume 1. Analytic Modeling and Subscale Tests (U).** Technical Report AFWL-TR-89-13-VOL-1, Air Force Weapons Laboratory, Kirtland Air Force Base, New Mexico, May 1990, **(SECRET).**

5. D. A. Simons. **Simplified Models for Motorcase Vulnerability to Lasers.** Technical Report DNA-TR-91-2, Defense Nuclear Agency, Alexandria, Va, June 1991.

6. H. A. Hogan and S. J. Harbert. **Improved Modelling of the Response of Pressurized Composite Cylinders to Laser Damage**, 31 December, 1990. 1989 USAF-UES Research Initiation Program, Final Report to WL/TALE Kirtland Air Force Base, New Mexico, Contract No. F49620-88-C-0053/SB5881-0378.

7. B. A. Boley and J. H. Weiner. **Theory of Thermal Stresses.** John Wiley & Sons, New York, 1960.

8. S. P. Timoshenko. **Analysis of Bi-Metal Thermostats.** *Journal of the Optical Society of America*, 11:233–255, 1925.

9. J. Dundurs. **Effect of Elastic Constants on Stress in a Composite Under Plane Deformation.** *Journal of Composite Materials*, 1:310–322, 1967.

10. J. Dundurs. **Discussion of D. B. Bogy's "Edge-Bonded Dissimilar Orthogonal Elastic Wedges under Normal and Shear Loading,".** *Journal of Applied Mechanics*, 36:650–652, 1969.

11. D. B. Bogy. **Edge-Bonded Dissimilar Orthogonal Elastic Wedges Under Normal and Shear Loading.** *Journal of Applied Mechanics*, 35:460–466, 1968.

12. D. B. Bogy. **On the Problem of Edge-Bonded Elastic Quarter-Planes Loaded at the Boundary.** *International Journal of Solids and Structures*, 6:1287–1313, 1970.

13. I. S. Raju, J. D. Whitcomb and J. G. Goree. **A New Look at Numerical Analyses of Free- Edge Stresses in Composite Laminates.** Technical Report NASA TN-1751, NASA, December 1980.

14. F. Delale. **Stress Singularities in Bonded Aristopian Materials.** *International Journal of Solids and Structures*, 20(1):31–40, 1984.

15. J. P. Blanchard and N. M. Ghoniem. **An Eigenfunction Approach to Singular Thermal Stresses in Bonded Strips.** *Journal of Thermal Stresses*, 12:501–527, 1989.

16. D. Munz, T. Fett and Y. Y. Yang. **The Regular Stress Term in Bonded Dissimilar Materials after a Change in Temperature.** *Engineering Fracture Mechanics*, 44:185–194, 1993.

17. D. Munz and Y. Y. Yang. **Stresses Near the Edge of Bonded Dissimilar Materials Described by Two Stress Intensity Factors.** *International Journal of Fracture*, 60:169–177, 1993.

18. J. N. Goodier. **On the Integration of the Thermo-Elastic Equations.** *Philosophical Magazine*, 23:1017–1032, 1937.

19. R. B. Pipes and N. J. Pagano. **Interlaminar Stresses in Composite Laminates under Uniform Axial Extension.** *Journal of Composite Materials*, 4:538, 1970.

20. A. H. Puppo and H. A. Evensen. **Interlaminar Shear in Laminated Composites under Generalized Plane Stress.** *Journal of Composite Materials*, 4:204, 1970.

21. M. Goland and E. Reissner. **The Stresses in Cemented Joints.** *Journal of Applied Mechanics*, 11:A17–A27, 1944.

22. C. E. S. Ueng and K. D. Zhang. **A Simplified Approach for Interlaminar Stresses in Orthotropic Laminated Strips.** *Journal of Reinforced Plastics and Composites*, 4:273–286, July 1985.

23. X. L. and D. Liu. **An Interlaminar Shear Stress Continuity Theory for Both Thin and Thick Composite Laminates.** *Journal of Applied Mechanics*, 6:502–509, September 1992.

24. C. Kassapoglou and P. A. Lagace. **Closed Form Solutions for the Interlaminar Stress Field in Angle-Ply and Cross-Ply Laminates.** *Journal of Composite Materials*, 21:292–308, April 1987.

25. N. O. Myklestad. **Two Problems of Thermal Stress in the Infinite Solid.** *Journal of Applied Mechanics*, 14:A136–A143, 1942.

26. C. D. Pionke and G. Wempner. **The Various Approximations of the Bimetallic Thermostatic Strip.** *Journal of Applied Mechanics*, 58:1015–1020, December 1991.

27. D. Chen, S. Cheng and T. D. Gerhardt. **Thermal Stresses in Laminated Beams.** *Journal of Thermal Stresses*, 5:67–84, 1982.

28. H. E. Williams. **Asymptotic Analysis of the Thermal Stresses in a Two-Layer Composite with an Adhesive Layer.** *Journal of Thermal Stresses*, 8:183–203, 1985.

29. K. Seo, M. Kusaka, F. Nogata, T. Terasaki, Y. Nakao and K. Saida. **Study on the Thermal Stress at Ceramics- Metal Joint.** *JSME International Journal, Series 1*, 33(3):342–348, 1990.

30. W. T. Chen and C. W. Nelson. **Thermal Stress in Bonded Joints.** *IBM Journal of Research and Development*, 23(2):179–188, March 1979.

31. Y. Weitsman. **Stresses in Adhesive Joints Due to Moisture and Temperature.** *Journal of Composite Materials*, 11:378–394, October 1977.

32. E. Suhir. **Stresses in Bi-Metal Thermostats.** *Journal of Applied Mechanics*, 53:657–660, September 1986.

33. E. Suhir. **Interfacial Stresses in Bimetal Thermostats.** *Journal of Applied Mechanics*, 56:595–600, September 1989.

34. S. K. Morton and J. P. H. Webber. **Interlaminar Failure Due to Mechanincal and Thermal Stresses at the Free Edges of Laminated Plates.** *Composites Science and Technology*, 47:1–13, 1993.

35. A. Y. Kuo. **Thermal Stresses at the Edge of a Bimetallic Thermostat.** *Journal of Applied Mechanics*, 56:585–589, 1989.

36. O. O. Ochoa and V. M. Marcano. **Thermal Stresses in Laminated Beams.** *International Journal of Solids Structures*, 20:579–587, 1984.

37. H. E. Williams. **Thermal Stresses in Bonded Solar Cells-the Effect of the Adhesive Layer.** *Journal of Thermal Stresses*, 6:231–252, 1983.

38. M. Y. Tsai and J. Morton. **The Stresses in a Thermally Loaded Bimaterial Interface.** *International Journal of Solids and Structures*, 28:1053–1075, 1991.

39. W. L. Yin. **Effects of Inclined Free Edges on the Thermal Stresses in a Layered Beam.** *Journal of Electronic Packaging*, 115:208–213, 1993.

40. Y. Y. Yang and D. Munz. **Determination of the Regular Stress Term in a Dissimilar Materials Joint under Thermal Loading by the Mellin Transform.** *Journal of Thermal Stresses*, 17:321–336, 1994.

41. Y. W. Kwon, D. Salinas and M. J. Neibert. **Thermally Induced Stresses in a Trilayered System.** *Journal of Thermal Stresses*, 17:489–506, 1994.

42. I. S. Gradshteyn and I. M. Ryzhik. **Table of Integrals Series and Products.** Academic Press, New York, 1965.

43. G. L. Camburn, J. R. Lippert and G. Maddux. **Response of Compression-Loaded Graphite Epoxy Laminates to Laser Energy.** Technical Report AFFDL TR-76-127, Air Force Flight Dynamics Laboratory, Wright-Patterson AFB, Ohio, November 1976.

44. N. A. Waterman and M. F. Ashby. **CRC-Elsevier Materials Selector.** CRC Press, Ann Arbor, Michigan, 1991.

45. ASM Handbook Committee. **Metals Handbook, Ninth Edition, Vol 2, Properties and Selection: Nonferrous Alloys and Pure Metals.** American Society for Metals.

46. J. P. Holman. **Heat Transfer.** McGraw-Hill Book Company, New York, 1981.

47. L. J. Broutman and R. H. Krock. **Composite Materials, Volume 5, Fracture and Fatigue.** Academic Press, New York, 1974.

48. G. Lubin. **Handbook of Composites**. Van Nostrand Reinhold Company, New York, 1982.

49. R. H. Perry and C. H. Chilton. **Chemical Engineers' Handbook, Fifth Edition**. McGraw-Hill, New York, 1973.

50. M. N. Özişik. **Heat Conduction**. John Wiley and Sons, New York, 1980.

51. R. O. Rivello. **Theory and Analysis of Flight Structures**. McGraw-Hill Book Company, New York, 1969.

Vita

Major Jerry Rodney (Rod) [redacted] September 1960 in Monroe, North Carolina. He graduated from High School in Monroe, North Carolina in 1976 and attended High Point College, High Point, North Carolina, from which he received the Bachelor of Science degree in Mathematics in May 1980. He worked as a computer programmer/analyst at Duke Power Company, Charlotte, North Carolina, until he entered the United States Air Force Officer Training School in May 1982. Upon his graduation from Officer Training School, he was commissioned a Second Lieutenant in the Air Force and was assigned to the Air Force Institute of Technology, from which he earned the Bachelor of Science degree in Aeronautical Engineering in March 1984 and the Master of Science degree in Aeronautical Engineering in March 1985. His master's thesis dealt with the subject of the thermal coupling of pulsed laser energy into metals. Following his graduation, Major Couick was assigned to the Air Force Weapons Laboratory at Kirtland AFB, New Mexico, where he served as a Laser Effects and Vulnerability Engineer for one year and as Chief of the Laser Test Facility for four years. In July 1990 he was selected to attend the Air Force Institute of Technology as a doctoral student. He entered the Doctor of Philosophy degree program in October 1990 and was admitted to candidacy in September 1992, with a major in solid mechanics and a minor in heat transfer. Following his admission to candidacy, he has performed research on the thermal stresses in layered dissimilar materials, working under the advice and guidance of Professor Peter J. Torvik of the Department of Aeronautics and Astronautics. In September 1993, Major Couick was assigned to Wright Laboratory as Thermal Structures Research Team leader, where he continued research on his dissertation on a part-time basis.

[redacted]

REPORT DOCUMENTATION PAGE

Form Approved
OMB No. 0704-0188

1. AGENCY USE ONLY *(Leave blank)*	2. REPORT DATE	3. REPORT TYPE AND DATES COVERED
	30 Nov 95	Dissertation, Dec 95

4. TITLE AND SUBTITLE

Thermal Stresses in End-Heated Layered Media

5. FUNDING NUMBERS

6. AUTHOR(S)

Jerry R. Couick, Major, USAF

7. PERFORMING ORGANIZATION NAME(S) AND ADDRESS(ES)

AFIT/ENY
2950 P Street
Wright-Patterson AFB OH 45433

8. PERFORMING ORGANIZATION REPORT NUMBER

AFIT/DS/ENY/95-6

9. SPONSORING/MONITORING AGENCY NAME(S) AND ADDRESS(ES)

Christopher Clay
WL/FIBEB, Bldg 45
2130 Eighth Street Suite 1
Wright-Patterson AFB OH 45433-7542

10. SPONSORING/MONITORING AGENCY REPORT NUMBER

11. SUPPLEMENTARY NOTES

12a. DISTRIBUTION/AVAILABILITY STATEMENT

Distribution Unlimited

12b. DISTRIBUTION CODE

13. ABSTRACT *(Maximum 200 words)*

Thermal stresses in semi-infinite layered beams heated on the end are calculated using an extension to simple bimetallic thermostat theory. Recently, researchers have used the concept of interfacial compliance to determine interlaminar stresses in a simple thermostat of finite length subjected to a uniform temperature increase. In the present work, the thermostat theory is extended to apply to the beams of interest. A closed-form solution to the problem is obtained. It is not applicable within about one beam thickness (St Venant boundary region) of the end. Various classes of layered materials are analyzed to determine if significant stresses exist outside the boundary region. Thermal stresses of sufficient magnitude to cause failure are confined to the boundary region if all layers of the beam are poor thermal conductors. Significant axial and bending stresses occur outside of the boundary region for layered beams in which one or more layers are relatively good thermal conductors. Very high stresses are found to exist in good conductors bonded to poor conductors of similar stiffness. Significant interlaminar stresses occur only in the boundary region, regardless of the layer thermal conductivities. The applicability of the solution to composite laminates is addressed.

14. SUBJECT TERMS

Thermal Stresses, Dissimilar Materials, Layered Media, Thermostats, Nonuniform Temperature

15. NUMBER OF PAGES

137

16. PRICE CODE

17. SECURITY CLASSIFICATION OF REPORT	18. SECURITY CLASSIFICATION OF THIS PAGE	19. SECURITY CLASSIFICATION OF ABSTRACT	20. LIMITATION OF ABSTRACT
UNCLASSIFIED	UNCLASSIFIED	UNCLASSIFIED	UL

GENERAL INSTRUCTIONS FOR COMPLETING SF 298

The Report Documentation Page (RDP) is used in announcing and cataloging reports. It is important that this information be consistent with the rest of the report, particularly the cover and title page. Instructions for filling in each block of the form follow. It is important to ***stay within the lines*** to meet ***optical scanning requirements***.

Block 1. Agency Use Only *(Leave blank)*.

Block 2. Report Date. Full publication date including day, month, and year, if available (e.g. 1 Jan 88). Must cite at least the year.

Block 3. Type of Report and Dates Covered. State whether report is interim, final, etc. If applicable, enter inclusive report dates (e.g. 10 Jun 87 - 30 Jun 88).

Block 4. Title and Subtitle. A title is taken from the part of the report that provides the most meaningful and complete information. When a report is prepared in more than one volume, repeat the primary title, add volume number, and include subtitle for the specific volume. On classified documents enter the title classification in parentheses.

Block 5. Funding Numbers. To include contract and grant numbers; may include program element number(s), project number(s), task number(s), and work unit number(s). Use the following labels:

C	- Contract	**PR**	- Project
G	- Grant	**TA**	- Task
PE	- Program Element	**WU**	- Work Unit Accession No.

Block 6. Author(s). Name(s) of person(s) responsible for writing the report, performing the research, or credited with the content of the report. If editor or compiler, this should follow the name(s).

Block 7. Performing Organization Name(s) and Address(es). Self-explanatory.

Block 8. Performing Organization Report Number. Enter the unique alphanumeric report number(s) assigned by the organization performing the report.

Block 9. Sponsoring/Monitoring Agency Name(s) and Address(es). Self-explanatory.

Block 10. Sponsoring/Monitoring Agency Report Number. *(If known)*

Block 11. Supplementary Notes. Enter information not included elsewhere such as: Prepared in cooperation with...; Trans. of...; To be published in.... When a report is revised, include a statement whether the new report supersedes or supplements the older report.

Block 12a. Distribution/Availability Statement. Denotes public availability or limitations. Cite any availability to the public. Enter additional limitations or special markings in all capitals (e.g. NOFORN, REL, ITAR).

- **DOD** - See DoDD 5230.24, "Distribution Statements on Technical Documents."
- **DOE** - See authorities.
- **NASA** - See Handbook NHB 2200.2.
- **NTIS** - Leave blank.

Block 12b. Distribution Code.

- **DOD** - Leave blank.
- **DOE** - Enter DOE distribution categories from the Standard Distribution for Unclassified Scientific and Technical Reports.
- **NASA** - Leave blank.
- **NTIS** - Leave blank.

Block 13. Abstract. Include a brief *(Maximum 200 words)* factual summary of the most significant information contained in the report.

Block 14. Subject Terms. Keywords or phrases identifying major subjects in the report.

Block 15. Number of Pages. Enter the total number of pages.

Block 16. Price Code. Enter appropriate price code *(NTIS only)*.

Blocks 17. - 19. Security Classifications. Self-explanatory. Enter U.S. Security Classification in accordance with U.S. Security Regulations (i.e., UNCLASSIFIED). If form contains classified information, stamp classification on the top and bottom of the page.

Block 20. Limitation of Abstract. This block must be completed to assign a limitation to the abstract. Enter either UL (unlimited) or SAR (same as report). An entry in this block is necessary if the abstract is to be limited. If blank, the abstract is assumed to be unlimited.